UTILIZATION OF NANOMATERIALS TO DEVELOP ANALYTICAL METHODS OF PROHIBITED SUBSTANCE IN SKINCARE PRODUCTS

By

MISS Kanokwan SAKUNRUNGRIT

A Thesis Submitted in Partial Fulfillment of the Requirements

for Master of Science CHEMISTRY

Department of CHEMISTRY

Silpakorn University

Academic Year 2023

การใช้ประโยชน์จากวัสดุนาโนเพื่อพัฒนาวิธีวิเคราะห์สารต้องห้ามในผลิตภัณฑ์ดูแลผิว

โดย
นางสาวกนกวรรณ สกุลรุ่งฤทธิ์

วิทยานิพนธ์นี้เป็นส่วนหนึ่งของการศึกษาตามหลักสูตรวิทยาศาสตรมหาบัณฑิต
สาขาวิชาเคมี แผน ก แบบ ก 2
ภาควิชาเคมี
มหาวิทยาลัยศิลปากร
ปีการศึกษา 2566

UTILIZATION OF NANOMATERIALS TO DEVELOP ANALYTICAL METHODS OF PROHIBITED SUBSTANCE IN SKINCARE PRODUCTS

By

MISS Kanokwan SAKUNRUNGRIT

A Thesis Submitted in Partial Fulfillment of the Requirements

for Master of Science CHEMISTRY

Department of CHEMISTRY

Silpakorn University

Academic Year 2023

Title	Utilization of nanomaterials to develop analytical methods of prohibited substance in skincare products
By	MISS Kanokwan SAKUNRUNGRIT
Field of Study	CHEMISTRY
Advisor	Assistant Professor Dr. Sumonmarn Chaneam, Ph.D.

Faculty of Science, Silpakorn University in Partial Fulfillment of the Requirements for the Master of Science

.....Dean of Faculty of Science
(Assistant Professor Dr. Narong Chimpalee, Ph.D.)

Approved by

.....Chair person
(Associate Professor Dr. Saowapak Teerasong, Ph.D.)

.....Advisor
(Assistant Professor Dr. Sumonmarn Chaneam, Ph.D.)

.....Committee
(Dr. Kanokwan Charoenkitamorn, Ph.D.)

.....External Examiner
(Associate Professor Dr. Purim Jarujamrus, Ph.D.)

640720024 : Major CHEMISTRY
Keyword : Prohibited substance, Nanomaterials, Skincare products

MISS Kanokwan SAKUNRUNGRIT : Utilization of nanomaterials to develop analytical methods of prohibited substance in skincare products Thesis advisor : Assistant Professor Dr. Sumonmarn Chaneam, Ph.D.

Recently, there has been a growing concern regarding the potential presence of prohibited substances in skincare products, especially preservatives, and mercury. Mercury is a toxic metal that can accumulate and be absorbed into the bloodstream. Preservatives are substances that are added to prevent microorganisms and prolong the shelf-life of the products. However, extended use of skin care products containing mercury and preservatives can have harmful side effects on the skin and internal organs. The usage of mercury and preservatives in skincare products is legally restricted in numerous countries owing to their damaging effects. There are various traditional methods employed for mercury and preservative detection, such as atomic absorption spectrophotometry (AAS), inductively coupled plasma optical emission spectroscopy (ICP-OES), inductively coupled plasma mass spectrometry (ICP-MS), and high-performance liquid chromatography (HPLC). However, despite their high accuracy and reliability, these techniques require costly equipment, skilled professionals, and complex sample preparation. Therefore, this study aimed to develop a fast, affordable, simple, and efficient approach to analyzing mercury and preservatives in skincare samples by using nanomaterials as key substances in the analysis reactions, followed by fluorometric detection. This work was divided into two sections.

First, determining mercury in skincare products using carbon dots (CDs) as a reagent combined with a sequential injection analysis (SIA) and spectrofluorometric detection was proposed. The fluorescence intensity of CDs is significantly decreased due to mercury ions. The CDs have been successfully synthesized using the microwave-assisted method. The properties of the CDs were characterized by transmission electron microscopy (TEM), X-ray diffractometry (XRD), X-ray photoelectron spectroscopy (XPS), Fourier-transform infrared spectroscopy (FT-IR),

UV–vis spectrometry, and spectrofluorometry. This proposed method showed a linear range from 0.5 to 600 ppm with a detection limit of 0.1 ppm and an acceptable percentage recovery. The relative standard deviation was 1.53% (n = 12) with a 20-sample per hour sample throughput. By comparison with ICP-MS, the accuracy of our approach was validated, and the results between the two methods are not significantly different. This work was the first time to present the use of CDs to determine mercury ions in skincare samples using the SIA method with an easy, automatic, and cost-effective detection.

Next, the fluorometric detection of preservatives in skincare products using Ni-MnFe-layered double hydroxides (Ni-MnFe-LDHs) as peroxidase-like mimicking was developed. 4-Hydroxybenzoic acid (PHBA) and benzoic acid were studied as preservative model targets. In the presence of preservatives, Ni-MnFe-LDHs can catalyze the oxidation of H_2O_2. The generated hydroxy radical ($^{\bullet}OH$) was then consumed by PHBA or benzoic acid to form phenoxy radical, leading to less of $^{\bullet}OH$ to catalyze *o*-phenylenediamine (OPD) into the yellow-fluorescent product of 2, 3-diamino phenazine (DAP). The yellow fluorescence signal of DAP significantly decreased, corresponding to the concentration of preservatives in skincare products. A smartphone captured the color of the solution under a UV-controlled lightbox within 20 minutes. Under the optimum conditions, this developed method showed a linear range of 0.008-1.0 and 0.008-1.0 mM for PHBA and benzoic acid, with a limit of detection of 0.0072 and 0.0042 mM for PHBA and benzoic acid, respectively. Our proposed method was validated with the HPLC-DAD and showed an acceptable percentage recovery.

ACKNOWLEDGEMENTS

I am deeply grateful to my advisor, Asst. Prof. Sumonmarn Chaneam, for her strong support and guidance throughout my master's program. Her expertise and patience have been invaluable to me and have played a crucial role in the success of this thesis.

I would like to thank the Faculty of Science, Silpakorn University, for the research assistant scholarship and the Department of Chemistry for the teaching assistant scholarship. Financial support from the Reinventing University System Program by the Ministry of Higher Education, Science, Research, and Innovation (fiscal year 2021) and the National Research Council of Thailand (N11A650144), chaired by Assoc. Prof. Dr. Duangjai Nacapricha is also gratefully acknowledged.

I would like to appreciative thank Assoc. Prof. Purim Jarujamrus, for providing me with the opportunity and collaboration to conduct my research at the Department of Chemistry, Faculty of Science, Ubon Ratchathani University, and for all the instrumental facilities and support. I am also grateful to thank Assoc. Prof. Saowapak Teerasong and Dr. Kanokwan Charoenkitamorn for serving on my thesis committee and providing valuable feedback and suggestions.

Finally, I would like to sincerely thank Mr. Akarapong Prakobkij, PJ group, and SCFlowLab members for their help, guidance, and support during this process.

Kanokwan SAKUNRUNGRIT

TABLE OF CONTENTS

Page

LIST OF TABLES

Page

LIST OF FIGURES

Page

CHAPTER 1

INTRODUCTION

1.1 Statements and significance of the problem

In recent years, the safety of skincare products has raised greater concern. It is important to be aware of some prohibited substances in these products, especially mercury and preservatives. Mercury is a highly hazardous metal that can be found in several skin-condition treatments intentionally or by mistakenly. Because mercury can accumulate in the skin when used frequently for a prolonged period, it may damage the skin and internal organs [1-3]. Preservatives are substances added to skincare products with the aim of maintaining quality and extending shelf life. Benzoic acid is the antimicrobial preservatives that are commonly found in skincare products. In addition, 4-hydroxybenzoic acid (PHBA) is also the preservative prohibited for use in certain types of cosmetics such as sunscreens [4-6]. Long-term use of these preservatives can exert harmful effects on the skin and internal organs [4, 7-9]. Accordingly, both mercury and preservatives have legislation that is restricted from use in skincare products in many countries.

The quantity of these prohibited substances in skincare products has been an increasing concern. Hence, sensitive, and accurate approaches are necessary. Several conventional techniques have been employed, including inductively coupled plasma-mass spectrometry (ICP-MS) for mercury analysis [10] and high-performance liquid chromatography (HPLC) for preservatives analysis [11-13]. Despite the high reliability and accuracy of these approaches, expensive equipment, long-time analysis and large amount of chemical reagents are still required.

This work reports method development of the simple, rapid, and cost effective for mercury and preservatives determination in skincare samples. Nanomaterials are employed as essential components in the analysis reactions. First, a spectrofluorometric method coupled with a sequential injection analysis (SIA) system

was used to analyze mercury utilizing carbon dots (CDs) as a reagent. This proposed method was based on the measurement of the fluorescence of CDs, which was correspondingly quenched after the addition of mercury. Fast and simple microwave-assisted method was used for the preparation of CDs. General compounds, citric acid and urea were used as precursors. Next, Ni-MnFe-layered double hydroxides (Ni-MnFe-LDHs) were employed as peroxidase-like mimicking for fluorometric preservative detection, with benzoic acid and PHBA serving as model analytes. The experiment was performed on a 96-well plate. The Ni-MnFe-LDHs catalyze the oxidation of H_2O_2 to produce $^{\bullet}OH$, which subsequently reacts with both PHBA and benzoic acid to create phenoxy radicals. The remaining $^{\bullet}OH$ interacts with the OPD substrate, dramatically decreasing the yellow fluorescence signal from the DAP. The fluorescent signal was later captured using a smartphone under a UV-controlled lightbox to detect preservatives within 20 minutes quantitatively.

1.2 Objectives of research

1.2.1 To develop the mercury determination using SIA system and CDs as a reagent

1.2.2 To develop the preservatives determination using Ni-MnFe-LDHs as peroxidase-like mimicking with OPD fluorescent substrate

1.2.3 To apply the developed methods to skincare samples and compare the sample analysis results with reference methods

1.3 Scope of research

1.3.1 Determination of mercury

1.3.1.1 Synthesis of CDs

1.3.1.2 Characterization of CDs

- The structures and morphologies; x-ray photo electron spectroscopy (XPS) and transmission electron microscopy (TEM)
- Crystalline identification; x-ray diffractometer (XRD)

- The functional group on the surface; Fourier-transform infrared spectroscopy (FT-IR)
- UV–visible absorption spectra and fluorescence spectra; UV-Vis spectrophotometry and spectrofluorometry

1.3.1.3 Utilization of the synthesized CDs as a reagent for mercury analysis using SIA system

- Physical optimization study; sample volume, reagent volume and flow rate
- Interference study
- Analytical performance and method validation
- Sample analysis

1.3.2 Determination of preservatives

1.3.2.1 Synthesis of Ni-MnFe-LDHs

1.3.2.2 Characterization of Ni-MnFe-LDHs

- Particle analysis; zeta potential analysis
- The structures and morphologies; x-ray photo electron spectroscopy (XPS), transmission electron microscopy (TEM), and field emission scanning electron microscope coupled with energy-dispersive spectrometer (FESEM-EDS)
- Crystalline identification; x-ray diffractometer (XRD)
- The functional group on the surface; Fourier-transform infrared spectroscopy (FT-IR)
- UV–visible absorption spectra and fluorescence spectra; UV-Vis spectrophotometry and spectrofluorometry

1.3.2.3 Proposed mechanism

1.3.2.4 Utilization of the synthesized Ni-MnFe-LDHs as an enzyme mimic for preservatives analysis

- Physical optimization study; concentration of reagent (including Ni-MnFe-LDHs, H_2O_2, and OPD substrate), and pH system

- Chemical optimization study; camera mode (including shutter speed, and ISO)
- Interference study
- Analytical performance and method validation
- Sample analysis

1.4 Definition

1.4.1 Nanomaterials are materials with at least one dimension that is 100 nm or smaller, or particles that are between 1 and 100 nm in size [14].

1.4.2 Carbon dots (CDs) are zero-dimension carbon-based nanomaterials with particle size less than 10 nm, which are composed of carbon, oxygen, hydrogen, and nitrogen, depending on the precursor [14]. This material exhibited good optical properties such as strong absorption, better light stability, and higher fluorescence properties [15].

1.4.3 Layered double hydroxides (LDHs) are two-dimension layered nanomaterials consist of anionic clays that contain brucite-like layers with hydrated interlayer anions species and cations that can be monometallic, two-metal, or three-metal in the body layer [16, 17].

1.4.4 Sequential injection analysis (SIA) is the flow-based technique which is automatically computer controlled and uses electrically multiple ports selection valve and syringe pump, which accurately delivered volumes of all the solution to detector [18].

CHAPTER 2

REVIEW OF RELATED LITERATURE

2.1 Determination of mercury

2.1.1 Mercury in skincare products

A particularly dangerous substance that can be found in skincare and cosmetic products is heavy metal, including lead, cadmium, nickel, arsenic and mercury [19]. Mercury is found in whitening products because it inhibits melanin formation [20, 21]. In addition, mercury can be added in skincare products from various sources such as contaminated raw materials (such as plants, herbals, and water), and production process[19]. Mercury is easily absorbed and accumulates within the skin, passes through the blood vessels and finally go into the internal organs [19] and exerts harmful side effects when uses repeatedly for a long duration of time. These findings can lead to damage in the brain, nervous system, and renal system [20]. Moreover, mercury has an impact on the body by reducing immune system response, inhibiting enzyme systems, and preventing the production of protein and DNA [20]. In addition, it leads to memory loss, tremors, insomnia, irritability, and trembling [21].

Due to the side effects of mercury, many countries have imposed restrictions on the quantity of mercury allowed in skincare and cosmetic products. For example, the permitted limit of mercury in skincare products in Thailand not higher than 1 ppm [22]. The U.S. FDA regulations legislated the maximum concentration of prohibited and restricted components in cosmetics is 1 mg Hg/L for all other cosmetics and 65 mg Hg/L for eye products [23].

2.1.2 Conventional method for mercury determination

Several conventional techniques have been employed to determine mercury ion (Hg^{2+}), including titration [24], neutron activation analysis [25], cold vapor atomic absorption spectrometry [26], inductively coupled plasma mass spectrometry (ICP-MS), that are highly efficient analytical method for Hg^{2+}

detection. Bussan D. *et. al.* (2015) [10] reported the mercury analysis in environmental solid samples. Their experiment pre-concentrated the mercury in the sample by amalgamation with gold and combusting the solid sample with direct mercury analyzer (DMA) to remove the matrix in sample. The detection was based on atomic absorption spectrophotometry (AAS) coupled to a sector field of ICP-MS. The limit of detection of this method was 0.37 pg. The percentage of relative standard deviation is less than 7 and the total analysis time was less than 8 min per sample.

2.1.3 Spectroscopy for mercury determination

Although the conventional ICP-MS method is highly accurate and precise, expensive instruments, highly skilled operators, and multistep sample preparation are still required. The spectrofluorometric method using organic ionophore/fluorophore reagent has been developed for a fast and highly sensitive sensor to detect Hg^{2+}. Petdum *et. al.* (2018) [27] synthesized a colorimetric and fluorometric sensor based on [5]helicene linked to rhodamine 6G through a hydrazide moiety for Hg^{2+} detection. The ring-opened rhodamine 6G-Hg^{2+} complex acceptor received energy from [5]helicene donor, increasing the fluorescence intensity and changing the sensor's color from greenish-yellow to orange, which is easily observed with the naked eye. The detection limit of this sensor was 2.3 ppb. Rasheed *et. al.* (2019) [28] designed the fluorometric sensor for Hg^{2+} detection with rhodamine B and 2-amino-5-bromopyridine. The spirolactam ring of the sensor was opened via photo-induced electron transfer (PET) of xanthene to enhance the fluorescence signal, and color of the sensor changed to red. The detection limit of this sensor was 0.63 μM. Although these sensors performed well, their applications were limited to water or spiked samples, lacking complexity in the matrix.

2.1.4 Nanomaterials for mercury determination

Determination of mercury based on the mentioned ionophore/fluorophore sensors required a multistep synthesis, considerable product amount, and chemical toxicity. Furthermore, most of these sensors exhibit insolubility in aqueous systems, which is unfavorable for sample preparation and delivery in the flow system. Recently, nanomaterials have been developed to become a mercury sensor for rapid, selective, and sensitive determination. Various types of nanomaterials such as gold nanoparticle, silver nanoparticle, and sulfur nanodots were reported as show in Table 1. However, these nanomaterials required some toxic chemicals for synthesis, involved modification and treated processes before used. Among these nanomaterials, carbon-based nanomaterials such as carbon dots (CDs) are increasingly used in different fields, especially, used as metal sensors.

Table 1 *Various nanomaterials for mercury analysis*

Type of nanomaterials	Synthesis procedure	Precursor	Modification reagent	Sample	Reference
Gold nanoparticle	One-pot citrate reduction method	Chloroauric acid	Rhodamine B and thiol ligand	Pond water and batteries	[29]
Silver nanoparticle	One-pot citrate reduction method	Silver nitrate	Rhodamine B	Drinking water and whitening lotion	[30]
Sulfur nanodots	Top-down method	Sublimed sulfur powder	PEG-1000	Tap water	[31]

Carbon dots (CDs) are zero-dimension carbon-based nanomaterials, which are composed of carbon, oxygen, hydrogen, and nitrogen, depending on the precursors [14]. The synthesis process and precursors have an impact on the structure as well as the composition of the surface of CDs, resulting in their fluorescence emission properties. Chien *et. al.* (2019) reported that oxidation on sp^2 carbon of CDs enhanced the excitation electrons [32, 33]. Several previous works found that different amount of nitrogen affected to fluorescence emission properties of CDs [33, 34].

In addition, CDs are reported as a specific sensor for heavy metals, particularly mercury ion (Hg^{2+}) due to their unique physical and chemical properties, easy synthesis, biocompatibility, and low toxicity [35, 36]. The carboxyl groups of CDs can interact with Hg^{2+} and the electron of CDs is then transferred to Hg^{2+}, resulting in CDs aggregation and a decrease in the fluorescence emission intensity [37]. This effect is named "Quenching effect" [37]. Notably, CDs are selective to Hg^{2+} compared to other metal ions due to higher stability formation constants (log K_f) between carboxyl group of CDs and Hg^{2+} [37].

Table 2 shows previous research that demonstrated the utilization of CDs as mercury sensors. As mentioned above, this work reported the utilized of CDs as a reagent for mercury analysis in skincare products for the first time.

Table 2 *The utilization of CDs as mercury sensors of previous works*

CDs precursor	Synthesis procedure	LOD	Sample	Reference
Flour	Microwave assisted	0.5 nM	Lake water	[38]
Urea and Ethylenediaminetetra acetic acid (EDTA)	One-step pyrolysis	14 nM	Tap water	[39]
Citric acid and triethylamine	Hydrothermal	2.8 nM	Tap water	[40]
Citric acid and melamine	Solid thermal method	0.44 µM	Breast milk	[41]
Citrus lemon juice and ethylenediamine	Hydrothermal	5.3 nM	Tap water and packed water	[42]
Citric acid and 2,2-dimethyl-1,3-propanediamine	Microwave assisted pyrolysis	7.63 nM	Tap water	[43]
Eggshell membrane	Hydrothermal	2.6 µM	Tap water and lake water	[44]

2.1.5 Sequential injection analysis for mercury determination

Sequential injection analysis (SIA) was developed from flow injection analysis (FIA) by J. Ruzicka and G. Marshall in 1990. This technique is based on the utilization of multi-port selection valve and high-precision syringe pump with computerized control. The zone of carrier, sample, standards, and reagent solution are precisely aspirated by this pump to a holding coil. The syringe pump then reversed the flow direction, leading to transport the product zone to the detector. The zone of solution in SIA system is operated in laminar profile. There is dilution and elongation in this laminar zone and the signal profile displays the typical asymmetric shape. [18, 45]

The SIA system offers many advantages over the FIA system such as reducing sample and reagent consumptions, minimizing the production of waste, suitable for hazardous reagents, short time analysis, and fully automatic operation. The SIA has been used in previous researches to determine the amount of Hg^{2+} in a variety of samples as shown in Table 3. [18, 45]

Table 3 *Determination of Hg^{2+} in a various samples by SIA system*

Sample	Detection method	LOD	Sample throughput	Reference
Certified fish, marine sediment, and fish liver	Cold-vapor atomic absorption spectroscopy	0.34 ppb	30 h^{-1}	[46]
Urine	UV-vis spectrophotometry	1 ppm	27 h^{-1}	[47]
Water	Anodic stripping voltammetry	0.22 ppb	Not reported	[48]
Commercial creams, local medicines, and water	UV-vis spectrophotometry	0.06 ppm	40 h^{-1}	[49]

According to related literatures, herein, this work report the first time to establish an approach for measuring Hg^{2+} in skincare products using the spectrofluorometric method and the SIA system to handle the sample and reagent in microliters and accomplish the automatic operation. The CDs were employed as the specific reagent with highly sensitive and selective determination.

2.2 Determination of preservatives

2.2.1 Preservatives in skincare products

Preservatives are commonly added to food, skincare, and cosmetic products. Their purpose is to prevent the growth of microorganisms and oxidants, which helps to maintain the quality of the products and increase their shelf life [4, 5]. Typically, preservatives are usually classified according to their purpose in skincare products; antioxidant preservatives (including nitrites, nitrates, and sorbates), anti-enzymatic preservatives (including citric acid and erythorbic acid), and antimicrobial preservatives (including 4-hydroxybenzoic acid, benzoic acid, and paraben), which are frequently added in skincare products [6].

4-Hydroxybenzoic acid or PHBA, is a derivative of benzoic acid that contains a benzene ring with a hydroxyl group attached at C-4. This molecule is formed through the hydrolysis reaction of paraben or alkyl esters of PHBA [50]. PHBA is commonly used in both the cosmetic and pharmaceutical industries [51]. Regrettably, consistent usage of products containing PHBA can cause skin irritation, leading to redness or burning and harm to the eyes [6, 7]. Furthermore, PHBA might promote the development of breast cancer in humans [8] and indirectly affect the production of proteins in the liver, leading to hepatotoxicity [9]. Many countries worldwide have permitted the use of preservatives in products. For instance, both the U.S. Food and Drug Administration (FDA) (Annex VI) [52] and the EU Cosmetics Regulation (Annex V) [53] have regulations regarding the amount of benzoic acid in leave-on products, which should not exceed 0.5% (40 mM) as an

acid. Also, the amount of PHBA and its methyl- and ethyl- esters, as well as their salts, should not exceed 0.4% (30 mM) for a single ester and 0.8% (60 mM) for a mixed esters.

2.2.2 Analytical methods for preservatives determination

Instrumental separation techniques have been employed to detect the preservatives, including capillary electrophoresis (CE) [54-56], gas chromatography (GC) [57-59], and high-performance liquid chromatography (HPLC). These techniques are typically used in various samples such as food, cosmetic, and pharmaceutical products as shown in Table 4. Although HPLC is accurate and high precision, expensive instruments, skilled operators, and sample preparation processes are still required.

Table 4 *Determination of preservatives by HPLC*

Sample	Analyte	LOD	Precision (%RSD)	Total analysis time[a] (min)	Reference
Food	Benzoic acid, sorbic acid, dehydroacetic acid	10 ppm	0.7-8.4	30	[11]
	Parabens	5 ppm			
Pharmaceutical dosage form	PHBA	0.0263 ppm	1.4	25	[12]
	Methylparaben	0.0257 ppm	1.5		
	Ethyl paraben	0.0252 ppm	0.5		
	Propylparaben	0.0259 ppm	0.5		
	Butylparaben	0.0259 ppm	0.6		
Cosmetics	Methylparaben	4 ppb	1-11	25	[13]
	Ethyl paraben	3 ppb			
	Propylparaben	5 ppb			
	Butylparaben	2 ppb			

[a]Including sample preparation

The colorimetric method based on UV-visible spectrophotometry was applied for preservative detection with the potential to evaluate preservatives in cosmetics products as shown in Table 5. However, this method has some limitations, such as costly equipment, large number of reagents, and hazardous chemicals.

Table 5 *Determine of preservatives by using UV-visible spectrophotometry of previous works*

Sample	Analyte	Reagent	LOD	Precision (%RSD)	Reference
Pharmaceutical oral solution	Methyl paraben (λ_{max} 442 nm)	*o*-aminobenzoic acid	0.0065 ppm	>1	[60]
Pharmaceutical and cosmetic products	Methyl paraben (λ_{max} 600 nm)	2,4-Dinitrophynel hydrazine	0.34 ppm	0.95	[61]

2.2.3 Enzyme mimicking nanomaterials

To overcome the limitations of the mentioned techniques (in section 2.2.2), peroxidase-mimicking nanomaterials have been utilized and proposed as an alternative for the natural enzyme, particularly horseradish peroxidase (HRP) such as carbon nanomaterials [62], metal oxide nanoparticles [63, 64], and metal complexes [65]. These nanomaterials are cost-effective preparation, biocompatible, and excellent stability [66].

Layered double hydroxides (LDHs) are two-dimensional nanomaterials and are defined as anionic clays that contain brucite-like layers with hydrated interlayer anions species and cations that can be monometallic, two-metal, or three-metal in the body layer [17, 67]. The general formula of LDHs is $[M_{1-x}^{2+}M_x^{3+}(OH)_2]^{x+}(A^{n-})_{x/n}\bullet mH_2O$, where M^{2+} and M^{3+} are divalent and trivalent cations in brucite-like layer and A^{n-} is interlayer anions [67]. The interlayer and

brucite-like layer of LDHs are bonded through a combination of hydrogen bonding and electrostatic forces [67].

LDHs have outstanding characteristics such as large surface area, nontoxicity, excellent stability, and high catalytic capacity [67]. The LDHshave been employed in many works as peroxidase mimics in a variety of fields, particularly colorimetric determination. For example, Zhan *et. al.* (2018) reported that NiFe-layered double hydroxide nanosheets (NiFe-LDHNS) that shows good peroxidase mimic activity for colorimetric determination of glucose and hydrogen peroxide (H_2O_2) in commercial beverage samples by detecting the dark blue product of an oxidized form of 3,3′,5,5′-tetramethylbenzidine (TMB) substrate [68]. Kitayanan *et. al*. (2019) described the colorimetric determination of H_2O_2 with Fe^{II} Fe^{III} layered double hydroxide nanosheets (Fe^{II} Fe^{III} LDHNS) for catalyzing the oxidation reaction of TMB and 2,2'-azino-bis (3-ethylbenzthiazoline-6-sulphonic acid) (ABTS) and detecting the blue and green product that corresponds to the amount of H_2O_2 in local pharmaceutical samples [69].

In previous work, Ni-MnFe-LDHs combined with nitrogen-doped carbon dot (N-CDs/Ni-MnFe-LDHs) as a novel peroxidase-like antibody labels in an immunoassay for low-density lipoprotein detection was developed by Prakobkij *et. al.* [70]. In the presence of H_2O_2 and under optimum conditions, N-CDs/Ni-MnFe-LDHs catalyzed the oxidation of TMB to produce the intense blue product due to the peroxidase-like activity of the metals with high surface area and layered structure of Ni-MnFe-LDHs. Eventually, this proposed method presents the potential of the effective nanomaterial for peroxidase-like activity, which could find application in other reactions as well.

Herein, a fluorometric method for determining preservatives was developed using PHBA and benzoic acid as model analytes. The Ni-MnFe-LDHs was employed as superior peroxidase mimics with *o*-phenylenediamine (OPD) substrate for the first time. The experiment was conducted using 96-well microplates that were

scaled down. Firstly, the oxidation reaction of H_2O_2 to generate •OH was catalyzed by the Ni-MnFe-LDHs. In the absence of the analyte, the produced •OH inducing *o*-phenylenediamine (OPD) to form the fluorescent product of 2,3-diamino phenazine (DAP). High amount of DAP led to high intensity of yellow fluorescence. In the presence of analyte, PHBA or benzoic acid, the produced •OH interacts with PHBA or benzoic acid and converts it into a phenoxy radical leading to a significantly decreased amount of DAP and led to low intensity of yellow fluorescence signal. The smartphone was then used to capture an image and imageJ was used for image processing. The concentration of preservative in sample was calculate via external calibration curve.

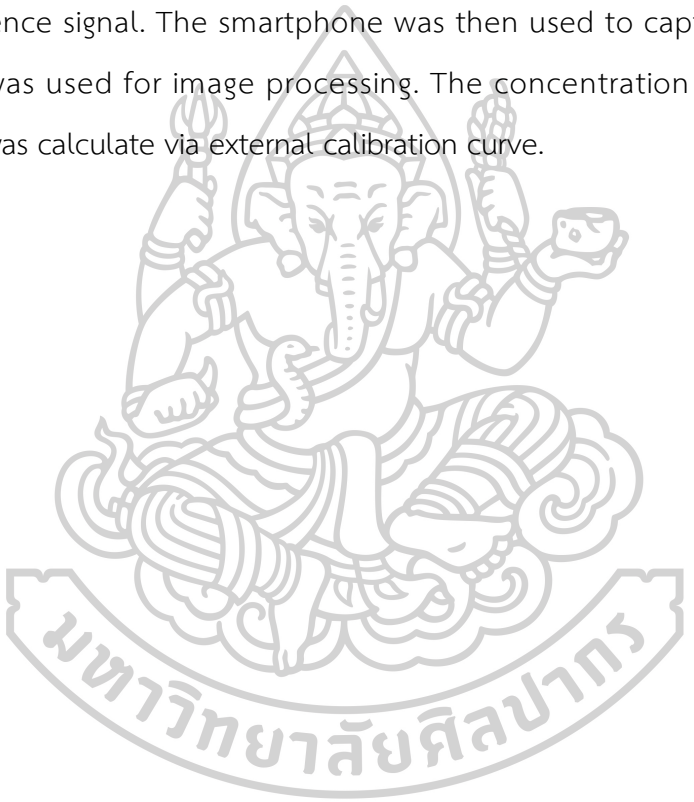

CHAPTER 3

RESEARCH METHODOLOGY

3.1 Research methodology

1) Interviewing and collecting relevant research

2) Examining an experiment

- Investigation and development of the optimum conditions for mercury and preservatives determination
- Application of mercury and preservatives determination in skincare products

3) Results summary and discussion

4) Writing thesis

5) Research presentation and publication

3.2 Material and instruments

Chemical	Manufacturing company	Grade
Citric acid anhydrous 99.5%	Loba chemie, India	Analytical reagent grade
Urea 99.5%	Loba chemie, India	Analytical reagent grade
Mercury (II) acetate	Sigma-Aldrich, USA	Analytical reagent grade
Sodium acetate	Sigma-Aldrich, USA	Analytical reagent grade
Acetic acid	Carlo Erba (Germany)	Analytical reagent grade
Sodium phosphate	Sigma-Aldrich, USA	Analytical reagent grade
4-Hydroxybenzoic acid	Sigma-Aldrich, USA	Analytical reagent grade
Benzoic acid	Riedel, US	Analytical reagent grade
Horseradish peroxidase (164 U/mg)	Sigma-Aldrich, USA	-
Hydrogen peroxide	Merck, Germany	Analytical reagent grade
o-Phenylenediamine (OPD)	Sigma-Aldrich, USA	Analytical reagent grade
Sodium benzoate	BDH chemicals, UAE	Analytical reagent grade
Methyl 4-hydroxybenzoate	Sigma-Aldrich, USA	Analytical reagent grade
Ethyl 4-hydroxybenzoate	Sigma-Aldrich, USA	Analytical reagent grade
Propyl 4-hydroxybenzoate	Sigma-Aldrich, USA	Analytical reagent grade
Salicylic acid	Sigma-Aldrich, USA	Analytical reagent grade
Magnesium chloride hexahydrate	Merck, Germany	Analytical reagent grade

Chemical	Manufacturing company	Grade
L-Ascorbic acid	Loba chemie, India	Analytical reagent grade
Sodium phosphate dibasic	Vivantis, Malaysia	Analytical reagent grade
Sodium citrate tribasic dihydrate	Sigma-Aldrich, USA	Analytical reagent grade

3.3 Determination of mercury

3.3.1 Synthesis of CDs

The CDs were prepared using a microwave-assisted approach according to previous report with slightly modified [35, 38]. Briefly, a 1.00 g of citric acid and 1.00 g of urea were mixed in 10.00 mL of deionized water. The mixture solution was irradiated in a microwave oven (Samsung model MW71B) at 750 W for 5 min until the dark brown suspension of CDs were form. Lastly, the as-synthesized CDs were collected and kept at 4 °C. Before analysis, the as-synthesized CDs were diluted 10 times in deionized water.

Fluorescence quantum yield (QY) of the synthesized CDs was measured by comparative method [71, 72]. Quinine sulfate in 0.1 M H_2SO_4 was used as a standard solution, which was dissolved in deionized water. UV-vis spectrophotometer (Cary 60, Agilent, US) was used to record the absorbance of all the solutions at the excitation wavelength of 360 nm (maintained under 0.05 to minimize self-absorption). Spectrofluorometer (LS-50B, PerkinElmer, US) was used to record the photoluminescence (PL) emission spectra of all the solutions at an excitation wavelength of 360 nm. The UV-vis absorbance and integrated fluorescence intensities of the synthesized CDs was compared with quinine sulfate solution to calculate QY to equation:

$$\varphi_u = \varphi_s \frac{F_u A_s \eta_u^2}{F_s A_u \eta_s^2}$$

where φ is the QY, F is the integrated fluorescence emission intensity, A is the optical density, and η is refractive indexes of the solvent. "s" and "u" correspond to the standard and sample solution.

3.3.2 Characterization of CDs

The synthesized CDs before and after reacting with Hg^{2+} were characterized. X-ray diffractometry (XRD) (Aris, PANalytical, UK), X-ray photoelectron spectroscopy (XPS) (Kratos Axis Ultra spectrometer, UK, with a monochromic Al K_α source at 1486.7 eV), and transmission electron microscopy (TEM) (FETEM/ STEM-EDS, Thermo Scientific Talos F200X STEM, USA) were used to study the structures and morphologies. Fourier-transform infrared spectroscopy (FT-IR) (Frontier, PerkinElmer, USA) was used to determine the functional group on the surface of standard mercury (II) acetate, dried CDs, and dried Hg-CDs. UV-vis spectrophotometer (Cary 60, Agilent, USA) was used to study UV-visible absorption spectra and spectrofluorometer (LS 55, PerkinElmer, USA) was used to study the fluorescence spectra.

3.3.3 SIA procedure

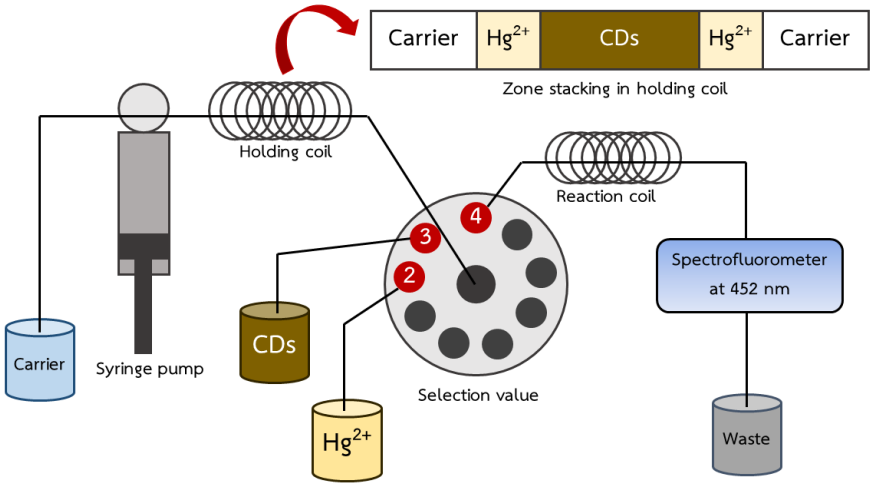

Figure 1 *SIA manifold in this work*

The SIA manifold is illustrated as in Figure 1. It is composed of a selection valve (Cavro Smart Valve, Switzerland) and 5 mL zero-dead-volume syringe pump (Cavro XLP 6000, Switzerland) that was fitted with a holding coil. The C# software, operating within the MS Windows environment, was employed to the programmable pump and valve using an RS-232 communication port, automatically. There are five steps in the typical sequential injection procedure for one cycle, as shown in Table 6. First, a 3000 µL carrier was aspirated with a flow rate of 10 mL/min. Then, at a flow rate of 10 mL/min, the system sequentially aspirated two 100 µL segments of standard or sample (port 2) partitioned with a 300 µL segment of the diluted CDs solution (port 3) into a holding coil, which is the sandwich pattern. Zone stacking was then continually delivered to a reaction coil (PTFE, 0.75 mm, 100 cm). and directly flushed to the detection cell through port 4 at a flow rate of 2.5 mL/min. The fluorescence intensity was measured at excitation and emission wavelengths of 360 and 452 nm, respectively. The fluorescence intensity decreased corresponding to the Hg^{2+} concentration.

Table 6 *Sequential injection procedure in this work*

Step	Event	Flow direction	Flow rate (mL/min)	Volume (mL)
1	Aspiration of carrier	Reverse	10	3.0
2	Aspiration of standard/sample zone segment 1	Reverse	10	0.1
3	Aspiration of reagent zone	Reverse	10	0.3
4	Aspiration of standard/sample zone segment 2	Reverse	10	0.1
5	Sent to spectrofluorometer	Forward	2.5	3.5

3.3.4 Sample analysis

This work aimed to determine the amount of Hg^{2+} in skincare products. The skincare sample in different formulations, particularly whitening cream, were purchased from the online market, local cosmetic shops, and supermarkets in Nakhon Pathom, Thailand. To prepare the sample, an exact weight of 0.1 g of the sample was dissolved in 0.50 mL of 5% (v/v) HNO_3 and the volume was made to 25 mL in a volumetric flask with 0.1 M acetate buffer at pH 7.0.

3.3.5 Method validation

In this work, ICP-MS (7900 ICP-MS, Agilent, USA), was employed as a reference method to validate the proposed mercury analysis with a detection limit of mercury of 0.001 mg/L. Microwave digestion was used for sample preparation. The exact weight of 0.20 g of each sample was added into the microwave vessel and was digested in digestion reagents, which are 9.00 mL of nitric acid (conc. 65%, w/w) and hydrogen peroxide (conc. 30% w/w), for 50 min. After digestion step, the sample solution was transferred into a volumetric flask and the final volume was adjusted to 100.00 mL with deionized water.

3.4 Determination of preservatives

3.4.1 Synthesis of Ni-MnFe-LDHs

The Ni-MnFe-LDHs were synthesized by using a co-precipitation method as previously reported by Prakobkij. *et. al.* [70]. A 0.30 M of $MnSO_4 \bullet H_2O$, 0.10 M $Fe_2(SO_4)_3$, and 0.03 M of $NiSO_4 \bullet 6H_2O$ in 25.0 mL of deionized water were mixed and stirred until a clear solution was obtained. Next, pH of the mixed solution was adjusted to 11 by adding 25.0 mL of 0.60 M NaOH. The yellow-brown precipitate obtained was stirred at room temperature for 1 hour and left at 70 °C overnight in order to completely precipitate. The process was followed by washing with DI water for three times to remove the excess soluble ions and adjust the pH of the filtrate down to 7. Then, the washed precipitate was dried in an oven for 3 hour at

60°C in order to receive the Ni-MnFe-LDHs. Before analysis, the Ni-MnFe-LDHs were dissolved in 60% ethanol-DI water.

3.4.2 Characterization of Ni-MnFe-LDHs

The synthesized Ni-MnFe-LDHs were fully characterized previously reported by Prakobkij. *et. al.* [70]. Zetasizer Nano ZS (Malvern Panalytical, Malvern, UK) was used for zeta potential analysis. X-ray diffractometry (XRD) (X' Pert, Malvern Panalytical, UK) was used for crystalline identification. X-ray photoelectron spectroscopy (XPS) (AXIS Ultra DLD, Kratos Analytical, UK), transmission electron microscopy (TEM) (FETEM/ STEM-EDS, Thermo Scientific Talos F200X STEM, USA), and field emission scanning electron microscope coupled with energy-dispersive spectrometer (FESEM-EDS) (JSM-7610FPlus, JEOL, Japan) with a copper stub with specimens platinum coated were used to study the structures and morphologies. Fourier-transform infrared spectroscopy (Nicolet 6700, Thermo Scientific, USA) was used to determine the functional group on the surface of Ni-MnFe-LDHs.

3.4.3 Fluorometric procedure for determination of preservatives

The fluorometric procedure for determination of preservatives showns in Figure 2. First, 96-well EIA/RIA polystyrene plate (Costar, Corning Incorporated, US) was filled with 15 µL of 500 mM H_2O_2, 25 µL of 200 ppm Ni-MnFe-LDHs, standard or sample solution, and citrate phosphate buffer pH 6 to make the final volume of 100 µL. This mixture solution was then allowed to incubate for 10 minutes at room temperature. After that, 10 µL of a 50 mM OPD substrate was added and mixed, the reaction was left for 20 minutes and the yellow fluorescence product was occurred. An image of the fluorescence product in 96 well plate was taken by a smartphone (Mi 10T Pro, Xiaomi, China) inside a UV-controlled lightbox (using a 365 nm UV lamp) [73]. The captured image was then examined using the ImageJ program (https://imagej.net/Downloads). Grey intensity of red channel of standard (R_s) and blank (R_0) was recorded. The calibration curve was plotted using

the difference between R_0 and R_s (R_0-R_s) as the y-axis and the preservative concentration as the x-axis.

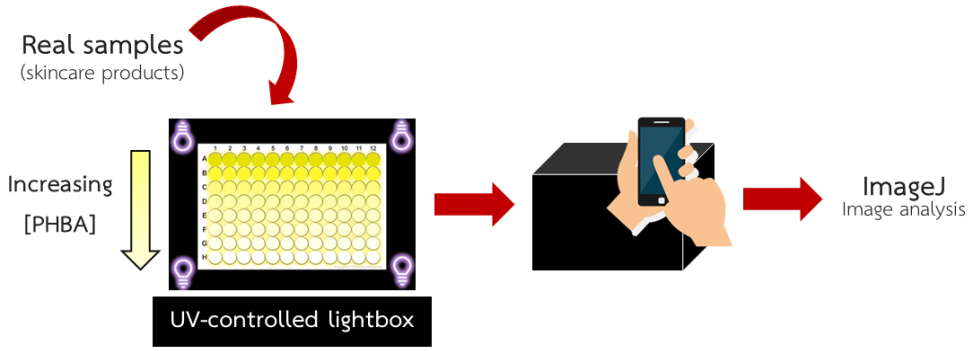

Figure 2 *Fluorometric procedure for determination of preservative in this work*

3.4.4 Enzyme kinetic study

The Michaelis–Menten kinetics was employed to determine the enzyme kinetic study of the Ni-MnFe-LDHs, functioning as an enzyme mimic, following to equation (1) [74] under the optimum concentration of Ni-MnFe-LDHs and fix the concentration of OPD substate. Next, the enzyme kinetic study was investigated by fixing the concentration of Ni-MnFe-LDHs at 75 ppm, fixing the concentrations H_2O_2 at 75 mM, and varying the OPD concentration. The molar absorption coefficient of 16,700 M^{-1} cm^{-1} [75] was used to calculate the oxidized OPD (yellow color) with observing absorbance at 417 nm using a UV-visible spectrophotometer. The Michaelis-Menten parameters, K_M (which stands for the enzyme's affinity) and V_{max} (which stands for the reaction's maximum rate), were calculated from the Lineweaver-Burk plot according to equation (2) [74].

$$V_0 = \left(\frac{V_{max}[S]}{K_M}\right) + [S] \qquad (1)$$

$$\frac{1}{V} = \left(\frac{K_M}{V_{max}}\right) \times \left(\frac{1}{[S] + K_M}\right) \qquad (2)$$

3.4.5 Sample analysis

In this work, we would like to detect the preservatives in skincare products in various formulations, including cleansing wipes, face toner, face serum, and sleeping mask. All samples were purchased from the local cosmetic shop and supermarket in Ubon Ratchathani, Thailand. For clear liquid sample, 2.50 mL were diluted in DI water. For cream samples, 1.00 g of were dissolved in DI water and further sonicated for 2 min. The samples were made up to 25.00 mL using DI water in a volumetric flask.

3.4.6 Method validation

In this work, HPLC-DAD (SHiMADZU, Nexera LC-40 series, USA), with guard column C-18 (4.0 × 10 mm, 5 µm, InertSustain) and analytical column C-18 (4.6 × 250 mm, 5 µm, InertSil), was employed as a reference method in order to compare the sample analysis results. For sample preparation, the clear samples were diluted in DI water and the high viscosity samples were dissolved in DI water and sonicated for 2 min. The final volume of the samples was made to 50 mL in a volumetric flask with DI water.

CHAPTER 4

RESULTS AND DISCUSSION

4.1 Determination of mercury

4.1.1 Characterization of CDs

The concentration of synthesized CDs was investigated by dropping 100 µL of the as-prepared CD solution on the glass slide and evaporating at 60°C for 24 h. Exact weight was recorded. The concentration was found to be 2.7 ± 0.6 mg/mL (n=3). The calculated QY of the synthesized CDs is 0.16% attributed to the low energy transfer of large untreated CDs. However, this QY value is enough for our application.

The optimum concentration of the CDs solution as a reagent in the SIA system was examined by dilution to 0.54, 0.27, and 0.14 mg/mL. The concentration of 0.27 mg/mL demonstrated the best sensitivity. Hence, the stock synthesized CDs solution was diluted 10 times with DI water to obtain the clear CDs solution and used as a reagent for determination of mercury ion in SIA system.

The stability of CDs was investigated by observing the fluorescence intensity and sensitivity obtained from the SIA operation. The result shows indicate that both sensitivity of synthesized CDs and sensitivity of this system remained stable a period of 3 months after preparation.

Next, the precision of CDs synthesis was also studied by measuring the emission fluorescence intensity at 452 nm of each batch and the inter-batch precision was reported to be 2.9% RSD (n = 3).

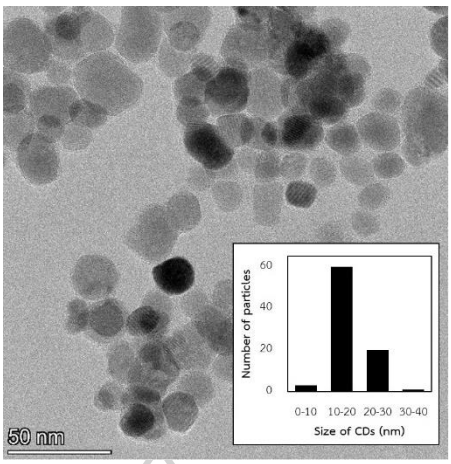

Figure 3 *TEM image of CDs and inset picture shows size distribution of CDs*

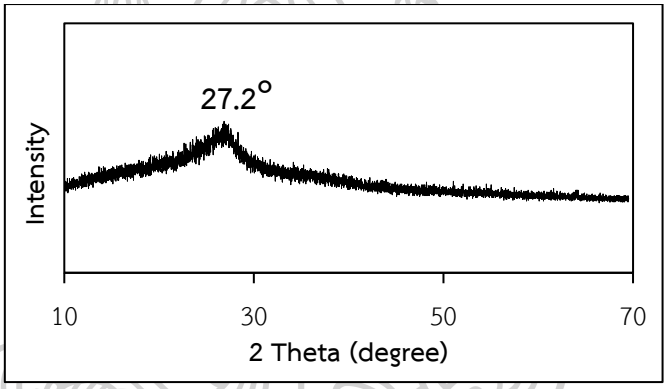

Figure 4 *XRD patterns of CDs*

The morphology of the untreated CDs was studied by TEM. TEM image in Figure 3 shows consistent distribution with spherical shape of the nanoparticles and 71% of size distribution is in the range of 10-20 nm as shown in the inset of Figure 3. The mean size of CDs was 14.7 ± 4.8 nm (by analyzing random particles), and we found the small number of bigger size particles due to the agglomeration of smaller particles.

Next, XRD patterns of the CDs were determined in the range from 10 to 70° as shown in Figure 4. The result shows a broad diffraction peak at 27.2° implying the (002) plane of graphitic carbon [76, 77] that indicates the amorphous structure of the as-prepared CDs.

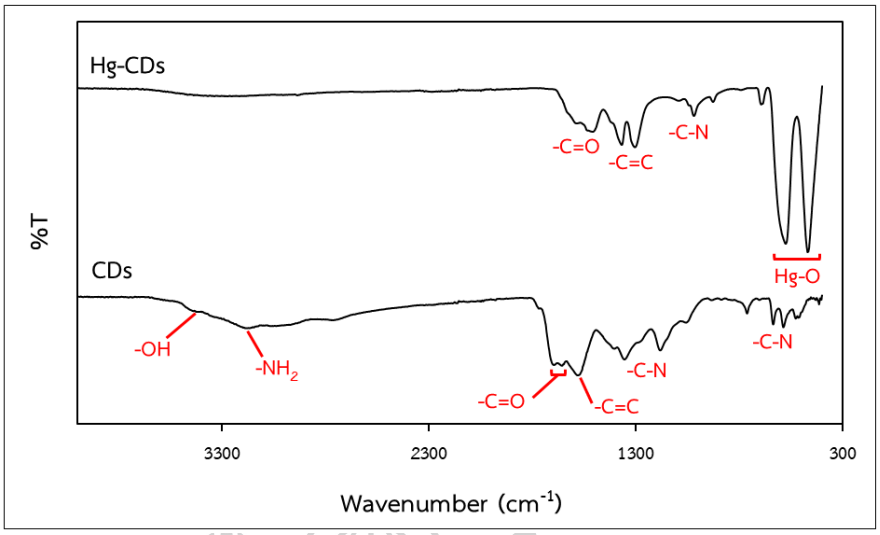

Figure 5 *FT-IR spectra of CDs and Hg-CDs*

In order to investigate the functional groups on the surface of nanomaterials, the synthesized CDs and Hg-CDs were dried and characterized by FT-IR. The results show in Figure 5. A broad peak that measured approximately 3420 cm^{-1} exhibited indications of OH stretching. The absorption bands at 3177 cm^{-1} were related to NH_2 group that typically found on the surface of CDs [71]. The typical peaks of the C=O stretching vibration, which are commonly found in CDs, are exhibited in 1701 and 1661 cm^{-1}. The C=C and C–N stretching vibrations were attributed to the 1576 and 1350 cm^{-1} peaks [78, 79]. For the dried Hg-CDs, two peaks of 400–600 cm^{-1} were found. The characteristic peaks at 576 and 468 cm^{-1} were identified as Hg-O in vibrational mode based on our reviews in previous reports, confirming the formation of Hg-O on the surface of Hg-CDs [80]. In addition, the broad peaks of -OH and $-NH_2$ as well as the peaks of C=O were shifted, and their intensities were decreased.

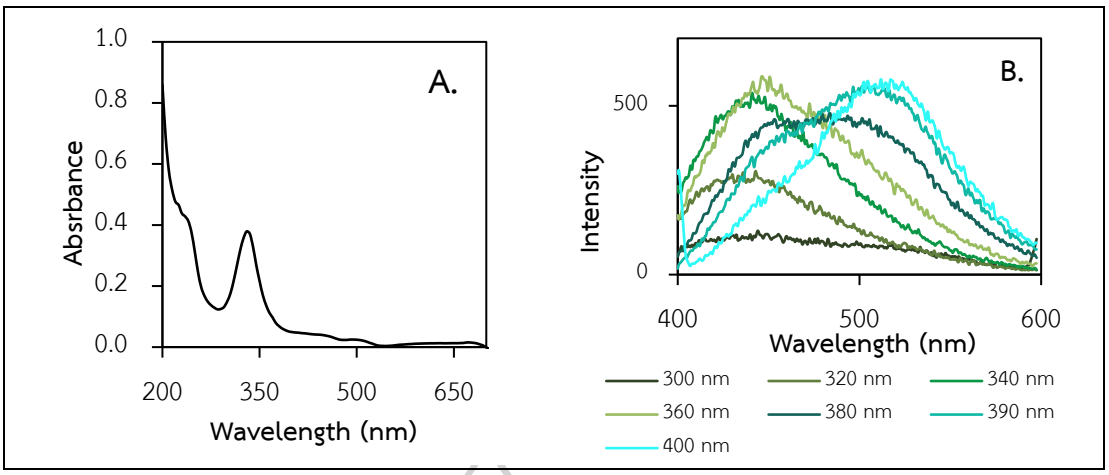

Figure 6 *UV-vis spectrum (A.) and fluorescence emission spectra (B.) of the CDs*

Next, Figure 6A shows the UV-vis spectrum of the CDs solution. From the result, absorption bands were mainly found at approximately 220, 260, and 340 nm. These bands correspond to the carbon-carbon double bond's $\pi \longrightarrow \pi^*$ and the aromatic ring's $\pi \longrightarrow \pi^*$ transitions. Moreover, according to the absorption peak of 340 nm, the C=C functional group of graphitic structure is present during the carbonization process [81, 82]. In Figure 6B, the CDs solution were excited at 360 nm, there was a noticeably strong fluorescence emission at 452 nm. With a shift in excitation wavelength from 300 to 400 nm, the highest fluorescence peak shifted from 420 to 530 nm.

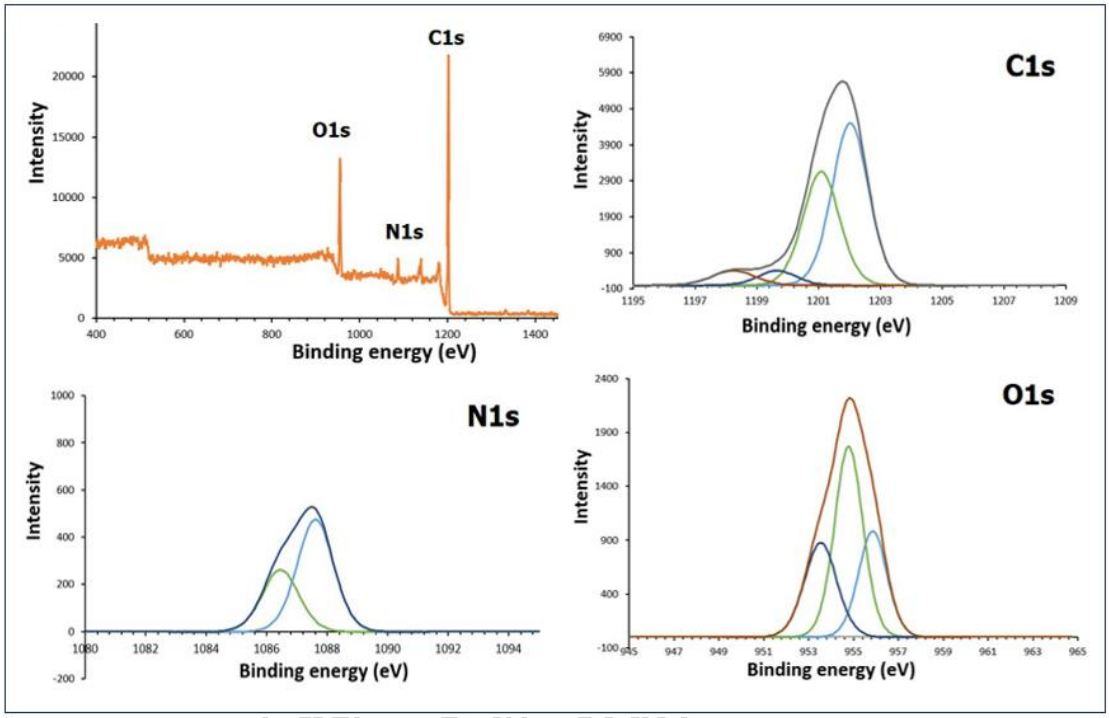

Figure 7 *XPS spectra of CDs*

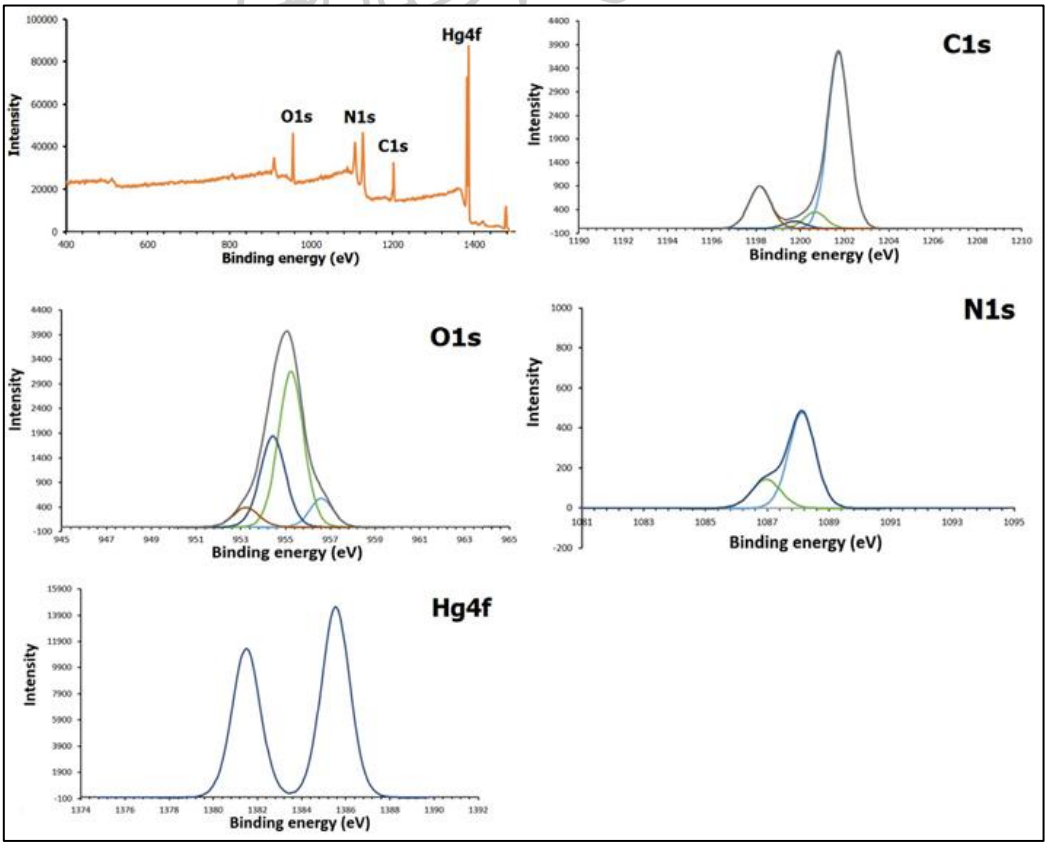

Figure 8 *XPS spectra of Hg-CDs*

Lastly, the elemental compositions of CDs and Hg-CDs were also examined by using the XPS [38, 82, 83]. Figure 7 and 8 show the high-resolution XPS spectra of C (1s), N (1s), O (1s), and Hg (4f) of CDs and Hg-CDs. The survey scan spectrum of CDs exhibited three apparent binding peaks implying the O (1s), N (1s), and C (1s) as shown in Figure 7. The C (1s) spectrum shows four peaks at 284.64, 285.59, 287.05, and 288.44 eV, which correspond to C=C (sp^2), C-N, C-OH/C-O-C, and C=O groups [84]. The N (1s) spectrum shows two peaks at 399.07 and 400.22 eV, implying C-NH_2 and O=N-C functional groups. The O (1s) spectrum shows three peaks at 530.84, 531.91, and 533.14 eV, corresponding to the -C-O/-N-O, -C=O, and C-O-C groups [39, 85]. The XPS results supported the FT-IR results that there are -NH_2, -COOH, and -OH functional groups on the surface of CDs. Next, the survey scan spectrum shows that Hg-CDs are composed of O, N, C, and Hg elements as shown in Figure 8. The C (1s) spectrum shows four peaks at 284.94, 286.03, 286.96, and 288.52 eV, corresponding to the C=C (sp^2), C-N, O-C=O, and C=O functional groups [84]. The N (1s) spectrum shows two peaks at 398.56 and 399.74 eV, which correspond to the amine group (C-NH_2 and O=N-C). The O (1s) spectrum shows four peaks at 530.09, 531.47, 532.28, and 533.47 eV, indicating to -C-O/-N-O, -C=O, C-OH, and C-O-C groups [39, 83, 85]. The Hg (4f) spectrum shows two peaks of 4f 5/2 and 4f 7/2 at 105.18 and 101.13 eV [40]. The results demonstrated that mercury ions were adsorbed on CDs via oxygen-containing functional groups and amine groups [40, 83].

4.1.2 Determination of mercury using the batch method

To analyze the fluorescence quenching of CDs, Figure 9 and 10 show images of the untreated CDs and the products after reacting with Hg^{2+} under visible (Figure 9A) and UV light (Figure 9B) that is simple to notice the intense photoluminescence of the bright blue color with naked eyes.

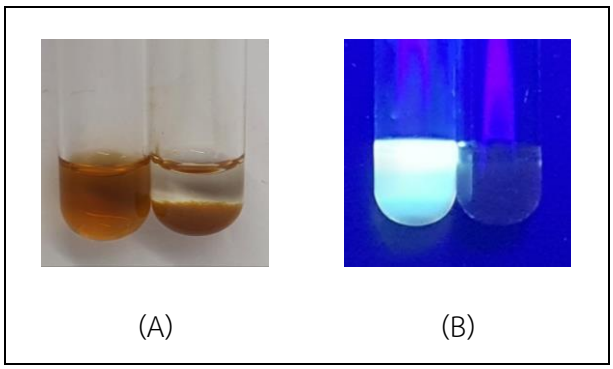

Figure 9 *Untreated CDs and the products after reacting with* Hg^{2+}

(A) under visible light

(B) under UV light (365 nm)

Then, a 100 µL of the diluted CDs and 3.00 mL of DI water were added into a quartz cuvette. This mixed solution was recorded for fluorescence intensity of CDs and denoted as a blank. Next, the standard solution of 0-100 µL of 1000 ppm Hg^{2+} was added and mixed by shaking the cuvette. Then, after adding Hg^{2+} to the CDs solution, the Hg-CD aggregation was occurred. As a result, fluorescence intensity of the CDs rapidly disappears. The presence of the Hg^{2+} promotes the aggregation of CDs and the color of solution changes from pale yellow to colorless. However, UV-visible absorption of CDs and CDs after adding Hg^{2+} is less sensitive and cannot be applied for quantitative analysis of Hg^{2+} in the samples.

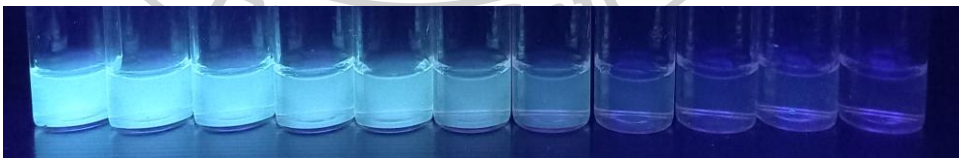

Figure 10 *CDs solution with adding of* Hg^{2+} *at various concentrations under the UV light*

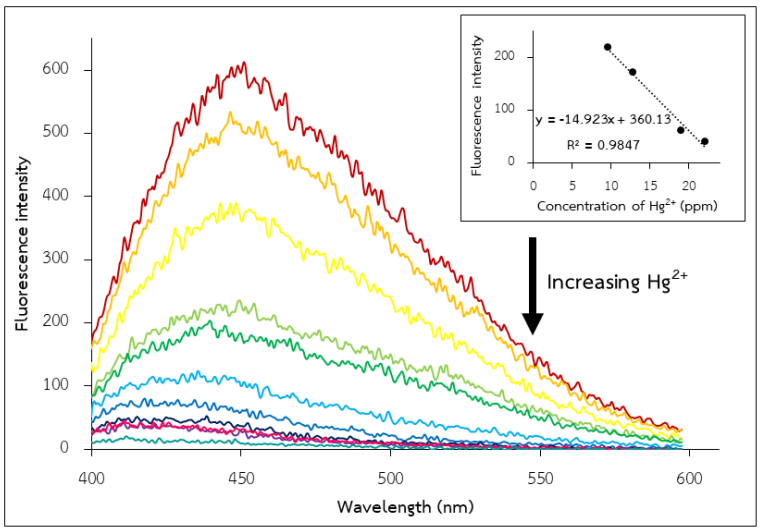

Figure 11 *Fluorescence emission spectra of the CDs solution with adding of* Hg^{2+} *at various concentrations and inset picture shows obtained linear calibration curve*

Hence, photoluminescence was then used to quantitative analysis instead of UV-visible absorption. The measurement was performed at the maximum emission peak at 452 nm and excitation at 365 nm. Figure 10 and 11 show that the fluorescence intensity gradually reduced as the Hg^{2+} concentration increased due to the formation of non-luminescent Hg-CDs aggregation. The fluorescence intensity of CDs was immediately quenched. A linear calibration curve was obtained as shown in the inset picture in Figure 11, indicating that the untreated CDs could be used for quantitative analysis of Hg^{2+}. The interaction between CDs and Hg^{2+} could be caused by a coordinate of Hg^{2+} and carboxyl and hydroxyl groups on the surface of the CDs via charge transfer, leading to the fluorescence quenching of the CDs [37, 86-88].

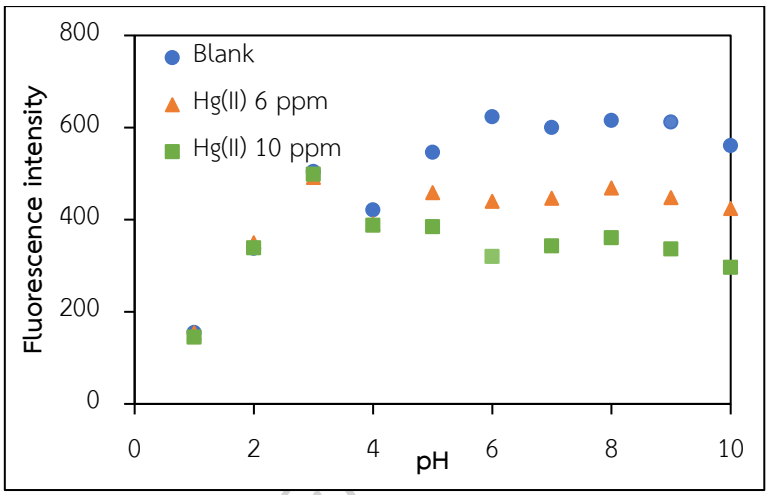

Figure 12 *Effect of pH on fluorescence intensity of CDs*

After that, the effect of pH on fluorescence intensity of CDs and Hg-CD was studied. It should be noted that the pH influences the intensity of CDs fluorescence similar to previous works [89]. Figure 13 shows that the fluorescence intensity decreased with decreasing pHof the CDs solution (lower than 5). In acidic system, low quenching efficiency was observed because of the dissociation of the Hg-CDs compound by the protonation of carboxyl group on the CDs surface. When the pH increases, the carboxylic groups on the CDs were deprotonated, therefore the quenching efficiency was higher with lower in fluorescence intensity due to the strengthen of the covalent bond between Hg^{2+} and CDs [38]. In high basic system, mercury hydroxide could precipitate that reduce the Hg-CDs compound. As a result, the pH of the solution was fixed at 7.0. Finally, several solutions at pH 7 were further examined, which are DI water, acetate buffer, and phosphate buffer. The results indicate that acetate buffer at pH 7 shows the best sensitivity.

4.1.3 Optimization of physical parameters of the SIA system

The physical parameters (including sample and reagent volumes, and flow rate) are affected to the performance of the proposed SIA method. The optimization experiment was set as shown in Figure 1. A set of working standard solutions of 0.5-600 ppm Hg^{2+} was used. The optimum condition was selected by considering the sensitivity (slope of calibration curve) and precision (error bar) obtained for each condition.

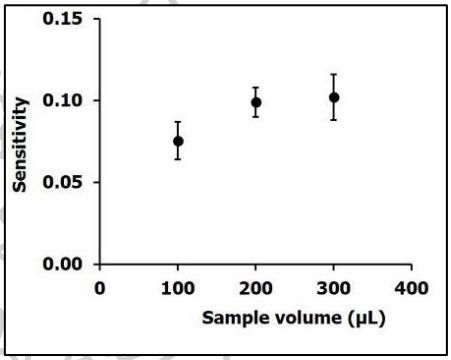

Figure 13 *Sensitivity obtained from calibration curves at various sample volumes*

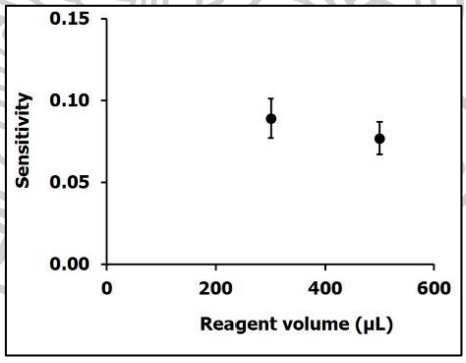

Figure 14 *Sensitivity obtained from calibration curves at various reagent volumes*

First, volume of the sample was studied at 100, 200, and 300 µL and the volume of the reagent was studied at 100, 300, and 500 µL. These parameters were optimized to minimize their amount. Figure 13 shows that 200 µL of the sample (divided in two aliquots of 100 µL intercalated with the reagent aliquot) and 300 µL of the reagent were sufficiently to provide the analytical range with a

satisfied signal as shown in Figure 14. Therefore, the 200 µL of the sample and 300 µL of the CDs reagent were chosen for further experiments.

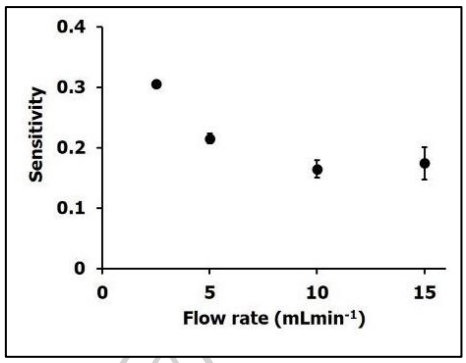

Figure 15 *Sensitivity obtained from calibration curves at various flow rates*

Next, the flow rate was studied at 2.5, 5, 10, and 15 mL/min. Figure 15 shows that the sensitivity decreased with increasing the flow rate. Moreover, sample throughput was not greatly improved, and a large noise was observed at flow rate higher than 10 mL/min. Sample throughput (20 sample/h) is higher when the flow rate was at 2.5 mL/min. Therefore, 2.5 mL/min of flow rate was chosen for the optimum condition in this work.

4.1.4 Interference study

The selectivity of the proposed method was investigated by study the influence of the possible interfering metal ions. Figure 16 is the batch experiment evaluated the fluorescence intensity under the UV light. A 100 µL of diluted CDs, 3.00 mL of DI water, and 80 µL of 100 ppm metal ion were added in a vial, and then, the fluorescence intensity was observed at the emission wavelength of 452 nm and excitation wavelength of 360 nm as shown in Figure 17.

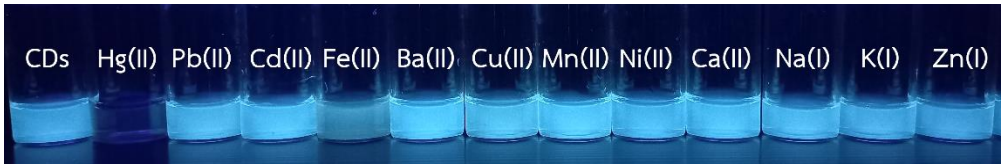

Figure 16 *CDs solution before and after adding of other metal ions*

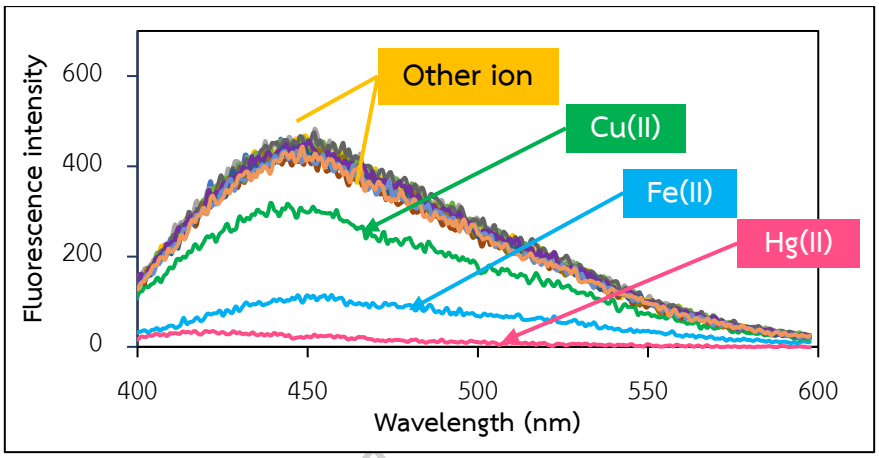

Figure 17 *Fluorescence emission spectra of CDs solution before and after adding of other metal ions*

The effect of interfering metal ions on this proposed SIA system was also examined by injecting 200 µL of 100 ppm for each metal ion solution into the system and used acetate buffer pH 7.0 solution as a carrier. The signal profile and bar graph are shown in Figure 18 and Figure 19.

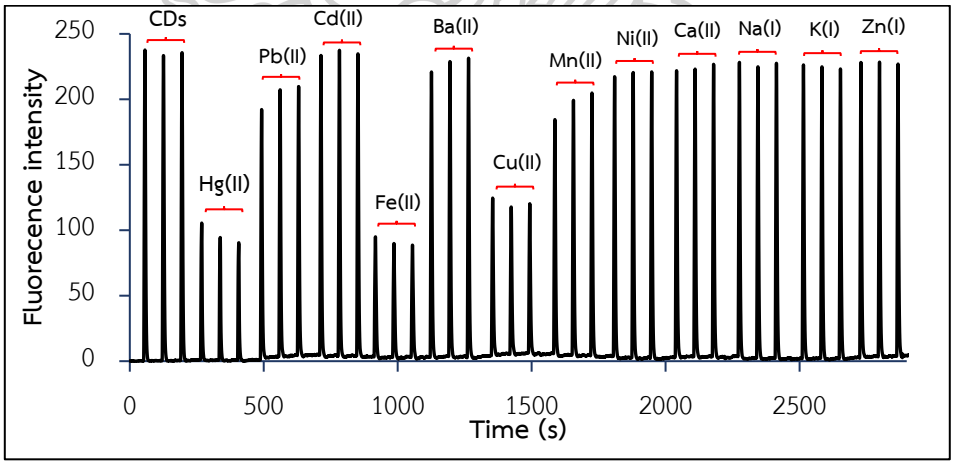

Figure 18 *Signal profile of the effect of interfering metal ions*

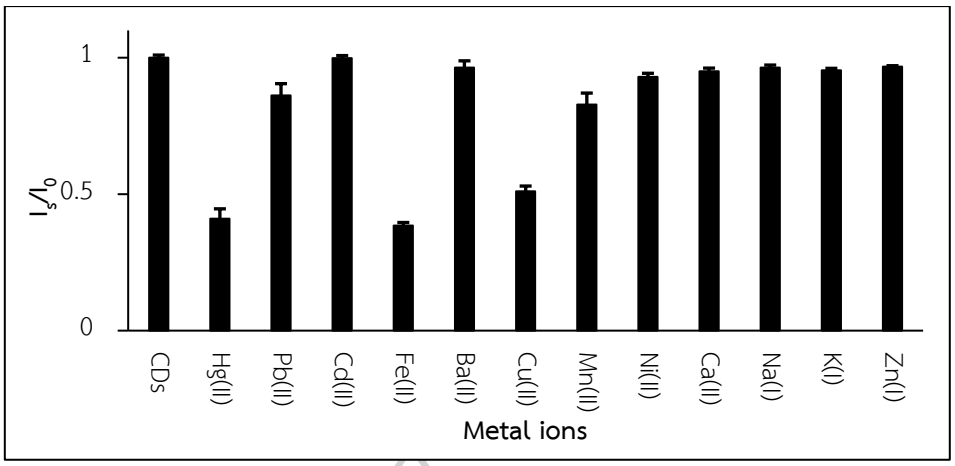

Figure 19 *Bar chart of fluorescence signal ratio of metal ions (I_s) and CDs (I_o)*

From the results, Cd^{2+}, Ba^{2+}, Ni^{2+}, Ca^{2+}, Na^{+}, K^{+} had no effect on the fluorescence intensity, and Zn^{2+}, Pb^{2+}, and Mn^{2+} exhibit slight effect on the fluorescence intensity, which was not significant. This result could be attributed to the higher stability constants between the Hg^{2+} and carboxylic group compared to other metal ions, which result in the production of a Hg-O non-fluorescent metal adduct [40]. In the case of Fe^{2+} and Cu^{2+}, metal hydroxide precipitation may result in reducing the fluorescence intensity and quenching of CDs by Fe^{2+} and Cu^{2+} was also previously reported [41]. Furthermore, 2 and 20 ppm Fe^{2+} and Cu^{2+} were tested to investigate the tolerance of the proposed SIA system. From the results, this method is tolerant of Fe^{2+} and Cu^{2+} at the tested concentrations. These ions, however, are rarely found in tested skincare samples.

4.1.5 Analytical performance

Figure 20 shows the signal profile obtained from the proposed SIA system at varied concentration of $Hg^{2+}$and Figure 21 shows the calibration curve of Hg^{2+}obtained under the optimum condition. The linear relationship between concentration of Hg^{2+} and the difference between fluorescence intensity of blank (I_0) and fluorescence intensity of the sample (I_s) is in the range of 0.5-10 ppm ($y = 0.5359x + 3.9681$) with $R^2 = 0.9965$ and of 10-600 ppm ($y = 0.1339x + 9.257$) with $R^2 = 0.9943$. The proposed method showed standard deviation and relative

standard deviation for Hg^{2+} are 2.30 and 1.53%, respectively (n = 12). Sample throughput of 20 samples per hour implying that our method has good precision and short-time analysis. The limit of detection (LOD) calculated from three times of SD of blank divided by the slope (3 SD/s) was 0.1 ppm which is lower than the maximum amount of mercury allowed in skincare products in Thailand [22] and also the U.S. Food and Drug Administration (FDA) (21 CFR 700.13) has regulations that limit the amount of mercury in eye area products and all other cosmetics not more than 65 and 1 ppm [23]. It should be noted that this proposed method has potential for mercury determination in skincare samples compared to previously reported as shown in Table 2.

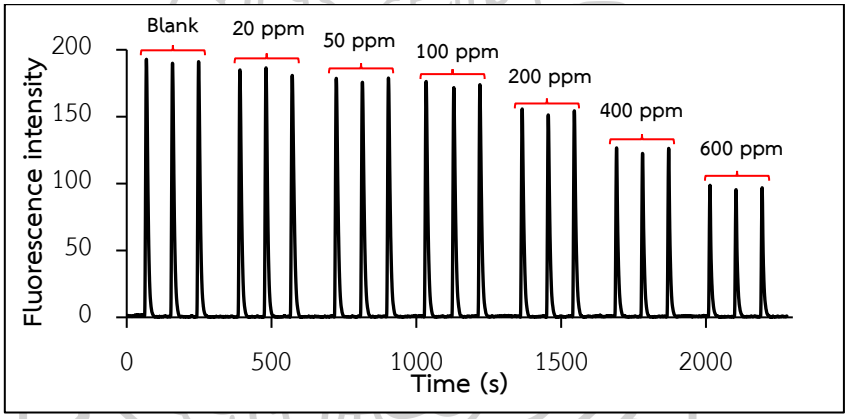

Figure 20 *Signal profile obtained from the proposed SIA system*

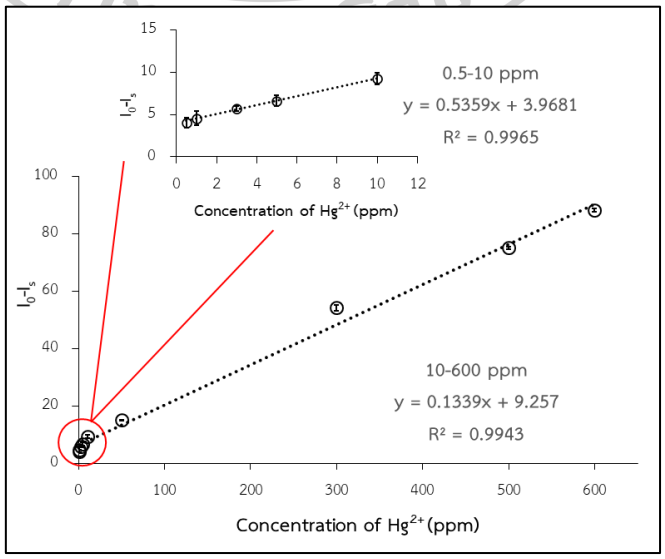

Figure 21 *Calibration curve obtained under the optimum condition*

4.1.6 Sample analysis

The efficacy of this method was assessed for its utility in analyzing Hg^{2+} in skincare samples. However, the results show that none of the samples contained Hg^{2+} (also confirm by ICP-MS). Even though Hg^{2+} was absent from the tested skincare samples. All the samples were spiked with the standard 1 ppm of Hg^{2+} was directly injected into the SIA system to investigate the matrix effect and. The result is shown in Table 7. Sample no. 1-5 were the whitening face serum, no. 6 was the soothing gel, and no. 7-9 were serum lotion. The percentage of recovery was calculated from equation:

$$\%Recovery = \left(\frac{C_{spiked\ std} - C_{sample}}{C_{std}}\right) \times 100$$

where $C_{spiked\ std}$ is the concentration of spiked standard mercury solution, C_{sample} is the concentration of the sample, and C_{std} is the concentration of standard mercury solution.

As a result, %recoveries obtained from the SIA system is 82.4-114% which is acceptable in accordance with AOAC method performance requirements for heavy metal analysis [90].

In addition, the accuracy of the proposed method was verified by triple measurements of the reference solution of Hg^{2+} (Agilent part number 8500-6940-HG), certified as 1.0 ppm [91]. The result showed that the fluorescence intensity measurement Hg^{2+} was 1.01 ± 0.02 ppm indicating that this proposed method has the potential for monitoring hazardous Hg^{2+}.

4.1.7 Method validation

This develop method was validated with reference ICP-MS. All the sample was diluted 100 times before injected into system and then calculated backward. The percentage of recovery was determined using the same formula as mentioned above. (In section 4.1.6) and reported in Table 7. The 1 ppm of standard mercury solution was spiked in the sample solution. By comparing with ICP-MS, although %recoveries obtained from two method show that certain samples had %relative errors carried out at ±5% [92], %recoveries are acceptable accordance with AOAC method performance requirements for heavy metal analysis [90].

Table 7 *Sample analysis and percentage recovery results from proposed method comparison with ICP-MS (n.d. = not detectable)*

Sample	Concentration of Hg^{2+} (ppm)				%relative error[a]
	Proposed method		Reference method (ICP-MS)		
	Found	%recovery	Found	%recovery	
1	n.d.	87.1±2.4	n.d.	101.10	-13.8
2	n.d.	82.4±3.9	n.d.	100.83	-18.3
3	n.d.	86.6±1.0	n.d.	90.77	-4.6
4	n.d.	81.8±6.6	n.d.	98.66	-17.1
5	n.d.	114.0±5.7	n.d.	109.56	4.05
6	n.d.	104.2±3.8	n.d.	105.42	-1.16
7	n.d.	85.2±2.7	n.d.	93.94	-9.30
8	n.d.	88.7±2.9	n.d.	100.60	-11.8
9	n.d.	92.6±3.4	n.d.	105.94	-12.6

[a]%relative error was calculated from [(%recovery of proposed method – %recovery of ICP-MS)/%recovery of ICP-MS] × 100.

4.2 Determination of preservatives

4.2.1 Characterization of Ni-MnFe-LDHs

UV-vis spectrometry, fluorescence spectrometry, FT-IR, FESEM-EDS, TEM, XRD, XPS, and cyclic voltammetry were used to investigate the properties of the synthesized Ni-MnFe-LDHs and previously reported by Prakobkij. *et. al*. [70]. The synthesized Ni-MnFe-LDHs were washed with DI water and centrifuged to remove unwanted particles before morphological and compositional characterization.

LDHs with peroxidase-like catalytic characteristics can be produced by combining nickel (Ni), manganese (Mn), and iron (Fe). This result indicated the potential for applications in this study involving fluorometric detection for preservatives.

4.2.2 Proposed mechanism

In this study, the Ni-MnFe-LDHs was employed as a superior peroxidase-like mimicking and OPD as a fluorescence substrate for the fluorometric detection of preservatives.

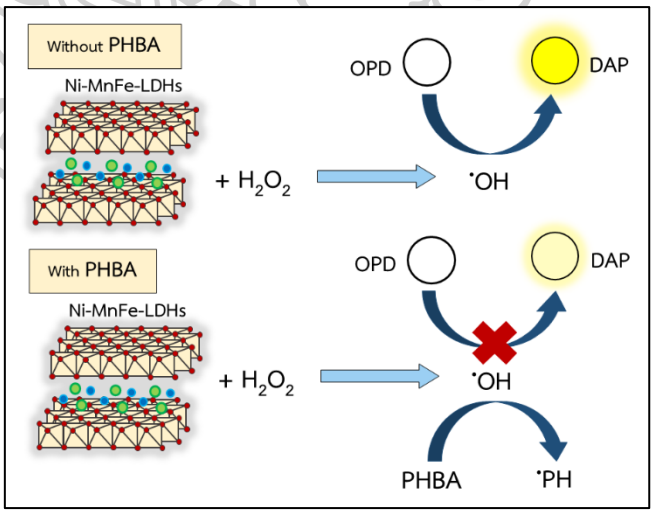

Figure 22 *Proposed mechanism for determination of preservative in this work*

According to Figure 22, the reaction is carried out in two steps. Under optimum conditions, Ni-MnFe-LDHs catalyzed the oxidation of H_2O_2 to form $^{\bullet}OH_{(1)}$ and ^{-}OH following equation (3). The produced $^{\bullet}OH$ was consumed by PHBA or

benzoic acid, which then converted into a phenoxy radical [93]. Based on the structure of PHBA, possible reactions that $^{\bullet}OH_{(1)}$ can react with the hydroxyl group for two routes as shown in Figure 23A. First, the decarboxylation reaction, involving $^{\bullet}OH_{(1)}$, can oxidize the hydroxyl of the carboxyl group [94] to produce phenol, H_2O, CO_2, and $^{\bullet}OH_{(2)}$ according to equation (4). The second route involves the dehydration reaction of phenols by removing the hydroxyl group [95, 96]. Following these reactions, the remaining $\bullet OH_{(1)}$ can then react with OPD, resulting in the production of yellow fluorescence DAP products as described in equation (5).

$$\text{Ni-MnFe-LDHs} + H_2O_2 \longrightarrow {}^{\bullet}OH_{(1)} + {}^{-}OH \quad (3)$$

$$\text{PHBA} + {}^{\bullet}OH_{(1)} \longrightarrow \text{Phenol} + {}^{\bullet}OH_{(2)} + H_2O + CO_2 \quad (4)$$

$$\text{OPD} + {}^{\bullet}OH_{(1)\text{leftover}} \longrightarrow \text{DAP} + H_2O \quad (5)$$

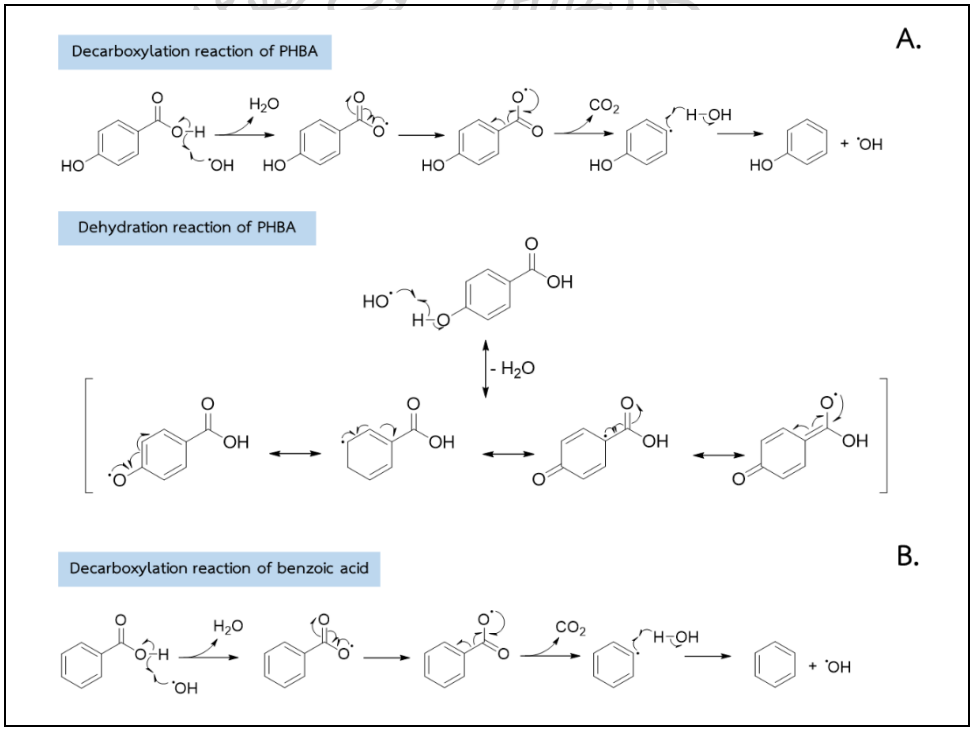

Figure 23 *Proposed mechanism of PHBA (A.) and benzoic acid (B.)*

In the case of benzoic acid, the decarboxylation reaction, also known as oxidation of the carboxyl group by •OH, occurred [94] and the possible mechanism is shown in Figure 23B. Next step is the leftover •OH from the previous step can then interact with OPD to produce yellow fluorescence products. The fluorescence signal decreased in an increase in amount of analyte in the sample.

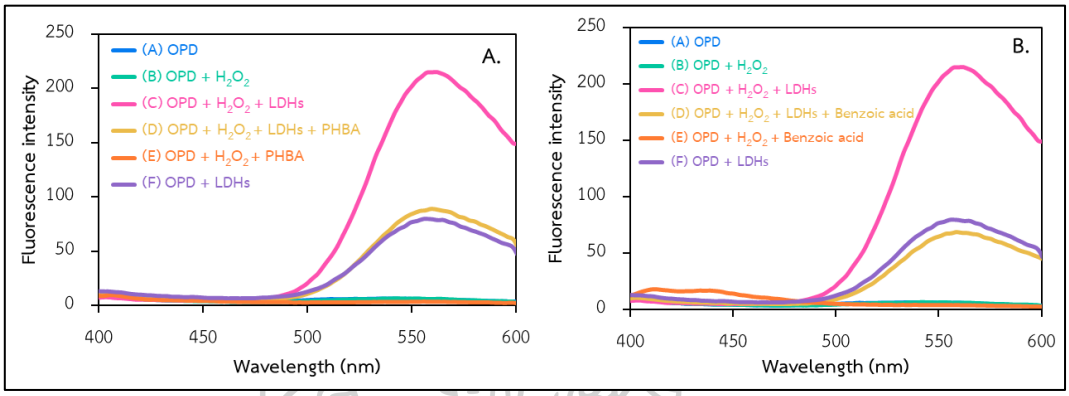

Figure 24 *Fluorescence spectra of catalytic reaction using Ni-MnFe-LDHs and OPD substrate of PHBA (A.) and benzoic acid (B.)*

Using a fluorescence spectrophotometer, the proposed mechanism was examined under the condition of 50 ppm Ni-MnFe-LDHs, 75 mM H_2O_2, 5 mM OPD, 3 mM PHBA, 3 mM benzoic acid, 20 minutes of reaction time, and pH 6. In Figure 24A, condition "C" shows that the fluorescence signal exhibits the highest intensity, indicating that Ni-MnFe-LDHs have the ability to oxidize H_2O_2 to form •OH and oxidize OPD to produce DAP, resulting in a yellow fluorescence product. Under condition "D", in the presence of PHBA, the intensity significantly decreased due to the decreased amount of •OH that could oxidize OPD after being consumed by PHBA, resulting in a phenoxy radical. The outcomes observed in the case of the benzoic acid (as depicted in Figure 24B) agreed with the earlier discussion concerning the PHBA system.

4.2.3 Steady-state kinetic study

The Michaelis-Menten parameters including K_M and V_{max} were evaluated by monitoring the absorbance of the Ni-MnFe-LDHs concentration in the range of 10-100 ppm with parallel studied the reaction time (10 to 130 min). The absorbance increases at the first 10 to 80 min when using 75 and 100 ppm as shown in Figure 25A and the obtained absorbance is not significantly different. From the results, the 75 ppm of Ni-MnFe-LDHs was chosen for the best sensitivity.

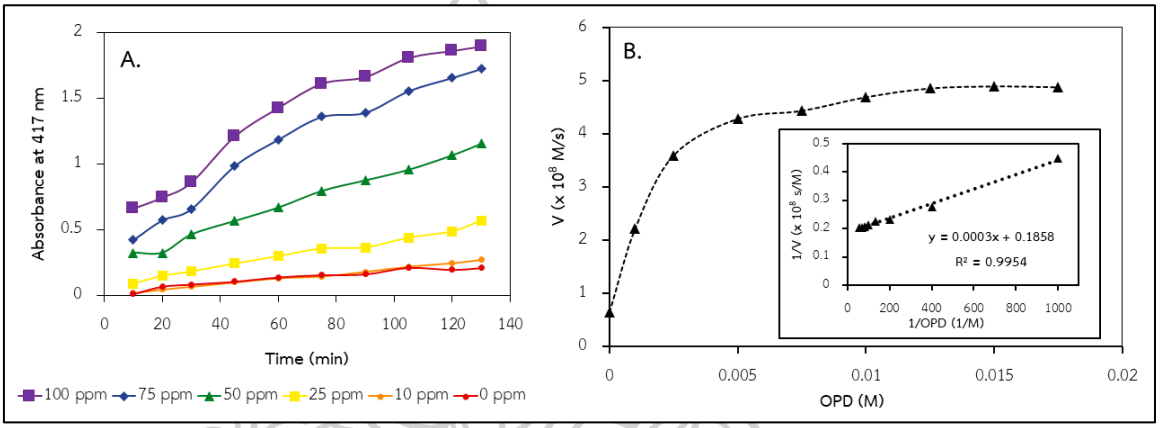

Figure 25 *Kinetic study of Ni-MnFe-LDHs by optimization of Ni-MnFe-LDHs concentration (A.) and observing OPD substrate concentration (B.)*

Next, Lineweaver–Burk plot for the OPD substrate was studied by evaluating the OPD concentration and fixing the Ni-MnFe-LDHs and H_2O_2 concentrations at 75 ppm and 75 mM. The results show in Figure 25B. The calculated K_M and V_{max} are 1.61 mM and 322.93 min^{-1}. Actually, there are no previous reports of OPD as a fluorescence substrate being employed with Ni-MnFe-LDHs.

In Table 8, the calculated K_M and V_{max} were compared to the various peroxidase-like activity in previously reported such as natural peroxidase enzyme [97-101] and hemoglobin [102] with OPD substrate. According to the results, our calculated K_M is lower than that of other catalysts, indicating a high efficiency of peroxidase-like activity in comparison to the previous reports due to the large surface area with the layered structure of Ni-MnFe-LDHs. These accelerated the interaction between Ni-MnFe-LDHs and H_2O_2, resulting in more generated $^{\bullet}OH$ and an increase in the flow of electrons to the OPD substrate, which increased the intensity of the yellow DAP product [67, 70].

Table 8 *Comparison of the Michaelis–Menten parameter of natural peroxidase and Ni-MnFe-LDHs using OPD substrate*

Catalyst	Source	V_{max} (min^{-1})	K_M (mM)	References
Natural peroxidase enzyme	*Ipomoea carnea* (Morning glory)	0.69	2.02	[97]
	Citrus jambhiri (Citrus)	23.25	2.85	[98]
	Triticum aestivum L. (Wheat grass)	Not report	2.9	[103]
	Ficus carica (Common fig)	116.28	3.33	[104]
	Chromolaena odorata (Siam weed)	Not report	9	[105]
Hemoglobin	Hb	1.60	8.75	[102]
	β-cyclodextrin-hemin	0.643	47.2	
	Hemin	0.493	55.9	
Ni-MnFe-LDHs	$MnSO_4 \bullet H_2O$, $Fe_2(SO_4)_3$, and $NiSO_4 \bullet 6H_2O$	322.93	1.61	This work

4.2.4 Optimization study

Some parameters that affect to the performance of this proposed method including chemical parameters (concentration of Ni-MnFe-LDHs, H_2O_2, OPD, and pH system) and physical parameters (camera mode; shutter speed, and ISO), were investigated to achieve the highest sensitivity.

4.2.4.1 Chemical parameters

First, the concentration of Ni-MnFe-LDHs varied at 10, 30, 50, 70, and 100 ppm and fixed 5.0 mM H_2O_2 and 10 mM OPD in 5.0 mM citrate phosphate buffer pH 6.0. The sensitivity increased with increasing Ni-MnFe-LDHs concentrations and reached its maximum at 50 ppm as shown in Figure 26A. There may be more $^{\bullet}OH$ produced due to the oxidation of H_2O_2, retulting in more leftover $^{\bullet}OH$ after the analyte consumed it. This cause high amount of yellow DAP products. At more than 50 ppm, the excess DAP product caused a slight variation in R0 and R value. As a result, 50 ppm of Ni-MnFe-LDHs was chosen as the optimal condition.

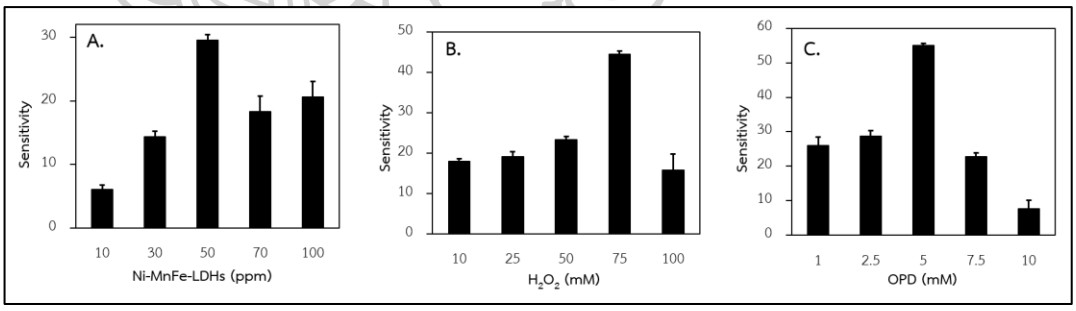

Figure 26 *Optimization of concentration of Ni-MnFe-LDHs (A.), H_2O_2 (B.), and OPD (C.)*

Subsequently, the H_2O_2 concentration was varied at 10, 25, 50, 75, and 100 mM. As depicted in Figure 26B, the sensitivity exhibited a corresponding rise with increasing H_2O_2 concentrations and reached the maximum at 75 mM. This result could be attributed to the increase in the quantity of generated $^{\bullet}OH$ through the oxidation of H_2O_2. When the

concentration of H_2O_2 exceeded 75 ppm, the grey intensity of the red channel did not show any significant difference. This is due to an excess of remaining $^{\bullet}OH$ after analyte consumption. Therefore, the concentration of H_2O_2 was fixed at 75 mM for further experiments.

For best sensitivity, the OPD substrate concentration was studied at 1.0, 2.5, 5.0, 7.5, and 10.0 mM. According to Figure 26C, it can be observed that the sensitivity increases as the concentration of OPD increases and reaches maximum at 5.0 mM. This is due to the increase in the amount of yellow DAP products. However, increasing the OPD concentration higher than 5.0 mM resulted in non significant amount of DAP product, causing the red channel's grey intensity to remain unchanged. Thus, the optimal condition was chosen to be 5.0 mM OPD concentration.

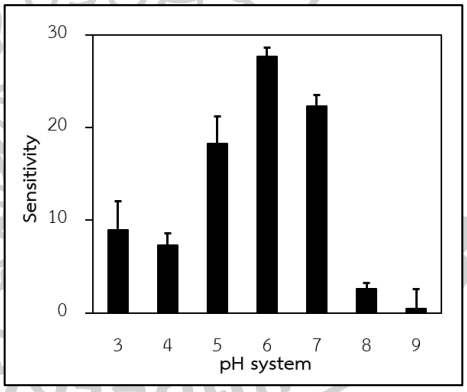

Figure 27 *Optimization of pH system*

Effect of pH range between 4-7 was investigated under the optimum conditions (50 ppm Ni-MnFe-LDHs, 75 mM H_2O_2, 5.0 mM OPD, and 20 minutes of reaction time). The results of this study indicated that the sensitivity increased when the pH system became higher, and maximum at pH 6 as shown in Figure 27. The oxidation of the OPD substrate is more effective in an acidic system (pH 3 to 5) compared to an alkaline system (pH 7 to 9). Additionally, the sensitivity considerably decreased above pH 6 because H_2O_2 can decompose into H_2O and O_2 rather than $^{\bullet}OH$, which

decreased the amount of yellow DAP products [70]. To achieve the best sensitivity, a citrate phosphate buffer with a pH of 6.0 was selected.

4.2.4.2 Physical parameters

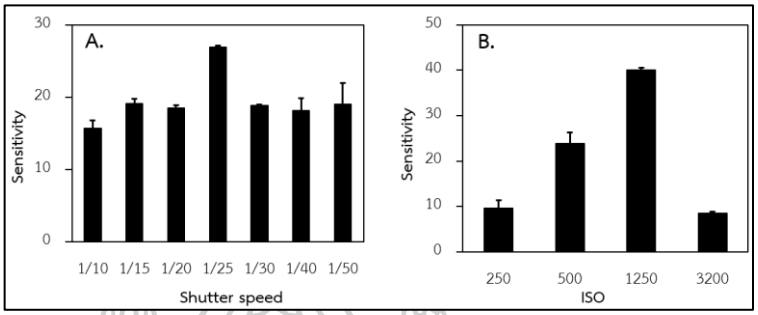

Figure 28 *Optimization of shutter speed (A.) and ISO (B.)*

In the case of camera mode, the shutter speed was studied at 1/10, 1/15, 1/20, 1/25, 1/30, and 1/15 s, while the ISO was studied at 250, 500, 1250, and 3200. As shown by Figure 28A and 28B, the maximum sensitivity can be observed at 1/25 s of shutter speed and 1250 of ISO. Therefore, for the best sensitivity in this work, 1250 of ISO and a shutter speed of 1/25 s were selected.

4.2.5 Interference study

To investigate the selectivity of the proposed method by studying the influence of the possible interfering substances commonly present in skincare products including sodium benzoate, methylparaben, ethylparaben, propylparaben, and other substances (including salicylic acid, $MgCl_2$, and ascorbic acid) in the coexisting system with PHBA (0.40 mM) or benzoic acid (0.40 mM).

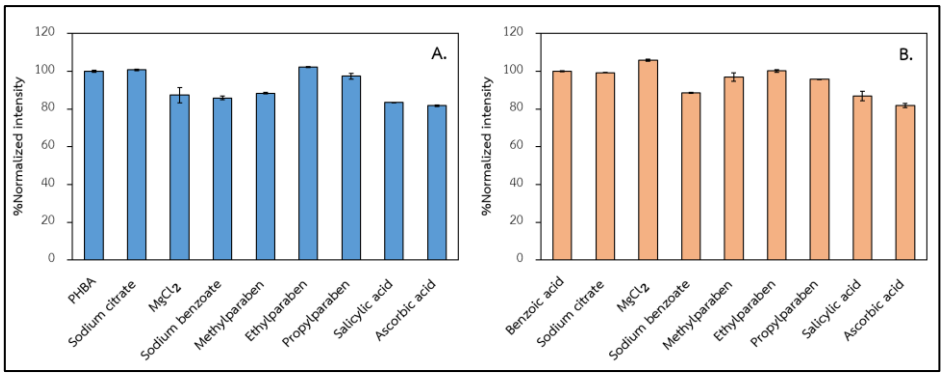

Figure 29 *Bar chart of interferences study of PHBA (A.) and benzoic acid (B.)*

Table 9 presents the concentrations of the tested compounds. The %normalized intensity was calculated from equation:

$$\%normalized\ intensity = \left(\frac{I_f}{I_0}\right) \times 100$$

where I_f is the obtained intensity with interferences, and I_0 is the obtained intensity without interferences. When compared to standard PHBA (Figure 29A) or benzoic acid (Figure 29B), the %normalized intensity changes slightly. According to the AOAC method performance requirements, the tolerance concentration of the possibly interfering substances was set at a range of 80–110% [106].

Table 9 *Tolerance concentrations of the tested compounds*

Testing compound	Tolerance concentration (mM)
Sodium citrate	30
$MgCl_2$	10
Sodium benzoate	60
Methylparaben	40
Ethylparaben	30
Propylparaben	60
Salicylic acid	10
Sodium citrate	30
Sodium benzoate	60
Ascorbic acid	5

4.2.6 Analytical performance

The performance of this suggested technique was examined. Figure 30 shows the obtained calibration curve of PHBA (Figure 30A) and benzoic acid (Figure 30B) under the optimum condition. As the concentration of PHBA or benzoic acid increased, the color of the solution gradually changes from bright orange-yellow to dark purple.

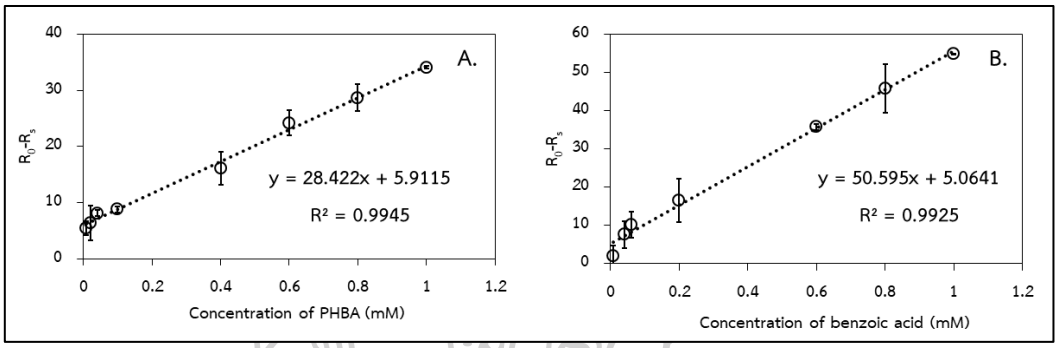

Figure 30 *Calibration curve of PHBA (A.) and benzoic acid (B.) under the optimum condition*

For PHBA determination, the linear association between R_0-R_s intensity and the concentration of PHBA is between 0.008 to 1.0 mM (y = 28.422x + 5.9115, R^2 = 0.9945). The limit of detection (LOD) was calculated from the 3SD of the first concentration in the calibration curve divided by the slope (n=3) and the limit of quantification (LOQ) was calculated from 10SD of the first concentration in the calibration curve divided by the slope (n=3) was 0.0072 and 0.024 mM. For benzoic acid determination, the linear association between R_0- R_s intensity and the concentration of benzoic acid is between 0.008 to 1.0 mM (y = 50.595x + 5.0641, R^2 = 0.9925) and the calculated LOD and LOQ was 0.0042 and 0.014 mM. As a result, the sensitivity of benzoic acid detection is better than PHBA. These might be driven by the structure of benzoic acid, which is more reactive than PHBA and only contains one hydroxyl group for the decarboxylation reaction with $^{\bullet}OH$. Based on these results, we may conclude that this developed method is capable of preservatives detection in skincare samples under the permitted limit of U.S.

FDA [52] and EU Cosmetics Regulation [53]. In addition, it should be noted that this proposed method has potential for preservative determination in skincare samples compared to standard HPLC, as shown in Table 4.

Table 10 *Intra-day and inter-day precision of this proposed method*

Standard concentration (mM)		Intra-day (n=3)		Inter-day (n=3)	
		SD	%RSD	SD	%RSD
PHBA	0.008	0.084	2.30	0.071	1.69
	0.1	0.14	2.06	0.18	2.47
	1.0	0.038	0.17	0.54	2.32
Benzoic acid	0.008	0.11	1.01	0.225	2.10
	0.1	0.29	1.91	0.171	1.12
	1.0	0.46	0.88	0.742	1.39

In addition, the intra-day and inter-day precision were also examined by calculating the percentage of relative standard deviation (%RSD) of the signal (R_0-R) acquired from each concentration of the standard. Table 10 shows that the %RSD values are less than 2.47% (n=3), demonstrating the acceptable reproducibility of the proposed method according to AOAC [106].

4.2.7 Sample analysis

The potential of the developed approach to determine preservatives in skincare products was tested. It should be noted that none of the sample contained PHBA and only cleansing wipes and facial toner contained benzoic acid. Each sample was spiked with the standard PHBA and benzoic acid in 0.20 and 0.60 mM (Each sample was spiked with standard PHBA in 28 and 83 ppm and standard benzoic acid in 24 and 73 ppm). The sample analysis and %recovery results of PHBA and benzoic acid are shown in Table 11 and 12. As a result, %recoveries are acceptable according to AOAC method performance requirements, which is in the range of 80 to 110% [106].

Table 11 *Real sample analysis and percentage of recovery results of PHBA analysis (n.d. = not detectable)*

Samples	Added (mM)	Found ± SD (mM)	%Recovery
Cleansing wipe	0	n.d.	-
	0.2	0.207 ± 0.010	103.5
	0.6	0.658 ± 0.003	109.7
Facial toner	0	n.d.	-
	0.2	0.189 ± 0.012	94.5
	0.6	0.658 ± 0.003	109.7
Facial serum	0	n.d.	-
	0.2	0.217 ± 0.006	108.5
	0.6	0.653 ± 0.014	108.8
Sleeping mask	0	n.d.	-
	0.2	0.200 ± 0.001	96.8
	0.6	0.613 ± 0.001	101.2

Table 12 *Real sample analysis and percentage of recovery results of benzoic acid analysis (n.d. = not detectable)*

Samples	Added (mM)	Found ± SD (mM)	%Recovery
Cleansing wipe	0	0.193 ± 0.007	-
	0.2	0.404 ± 0.042	105.4
	0.6	0.802 ± 0.012	101.5
Facial toner	0	0.024 ± 0.010	-
	0.2	0.241 ± 0.011	108.2
	0.6	0.652 ± 0.180	103.5
Facial serum	0	n.d.	-
	0.2	0.198 ± 0.008	95.8
	0.6	0.608 ± 0.012	100.3
Sleeping mask	0	n.d.	-
	0.2	0.200 ± 0.030	95.7
	0.6	0.585 ± 0.004	96.0

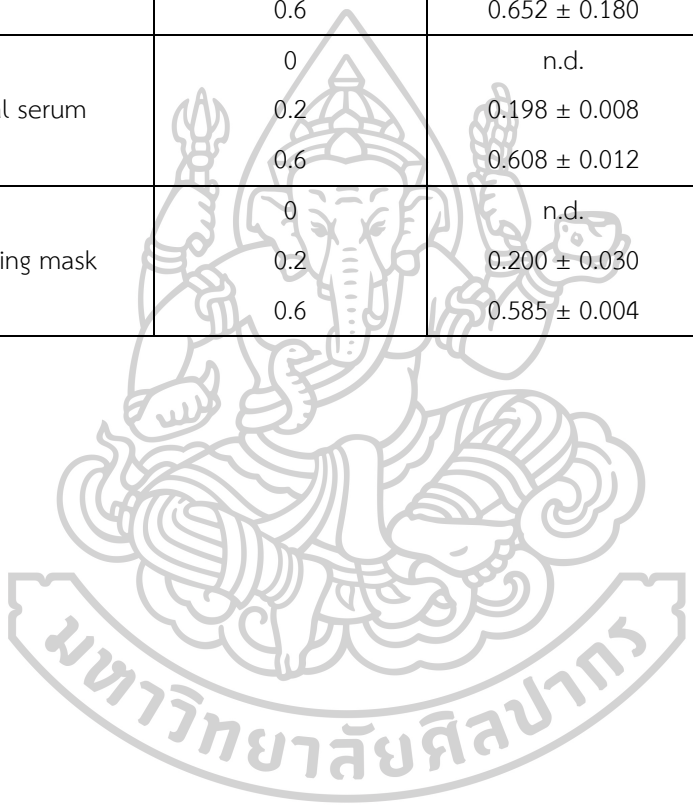

4.2.8 Method validation

To validate the proposed method, HPLC was used as a standard method. Table 12 shows that the determination of benzoic acid in real sample between two methods were acceptable according to Codex recommendations guideline that %relative error is at ± 5% [92]. This result demonstrated the feasibility of the proposed method for analyzing preservatives in real samples.

Table 13 *The determination of benzoic acid in real sample results comparison with standard HPLC method*

Samples	Found ± SD (mM)		%Relative error[a]
	Proposed method	HPLC method	
Cleansing wipe	0.193 ± 0.007	0.189 ± 0.002	+1.82
Facial toner	0.024 ± 0.010	0.025 ± 0.001	-2.56

[a]%relative error was calculated from [(Found of proposed method - Found of HPLC)/ Found of HPLC] × 100.

CHAPTER 5

CONCLUSION

This work aimed to establish quick, low-cost, and highly effective methods for determining the amount of mercury and preservatives in skincare products. It was divided into two main parts; mercury detection based on spectrofluorometric approach coupled SIA system with CDs as a reagent and fluorometric preservative determination utilizing Ni-MnFe-LDHs with OPD substrate.

For the first part, the CDs were easily synthesized by microwave-assisted method and were used as a specific reagent for mercury analysis in this work. The as-prepared CDs have an average size of 14.7 ± 4.8 nm that exhibited good optical properties. This proposed method is based on spectrofluorometric method coupled with SIA system. The fluorescence intensity of CDs was measured, which was quenched after adding mercury. The LOD is low to 0.1 ppm with a wide linear range. There is no significant difference between the proposed method and ICP-MS, with an acceptable percentage recovery of 81.8 - 114. In comparison to ICP-MS, this approach offers less recovery, but it is more convenient and cost-effective. Our approach uses a non-harmful chemical reaction for detection, as well as is simple to prepare CDs without the need for additional purification or modification steps. This work is the first time to develop the SIA system based on CDs for mercury analysis in skincare products and heavy metal ion contamination to achieve a simple, automatic, rapid, and low-cost analysis. This system could be applied for quality control or working for safety and inspection service agencies and developed as a portable device for on-site analysis.

Next, the fluorometric determination based on the peroxidase-like activity of Ni-MnFe-LDHs with OPD substrate was developed for low-cost and rapidly determining preservatives in skincare products. The produced $^{\bullet}OH$ from the decomposition of H_2O_2 was consumed by the target analyte, which are PHBA and

benzoic acid, and the leftover •OH oxidized the OPD into the yellow-fluorescent DAP product. The yellow fluorescence intensity dramatically decreased as the preservative concentration increased. This procedure was carried out on miniaturized 96-well microplates to obtain simultaneous color capturing and reducing the reagent (100 µL/well) for rapid and cost-effective detection. Additionally, the image-capturing step just needed a smartphone under a UV-controlled lightbox. This proposed method exhibited a wide linear range of 0.008 to 1.0 mM for both PHBA and benzoic acid. The detection limit is as low as 0.0072 and 0.0042 mM for PHBA and benzoic acid, making it significant potential for detecting preservatives in real samples. This system showed an acceptable percentage of recovery with no significant differences from the conventional HPLC method. Finally, this developed method is expected to be a pioneering platform for detecting other interesting analytes.

CHAPTER 6

INDEX

6.1 Output: presentation

This work was presented in three international conferences. First conference is the 47th International Congress on Science, Technology, Technology-Based Innovation (STT 47th) at Nakhon Pathom, Thailand in title “Rapid and sensitive method for determination of mercury in pharmaceutical products based on green synthesis of carbon nanodots” on October 5 – 7, 2021. This presentation was received silver prize award in Young Rising Stars of Science 2021 from this conferences.

Second conference is the Pure and Applied Chemistry International Conference 2022 (PACCON2022) at Bangkok, Thailand in title “Charecterization of untreated eco-friendly synthesis carbondots and application for determination of mercury in pharmaceutical products by sequential injection analysis” on June 30 - July 1, 2022.

And third conference is the 4th Materials Research Society of Thailand International Conference (MRS-Thailand 2023) at Ubon Ratchathani, Thailand in title “Fluorometric Determination of Preservatives in Skincare Products using Layered Double Hydroxides as Peroxidase Enzyme Mimicking” on February 28 – March 4, 2023. This presentation was received best poster presentation award.

RAPID AND SENSITIVE METHOD FOR DETERMINATION OF MERCURY IN PHARMACEUTICAL PRODUCTS BASED ON FLUORESCENCE QUENCHING OF GREEN SYNTHESIS CARBON NANODOTS

Kanokwan Sakunrungrit[1], Cheewita Suwanchawalit[1], Kanokwan Charoenkitamorn[1], Apisake Hongwitayakorn[2], Kamil Strzelak[3] and Sumonmarn Chaneam[1,4,*]

[1]Department of Chemistry, Faculty of Science, Silpakorn University, Nakhon Pathom, 73000, Thailand
[2]Department of Computing, Faculty of Science, Silpakorn University, Nakhon Pathom, Thailand
[3]University of Warsaw, Faculty of Chemistry, Pasteura 1, 02-093, Warsaw, Poland
[4]Flow Innovation Research for Science and Technology Laboratories (FIRST Labs), Bangkok, 10400, Thailand
*e-mail: schaneam@gmail.com

Mercury is a highly toxic metal that presents intentionally or accidentally in some treatments of skin conditions, especially whitening products. **ICP-MS** has become one of the most powerful analytical techniques for mercury analysis. However, this method is very cost intensive and requires highly skilled operators which results in the method being expensive. Later, detection of mercury with **spectrofluorometry by ionophore/fluorophore** reagent has been reported. However, the reagent is difficult and multi-step synthesis, hard to predict amount of product and sometimes chemical toxicity. In recent years, **Carbon nanodots (CNDs)** has been replaced to overcome these problems.

OBJECTIVE

The aim of this study was using **CNDs** as a specific reagent for determination of mercury(II) in pharmaceutical products based on spectrofluorometry with a **sequential injection analysis (SIA)** system.

GREEN SYNTHESIS OF CNDs

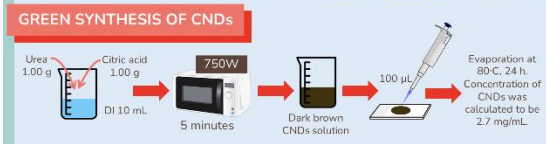

Scheme 1. The environmentally friendly CNDs synthesized by a microwave-assisted

CHARACTERIZATION OF CNDs

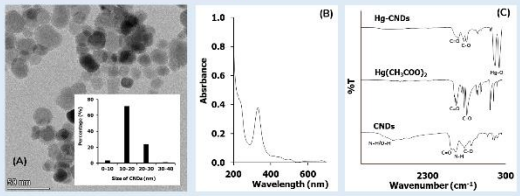

Fig 1. (A) TEM image of CNDs powder inset; Size distribution of CNDs powder, (B) Absorption spectrum of CNDs solution, and (C) FTIR spectra of CNDs, pure $Hg(CH_3COO)_2$, and Hg-CNDs precipitate.

SPECTROFLUOROMETRY: Batch method

The method is based on the measurement of fluorescence intensity of CNDs which was quenched proportionally after adding mercury ion.

After adding mercury(II)acetate to the diluted CNDs 10 times solution, the Hg-CNDs precipitate appears and fluorescence of CNDs solution decrease.

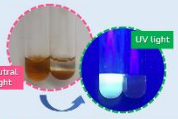

Effect of excitation wavelength

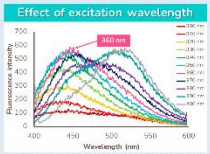

Fig 3. Fluorescence emission spectra of the CNDs solution at different excitation wavelength (300 – 400 nm). Here, excitation wavelength at 380 was selected.

Effect of slit width

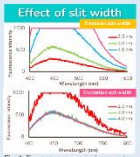

Fig 4. Fluorescence emission spectra of the CNDs solution at different slit width.

Effect of pH

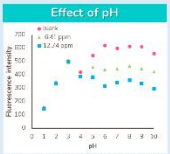

Fig 5. Fluorescence intensity of CNDs solution (blank) and after adding Hg^{2+}. The result show the intensity at pH more than 8 are resemblance. Thus, pH of the medium should be controlled around 6 – 7.

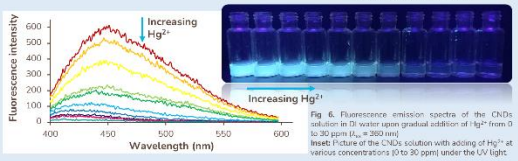

Fig 6. Fluorescence emission spectra of the CNDs solution in DI water upon gradual addition of Hg^{2+} from 0 to 30 ppm (λ_{ex} = 360 nm)
Inset: Picture of the CNDs solution with adding of Hg^{2+} at various concentrations (0 to 30 ppm) under the UV light.

GREEN ANALYSIS OF MERCURY USING THE SIA SYSTEM

The first time that using CNDs as a specific reagent for determination of mercury(II) in pharmaceutical products with a **sequential injection analysis (SIA)** system and the as-prepared CNDs stock solution was diluted 10 times and used as a reagent in SIA system.

SIA manifold

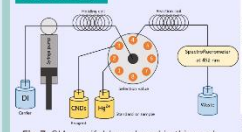

Fig 7. SIA manifold employed in this work

Optimization of SIA parameters

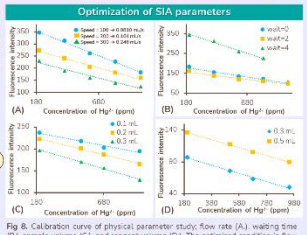

Fig 8. Calibration curve of physical parameter study; flow rate (A), waiting time (B), sample volume (C), and reagent volume (D). The optimized condition is flow rate is 0.164 mL/s, wait time 0 s, volume of reagent and sample is 0.3 and 0.2 mL.

Pattern of zone

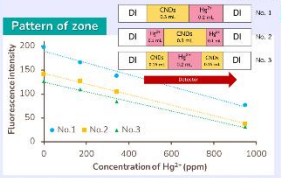

Fig 9. Calibration curves obtained from different zone patterns. Pattern no. 1 is a normal zone pattern. Pattern no. 2 and no. 3 are a sandwich pattern. The sandwich pattern of no. 2 showed the best sensitivity.

Effect of pH of carrier

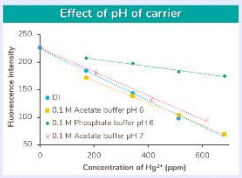

Fig 10. Calibration curves show the effect of pH of carrier. In this work 0.1 M acetate buffer pH 7 was chosen.

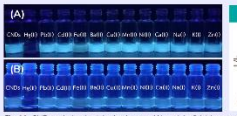

Selectivity test

Fig 11. CNDs solution in deionized water (A) and in 0.1 M acetate buffer pH 7 (B) before and after adding of other metal ions under UV light. (C) Bar chart of fluorescence signal ratio of metal ions (I_0) and CNDs (I_0) in deionized water (pink) and 0.1 M acetate buffer pH 7 (green).

Signal profile and calibration curve

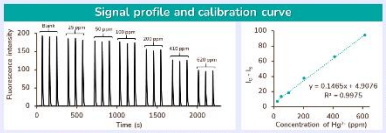

Fig 12. Signal profile (A) and calibration curve (B) obtained from the SIA system with various concentrations of mercury (II) used for determination mercury(II) in sample.

Sample Analysis

Table 1. Validation method by comparison with ICP-MS and percent recovery.

Sample	Hg^{2+} (ppm) Standard method (ICP-MS)	Proposed method	% Recovery
1	ND	ND	84.97
2	ND	ND	84.70
3	ND	ND	109.19
4	ND	ND	84.46
5	ND	ND	82.45

ND: not detectable

Analytical performance

- Linear range : 25 to 620 ppm
- Limit of detection : 4 ppm
- Standard deviation : 2.30 (200 ppm, n=12)
- Relative standard deviation : 1.53% (200 ppm, n=12)
- Sample throughout : 41 samples per hour

CONCLUSIONS

Green synthesis + Green analysis

- ✓ At the optimum condition, linear range between 25 to 620 ppm with R^2 more than 0.99 was obtained and sample analysis result shows acceptable recovery value.
- ✓ This proposed approach is fist time that using CNDs as a reagent in SIA system and expected to be an alternative method for the analysis of mercury in pharmaceutical products and other sample applications.

Acknowledgements

Financial support from Reinventing University System Program by The Ministry of Higher Education, Science, Research and Innovation is gratefully acknowledged. (Fiscal Year 2021)

PACCON KMITL 2022
" Frontiers in Chemical Sciences "
for Health, Energy, and Sustainability
June 30th - July 1st of 2022, KMITL Convention Hall, King Mongkut's Institute of Technology Ladkrabang, Bangkok, Thailand

CHARECTERIZATION OF UNTREATED ECO-FRIENDLY SYNTHESIS CARBONDOTS AND APPLICATION FOR DETERMINATION OF MERCURY IN PHARMACEUTICAL PRODUCTS BY SEQUENTIAL INJECTION ANALYSIS

Kanokwan Sakunrungrit[1], Cheewita Suwanchawalit[1], Kanokwan Charoenkitamorn[1], Apisake Hongwitayakorn[2], Kamil Strzelak[3], and Sumonmarn Chaneam[1,4,*]

[1] Department of Chemistry, Faculty of Science, Silpakorn University, Nakhon Pathom, 73000, Thailand
[2] Department of Computing, Faculty of Science, Silpakorn University, Nakhon Pathom, Thailand
[3] University of Warsaw, Faculty of Chemistry, Pasteura 1, 02-093, Warsaw, Poland
[4] Flow Innovation Research for Science and Technology Laboratories (FIRST Lab), Bangkok, 10400, Thailand
Department of Chemistry, Faculty of Science, Silpakorn University, Nakhon Pathom, 73000, Thailand
(Email: schaneam@gmail.com, +66-0865355053)

Mercury is the one of toxic metal that presents intentionally or accidentally in pharmaceutical products, especially whitening products. It may exert harmful side effects on skin and internal organs. Therefore, many countries, including Thailand, have prohibited the use of mercury in these skin conditions. **This work reports the analysis of mercury(II) using a spectrofluorometric method combining with a sequential injection analysis (SIA) system and measure the fluorescence intensity of carbondots (CDs) which was quenched proportionally after adding mercury(II) ion.** The CDs was environmentally friendly synthesized by a microwave-assisted approach that provide intensive, efficient energy, and shorten reaction time. The as-prepared CDs stock solution was diluted 10 times and used as a reagent. **The properties of CDs were entirely characterized by TEM, XPS, XRD, FTIR, and UV-Vis spectrometry.** Excitation and emission wavelength at 360 nm and 452 nm was used to construct a calibration curve. Physical parameters affected to the SIA performance were optimized.

In addition, effect of pH and other ions were investigated. At the optimum condition, our method showed a linear range between 0.5 to 600 ppm with R^2 of 0.99. Limit of detection was 0.4 ppm, which was enough for the proposed application. Relative standard deviation was 1.53% (n=12) with high sample throughout of 20 sample/h. Accuracy of our method was validated by comparison with ICP-MS. Recovery study showed acceptable result without matrix effect. Finally, **this work presented for the first time that using CDs as a specific reagent for determination of mercury(II) in pharmaceutical products with the SIA system to achieve sensitive and rapid analysis.**

Introduction

Nowadays, there has been increasing concern about the safety of pharmaceutical products used in everyday life. Mercury is a toxic metal that can be presented in these products. Thailand have prohibited the use of mercury in these products and the level of mercury should not over than 1 ppm. Therefore, increasing public awareness about mercury contamination in pharmaceutical products is necessary. ICP-MS has become the most powerful technique for mercury analysis but this method is very cost intensive and requires highly skilled operators. Many fluorescent probes, including organic molecules, have been developed for fluorescent mercury detection in various samples based on ionophore/fluorophore reagent has been reported but these reagents are difficult synthesis, hard to predict amount of product and sometimes chemical toxicity. CDs has been replaced to overcome these problems with low toxicity, simple synthetic routes, environmentally friendly synthesis. Moreover, CDs can be prepared in aqueous system which is favorable for sample preparation medium. This proposed SIA is fully automatic controlled and rapid analysis. It is expected to be an alternative method for the analysis of mercury(II) in pharmaceutical products and other sample applications.

Experimental

Eco-friendly synthesis of CDs

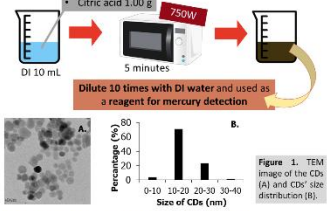

Figure 1. TEM image of the CDs (A) and CDs' size distribution (B).

Rapid analysis using the SIA system

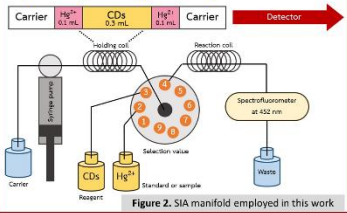

Figure 2. SIA manifold employed in this work

Results and discussion

Characterization of CDs

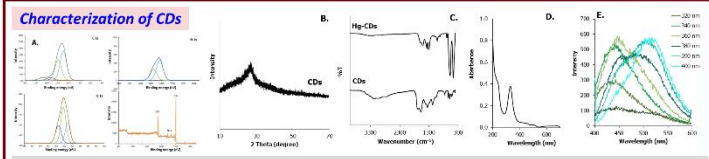

Figure 3. XPS spectra of the CDs (A). XRD of CDs (B). FT-IR spectra of the CDs and Hg-CDs (C). UV-Vis spectrum of the CDs solution show absorption at approximately 220-340 nm (D). Photoluminescence emission spectra of the CDs in aqueous solutions at different excitation wavelengths (300-400 nm) (E).

Batch method

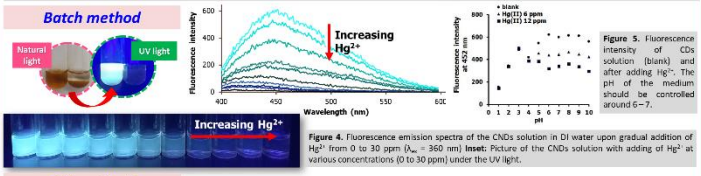

Figure 4. Fluorescence emission spectra of the CNDs solution in DI water upon gradual addition of Hg^{2+} from 0 to 30 ppm (λ_{ex} = 360 nm) **Inset:** Picture of the CNDs solution with adding of Hg^{2+} at various concentrations (0 to 30 ppm) under the UV light.

Figure 5. Fluorescence intensity of CDs solution (blank) and after adding Hg^{2+}. The pH of the medium should be controlled around 6−7.

SIA method

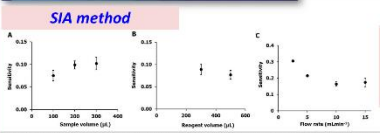

Analytical performance under the optimum condition

- Linear range : 0.5 to 600 ppm
- Limit of detection : 0.4 ppm
- Relative standard deviation : 1.53% (200 ppm, n=12)
- Sample throughput : 20 samples/h

Figure 6. Sensitivity from calibration curves obtained from physical parameter studies: sample volume (A), and reagent volume (B) and flow rate to detector (C). The optimized conditions are as follows: flow rate of 2.5 mL min^{-1}, volume of sample and reagent of 0.2 and 0.3 mL, respectively, and no waiting time.

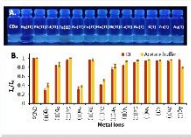

Figure 7. CDs solution in 0.1 M acetate buffer pH 7 (A) before and after adding of other metal ions. (B) Bar chart of fluorescence signal ratio of metal ions (I_o) and CDs (I_o) in deionized water (red) and acetate buffer (yellow).

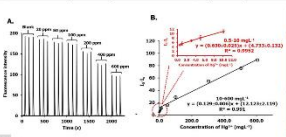

Figure 8. Signal profile (A) and calibration curve (B) obtained from the proposed SIA operated at the optimum condition. Error bars are derived from three injections.

Table 1. Sample analysis results. Comparison of our method with standard ICP-MS.

Sample	Hg^{2+} (ppm) Standard method (ICP-MS)	Proposed method	% Recovery
1	ND	ND	87.1±2.4
2	ND	ND	86.6±1.0
3	ND	ND	104.2±3.8
4	ND	ND	88.7±2.9
5	ND	ND	92.6±3.4

ND= not detectable

Conclusions

- ✓ **This proposed method is the combination of green synthesis of CDs and green analysis by SIA system.**
- ✓ At the optimum condition, linear range between 0.5 to 600 ppm with R^2 more than 0.99 was obtained and sample analysis result shows acceptable recovery value.
- ✓ The SIA application based on CDs was developed for the first time, providing a simple, automatic, rapid, and low-cost analysis platform for the detection of mercury ion in pharmaceutical products and heavy metal ion contamination.
- ✓ **This method expected to be an alternative method for the analysis of mercury in pharmaceutical products and other sample applications.**

References

1. M. Pajewska-Szmyt, B. Buszewski, R. Gadzała-Kopciuch, *Spectrochimica Acta Part A*, 2020, **236**, 118320.
2. S. Qu, X. Wang, Q. Lu, X. Liu, L. Wang, *Angewandte Chemie International Edition*, 2012, **51**, 12215-12218.
3. X. Qin, W. Lu, A.M. Asiri, A.O. Al-Youbi, X. Sun, *Sensors and Actuators: B*, 2013, **184**, 156-162.

Acknowledgements

Financial support from Reinventing University System Program by The Ministry of Higher Education, Science, Research and Innovation is gratefully acknowledged. (Fiscal Year 2021)

Fluorometric Determination of Preservatives in Skincare Products using Layered Double Hydroxides as Peroxidase Enzyme Mimicking

Kanokwan Sakunrungrit[a], Akarapong Prakobkij[b,c], Purim Jarujamrus[b,c], Sumonmarn Chaneam[a,d*]

[a] Department of Chemistry, Faculty of Science, Silpakorn University, Nakhon Pathom, 73000, Thailand.
[b] Department of Chemistry and Center of Excellence for Innovation in Chemistry, Faculty of Science, Ubon Ratchathani University, Ubon Ratchathani 34190, Thailand.
[c] Nanomaterials Science, Sensors & Catalysis for Problem-Based Projects, Faculty of Science, Ubon Ratchathani University, Ubon Ratchathani 34190, Thailand.
[d] Flow Innovation Research for Science and Technology Laboratories (FIRST Labs), Bangkok 10400, Thailand

*Corresponding e-mail: chaneam_s@su.ac.th

(N11A650144) chaired by Assoc. Prof. Dr. Duangjai Nacapricha.

p-Hydroxybenzoic acid (PHBA), a preservative, was added to many skincare products to prohibit microorganisms and oxidants from extending shelf-life. However, it can be toxic, irritate, and damage the eyes. Many countries, including Thailand, have legislated using preservatives in these products **not more than 0.8% for a mixture of esters**.

In this work, a fluorometric determination of preservatives using PHBA as a model target was developed. **Layered double hydroxides (LDHs)** were employed as a **peroxidase enzyme mimic**. The LDHs were easily synthesized by the co-precipitation method. Under optimum conditions, a certain amount of hydrogen peroxide (H_2O_2), H_2O_2 could be oxidized by the LDHs to form hydroxyl radicals ($HO^•$), followed by the reaction of $HO^•$ and PHBA as target analyte to for followed the phenoxy radical of PHBA. The remaining $HO^•$ could subsequently react with o-phenylenediamine (OPD), producing a yellow fluorescence product. **The fluorescence signal was dramatically decreased correspondingly to the PHBA concentrations in the sample.**

Fluorometric application for determination of preservatives in skincare products

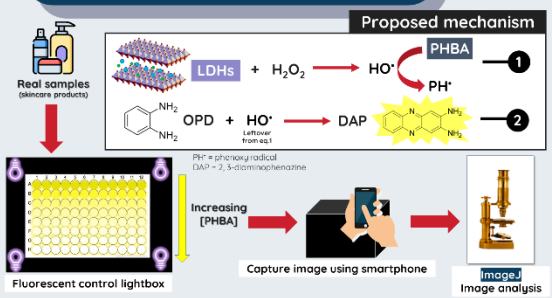

Figure 1. Fluorometric determination of preservatives by using LDHs as enzyme mimics

Mechanism

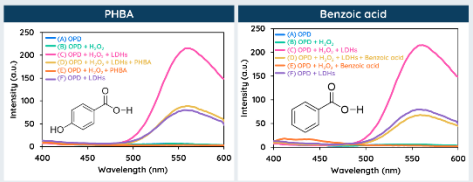

Figure 3. Fluorescence spectra of catalytic reaction by using LDHs as an enzyme mimics and OPD as a fluorescence substate (optimum condition: 50 ppm of LDHs, 75 mM of H_2O_2, 5 mM of OPD, 3 mM of PHBA, 3 mM of benzoic acid, 20 minutes of reaction time, and pH 6)

Optimization

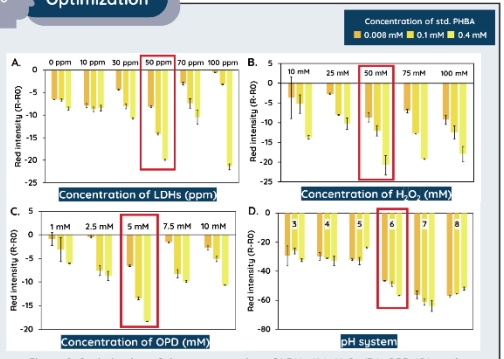

Figure 2. Optimization of the concentration of LDHs (A.), H_2O_2 (B.), OPD (C.), and pH system (D.) for fluorometric determination of PHBA

Analytical performance

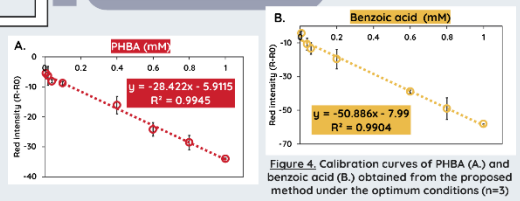

Figure 4. Calibration curves of PHBA (A.) and benzoic acid (B.) obtained from the proposed method under the optimum conditions (n=3)

Analytical performance	PHBA	Benzoic acid
Linearity range	0.008 to 1 mM	0.008 to 1 mM
Limit of quantification (LOQ)	0.024 mM	0.014 mM
Limit of detection (LOD)	0.0072 mM	0.0042 mM

Table 1. Analytical performance of PHBA and benzoic acid under optimum conditions

Table 2. The analysis of preservatives in various samples using our proposed method

Sample	PHBA (mM) Added	PHBA (mM) Found	%Recovery	Benzoic acid (mM) Added	Benzoic acid (mM) Found	%Recovery
Cleansing wipe*	0 0.2 0.6	0.011±0.33 0.206±0.31 0.657±0.04	- 97.1 107.6	0 0.2 0.6	0.194±0.26 0.397±1.13 0.807±0.28	- 101.7 102.1
Facial toner*	0 0.2 0.6	0.034±0.37 0.241±0.58 0.633±0.27	- 103.9 99.5	0 0.2 0.6	0.198±0.23 0.404±0.04 0.807±0.27	- 102.8 101.9
Facial serum*	0 0.2 0.6	0.018±0.45 0.219±0.12 0.650±0.04	- 100.4 105.3	0 0.2 0.6	0.004±0.10 0.200±0.19 0.603±0.24	- 98.0 99.8
Soothing gel*	0 0.2 0.6	0.002±0.22 0.203±0.22 0.588±0.11	- 100.8 97.8	0 0.2 0.6	0.233±0.45 0.448±0.18 0.843±0.40	- 107.3 101.6

*All samples were diluted before analysis

Conclusions

- ✓ This low-cost and rapid method is the first report on the use of LDHs as a peroxidase enzyme mimic and OPD substate for fluorometric determination of preservatives.
- ✓ The smartphone was used to capture an image of the fluorescent signal under a fluorescent control lightbox for quantitative determination of preservatives.
- ✓ Under the optimum conditions, the method showed a linearity range from 0.008 to 1 mM (PHBA and Benzoic acid) with acceptable percentage of recovery.
- ✓ This method is expected to be an alternative method for the determination of preservatives in skincare products and other interesting analytes.

Acknowledgements

This work was supported by the National Research Council of Thailand (N11A650144), chaired by Assoc. Prof. Dr. Duangjai Nacapricha. The Department of Chemistry, Faculty of Science, Ubon Ratchathani University, is recognized for its instrumental facilities. The research scholarships of the Faculty of Science, Silpakorn University is also gratefully acknowledged.

6.2 Output: publication

This work was published in ACS omega journal (Q1, IF 4.1) in title “Sequential Injection Analysis for Rapid Determination of Mercury in Skincare Products Based on Fluorescence Quenching of Eco-Friendly Synthesized Carbon Dots”

ACS OMEGA

http://pubs.acs.org/journal/acsodf

Article

Sequential Injection Analysis for Rapid Determination of Mercury in Skincare Products Based on Fluorescence Quenching of Eco-Friendly Synthesized Carbon Dots

Kanokwan Sakunrungrit, Cheewita Suwanchawalit, Kanokwan Charoenkitamorn, Apisake Hongwitayakorn, Kamil Strzelak, and Sumonmarn Chaneam*

Cite This: *ACS Omega* 2023, 8, 7615−7625

Read Online

ACCESS | Metrics & More | Article Recommendations

ABSTRACT: This work reports the analysis of mercury using a spectrofluorometric method combined with a sequential injection analysis (SIA) system. This method is based on the measurement of fluorescence intensity of carbon dots (CDs), which is quenched proportionally after adding mercury ions. Herein, the CDs underwent environmentally friendly synthesis using a microwave-assisted approach that provides intensive and efficient energy and shortens reaction time. After irradiation at 750 W for 5 min in a microwave oven, a dark brown CD solution with a concentration of 2.7 mg mL^{-1} was obtained. The properties of the CDs were characterized by transmission electron microscopy, X-ray diffractometry, X-ray photoelectron spectroscopy, Fourier-transform infrared spectroscopy, and UV−vis spectrometry. We presented for the first time the use of CDs as a specific reagent for the determination of mercury in skincare products with the SIA system to achieve rapid analysis and full automatic control. The as-prepared CD stock solution was diluted 10 times and used as a reagent in the SIA system. Excitation and emission wavelengths at 360 and 452 nm, respectively, were used to construct a calibration curve. Physical parameters affecting the SIA performance were optimized. In addition, the effect of pH and other ions was investigated. Under the optimum conditions, our method showed a linear range from 0.3 to 600 mg L^{-1} with an R^2 of 0.99. The limit of detection was 0.1 mg L^{-1}. Relative standard deviation was 1.53% (n = 12) with a high sample throughput of 20 samples per hour. Finally, the accuracy of our method was validated by comparison using inductively coupled plasma mass spectrometry. Acceptable recoveries were also presented without a significant matrix effect. This method was also the first time that uses the untreated CDs for the determination of mercury(II) in skincare products. Therefore, this method could be an alternative for mercuric toxic control in other sample applications.

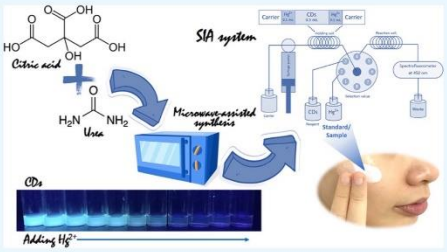

1. INTRODUCTION

At present, there has been increasing concern about the safety of cosmetic and pharmaceutical products used in everyday life. Mercury is a toxic metal that presents intentionally or accidentally in some treatments of skin conditions, particularly whitening products. Mercury can be presented in these products, although it is not listed on the label or on the product information. However, it may accumulate in the skin and exert harmful side effects on the skin and internal organs when used in large quantities for a long period of time. For example, in the case of a woman who uses mercury-containing cream, mercury levels are high in the hair, blood, and urine. The long-term use of mercury-containing lighteners often produces a gray skin color.[1−3] Therefore, many countries, including Thailand, have prohibited the use of mercury in these products not higher than 1 mg L^{-1}.[4] In Thailand, face whitening cream holds a 60% share of the national market for facial lotion, with approximately 2100 million Baht ($70 million).[5] Therefore, increasing public awareness about mercury contamination in skincare products is necessary.

Traditional techniques have been utilized for detecting mercury ions (Hg^{2+}) in skincare and cosmetic products such as titration,[6] neutron activation analysis,[7] and cold vapor atomic absorption spectrometry.[8] Inductively coupled plasma mass spectrometry (ICP-MS) has become a powerful analytical technique for Hg^{2+} analysis.[9,10] However, the instrument is

Received: November 7, 2022
Accepted: February 1, 2023
Published: February 14, 2023

https://doi.org/10.1021/acsomega.2c07175
ACS Omega 2023, 8, 7615−7625

expensive, and it requires highly skilled operators. An alternative for optical sensing systems for the detection of Hg^{2+} can also be based on the fluorescence assay because of its high sensitivity and fast analysis. Many fluorescent probes, including organic molecules, have been developed for fluorescent Hg^{2+} detection in various samples based on the ionophore/fluorophore reagent.[11−14] However, some reagents have difficult and multistep synthesis, a considerable amount of products, and chemical toxicity. In addition, most reagents are insoluble in an aqueous medium, which is an unfavorable condition of the sample preparation medium and of the flow-based system including the sequential injection analysis system (SIA). There are previous works reported using the SIA for determination of Hg^{2+}, for example, SIA with cold vapor atomic absorption spectrometry,[15] SIA with anodic stripping voltammetry,[16] and SIA with spectrophotometry.[17]

Nanoparticles have been used to address the abovementioned problems. Recent advances in nanotechnology have provided new methodologies for Hg^{2+} sensing contaminants.[18,19] For example, colorimetric methods based on surface plasmon resonance of gold nanoparticles have been used for testing Hg^{2+}.[20] However, these gold nanoparticles are unstable, and they require time-consuming modification processes. Among these nanoparticles, carbon-based nanomaterials such as carbon dots (CDs) are increasingly used in various fields, including food, agricultural, industrial, health, and medical purposes, because of their unique physical and chemical properties. CDs have easy synthesis, biocompatibility, and low toxicity.[21] Elemental analysis showed that CDs are composed of C, H, O, and N, depending on the carbon precursors. In general, CDs should be further purified by using centrifugation, dialysis, electrophoresis, or another separation technique to control the size and improve the photoluminescence properties. Some studies use CDs as a specific sensor for heavy metals.[22−27] Most of the CD probes for Hg^{2+} were applied to analyze Hg^{2+} in water samples[28−32] and breast milk.[33] In addition, CDs were investigated as the Hg^{2+} sensor for bioimaging.[34,35]

As described previously, CDs have been applied for Hg^{2+} analysis. However, CDs have never been applied for the assessment of Hg^{2+} in skincare products. Herein, we presented an easy preparation of CDs through a one-step and short-time method under a microwave-assisted approach by using common chemical reagents such as citric acid and urea as initial substances. The resultant CDs exhibited strong blue fluorescence emission in aqueous solution. After adding Hg^{2+} to the untreated CD solution, precipitation and aggregation of Hg-CDs occurred. Simultaneously, fluorescence emission of the solution turned off. Based on this phenomenon, a fluorometric detection was explored and used for quantitative analysis of mercury.

In this work, the feasibility of CDs for Hg^{2+} analysis in a real sample was also demonstrated by employing the SIA system for microliter handling to reduce the sample and reagent as well as achieve the automatic operation. The developed procedure was applied to monitor the Hg^{2+} content in skincare products, particularly whitening cream.

2. EXPERIMENTAL SECTION

2.1. Materials and Instruments. All the experiments were performed in aqueous solution. Citric acid anhydrous 99.5% (Loba Chemie Pvt., Ltd., India) and urea 99.5% (Loba Chemie Pvt., Ltd., India) were used for CD synthesis. The standard solution of 1000 mg/L Hg^{2+} was prepared by dissolving mercury(II) acetate (Sigma-Aldrich, USA) in deionized water and used as a stock solution. The working standard solution of 0.3−600 mg L^{-1} Hg^{2+} was prepared by diluting the stock solution. Acetate buffer (0.10 M) at pH 6 and 7 was prepared from acetic acid (Carlo Erba, Italy) and sodium acetate (Sigma-Aldrich, USA). Phosphate buffer (0.1 M) at pH 6 was prepared from sodium phosphate (Sigma-Aldrich, USA). All of the solutions were prepared in deionized water.

In this work, we aimed to quantitatively analyze Hg^{2+} in skincare products. Different products for skin conditions, particularly whitening cream, were purchased from the online market, local cosmetic shops, and supermarkets in Nakhon Pathom, Thailand. For analysis, the exact weight of 0.10 g of the sample was dissolved in 0.50 mL of 5% (v/v) HNO_3 (Carlo Erba, Italy), and the volume was made to 25 mL in a volumetric flask by 0.1 M acetated buffer at pH 7.0, which was then injected to the SIA system. All samples were analyzed using the proposed flow system and the ICP-MS reference method.

2.2. Microwave-Assisted Synthesis of CDs. The CDs were synthesized by a microwave-assisted method of the previously reported procedure with a slight modification.[36,37] The mixed solution composed of 1.00 g of citric acid and 1.00 g of urea to 10.00 mL of deionized water was irradiated at 750 W for 5 min in a microwave oven (Samsung model MW71B) to give the CD suspension. Finally, the as-synthesized CDs were collected and stored at 4 °C for further characterization and application of Hg^{2+} detection.

Fluorescence quantum yield (QY) was determined by a comparative method.[38−40] Quinine sulfate in 0.1 M H_2SO_4 was used as a standard solution to calculate the QY of synthesized CD samples, which were dissolved in deionized water. All the absorbance values of the solutions at the excitation wavelength were measured with a UV−vis spectrophotometer. Photoluminescence (PL) emission spectra of all the sample solutions were recorded by a PerkinElmer LS-50B luminescence spectrometer at an excitation wavelength of 360 nm. The fluorescence quantum yield of the as-prepared CDs was calculated by comparing the UV−vis absorbance values and the integrated fluorescence intensities (λ_{ex} = 360 nm) of the CDs with those of quinine sulfate solution. The absorbance values of all solutions were maintained under 0.05 to minimize self-absorption. The fluorescence quantum yield of obtained CDs was calculated using the following equation:

$$\varphi_u = \varphi_s \frac{F_u A_s \eta_u^2}{F_s A_u \eta_s^2}$$

where φ is the quantum yield, A stands for the optical density, F represents the integrated emission intensity, and η is the refractive index of the solvent. "s" and "u" correspond to the standard and the sample, respectively.

2.3. Microwave Digestion and ICP-MS for Method Validation. For sample preparation, microwave digestion was used. The exact weight of 0.20 g of each sample was transferred into a microwave vessel. Then, 9.00 mL of nitric acid (conc. 65%, w/w) and hydrogen peroxide (conc. 30% w/w) was added into the microwave vessel as digestion reagents. Finally, under microwave digestion around 50 min, the sample solution was transferred into a volumetric flask, and the volume was made up to 100 mL with deionized water. Afterward, the prepared sample solutions were analyzed by ICP-MS. ICP-MS (7900 ICP-MS, Agilent, USA), with a detection limit of mercury of 0.001 mg

https://doi.org/10.1021/acsomega.2c07175
ACS Omega 2023, 8, 7615−7625

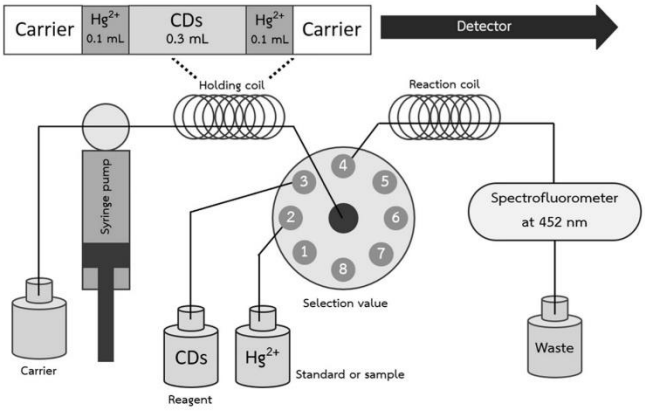

Figure 1. Schematic diagram of the SIA system for the determination of mercury.

L^{-1}, was used as the standard method to validate mercury analysis.

2.4. Characterizations. The properties of the as-prepared CDs before and after reacting with Hg^{2+} were characterized extensively. The structures and morphologies were examined using X-ray diffractometry (XRD; Aris, PANalytical, UK), X-ray photoelectron spectroscopy (XPS) (Kratos Axis Ultra spectrometer, Manchester, UK, with a monochromic Al Kα source at 1486.7 eV), and transmission electron microscopy (TEM) (FE-TEM/STEM-EDS, Thermo Scientific Talos F200X STEM, USA). Fourier-transform infrared spectra of standard mercury-(II) acetate, dried CDs, and dried Hg-CDs were recorded on Frontier, PerkinElmer, USA. UV−visible absorption spectra were recorded on Cary 60, Agilent, USA, and fluorescence spectra were recorded using a spectrofluorometer (LS 55, PerkinElmer, USA).

2.5. Sequential Injection Procedure. The SIA with a syringe pump (Cavro XLP 6000, Switzerland) and a selection valve (Cavro Smart Valve, Switzerland) was operated (Figure 1). A 5 mL zero-dead-volume syringe was fitted with a holding coil. The programmable pump and valve were automatically controlled, via an RS-232 communication port, using the program developed in C# language running under an MS-Windows environment. The graphical user interface of the program practically guided users to input parameters and steps of the procedure as necessary. The amount of Hg^{2+} in skincare products was determined using an SIA coupled spectrofluorometer. As shown in Table 1, the common sequential injection procedure has five steps for one cycle. First, a 3000 μL carrier was aspirated into the system at a flow rate of 10 mL min^{-1}. Next, two 100 μL segments of standard or sample (port 2) partition with a 300 μL segment of the diluted CD solution (port 3) were sequentially aspirated into a holding coil, namely, sandwich pattern, at a flow rate of 10 mL min^{-1}. Then, zone stacking was sent to a reaction coil (PTFE, 0.75 mm, 100 cm) and continuously propelled to the detection cell through port 4 at a flow rate of 2.5 mL min^{-1} with no need of any cleaning step. The fluorescence intensity was recorded at an excitation wavelength and emission wavelength of 360 and 452 nm, respectively. A decreased signal (compared with the blank sample) was observed because the fluorescence of the CDs was quenched by Hg^{2+} in the sample.

Table 1. SIA Procedure Operated in This Work

step	flow rate (mL min^{-1})	volume (μL)	flow direction	event
1	10	3000	reverse	carrier aspirated
2	10	100	reverse	standard/sample zone segment 1 aspirated
3	10	300	reverse	reagent zone aspirated
4	10	100	reverse	standard/sample zone segment 2 aspirated
5	2.5	3500	forward	zones sent to the spectrofluorometer

3. RESULTS AND DISCUSSION

3.1. Concentration and Size of CDs. The CDs were synthesized by a microwave-assisted method as described above. A hundred microliters of the as-prepared CD solution was pipetted onto a glass slide and was evaporated at 80 °C for 24 h. Finally, the concentration of the synthesized CDs was found to be 2.7 mg mL^{-1}. The fluorescence quantum yield of the CDs was calculated to be about 0.16%. This result might be due to the effect of low energy transfer of large untreated CDs. However, this QY value is sufficient for our application. To use the CDs as a reagent in the SIA system, the optimal concentration of the CD solution was investigated by dilution to 0.54, 0.27, and 0.14 mg mL^{-1} and the concentration of 0.27 mg L^{-1} showed the best sensitivity. Therefore, the as-prepared stock CD solution was diluted 10 times in deionized water. The clear diluted CD solution was used as a reagent for Hg^{2+} analysis with the SIA. The stability of the CDs was also investigated by measuring the fluorescence intensity and sensitivity of the flow system for Hg^{2+} determination. The results revealed that the sensitivity of our system was stable up to 3 months after preparation. Precision of synthesis was considered by measuring the emission intensity at 452 nm of the 10 times dilution of the as-prepared CDs obtained from each batch. Therefore, inter-batch precision of the synthesis of CDs was reported as 2.9%RSD (n = 3).

https://doi.org/10.1021/acsomega.2c07175
ACS Omega 2023, 8, 7615−7625

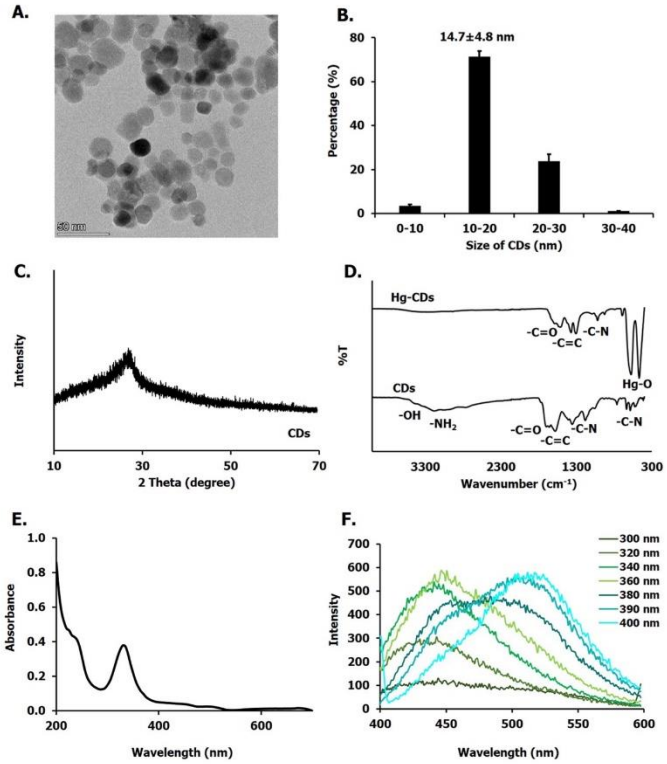

Figure 2. Typical TEM image of as-prepared CDs (A) and CDs' size distribution (B). XRD pattern of the as-prepared CDs (C). FT-IR spectra of the synthesized CDs and Hg-CDs (D). The UV−vis spectrum of the CD solution shows absorption at approximately 220−340 nm (E). Photoluminescence emission spectra of the CDs in aqueous solutions at different excitation wavelengths (300−400 nm) (F).

3.2. Characterization of CDs. In this paper, the CDs were synthesized using a microwave-assisted method. TEM was used to characterize the morphology of the untreated CDs. The TEM image (Figure 2A) shows spherical nanoparticles with consistent dispersion. In this work, about 71% of the size distribution is in the range of 10−20 nm (Figure 2B). After analyzing random particles, the CD mean size was 14.7 ± 4.8 nm. A small number of particles are relatively of bigger size because of the agglomeration of smaller particles. Figure 2C shows the XRD patterns of the CDs obtained in the range from 10 to 70°. The XRD pattern shows that the CDs have a broad diffraction peak at 27.2°, which indexes to the (002) plane of graphitic carbon.[41,42] This peak reveals the predominately amorphous structure of the as-prepared CDs.

The surface functional groups of CDs were characterized by FT-IR (Figure 2D). A broad peak of approximately 3420 cm^{-1} was indicative of OH stretching. Absorption bands at 3177 cm^{-1} were attributed to NH_2. These functional groups typically existed on the surface of CDs.[38] The characteristic peaks of the C═O stretching vibration, which are a typical observation for CDs, are shown at 1701 and 1661 cm^{-1}. The 1576 and 1350 cm^{-1} peaks were attributed to the stretching vibrations of C═C and C−N, respectively.[43,44] The FT-IR spectrum of dried Hg-CDs was also evaluated. Two peaks at approximately 400−600 cm^{-1} were found dominant. Based on our reviews in previous works, the characteristic peaks at 576 and 468 cm^{-1} were defined as Hg−O in vibrational mode, which confirms the formation of Hg−O on the surface of Hg-CDs.[45] Notably, the peaks of C═O and broad peaks of −OH and $-NH_2$ were shifted, and their intensities were reduced. The UV−vis spectrum of the CD solution (Figure 2E) shows main absorption bands at approximately 220, 260, and 340 nm, which correspond to the carbon−carbon double bond's $\pi \rightarrow \pi^*$ and aromatic ring's $\pi \rightarrow \pi^*$ transitions. The absorption peak at 340 nm in the UV−vis absorption spectra of the synthesized CDs confirmed that the presence of the C═C functional group of the graphitic structure occurs during the carbonization process.[46,47] As shown in Figure 2F, when the CDs were excited at 360 nm, strong fluorescence emission at 452 nm was observed. The maximum fluorescence peak shifted from 420 to 530 nm with a change of excitation wavelength from 300 to 400 nm, respectively.

https://doi.org/10.1021/acsomega.2c07175
ACS Omega 2023, 8, 7615−7625

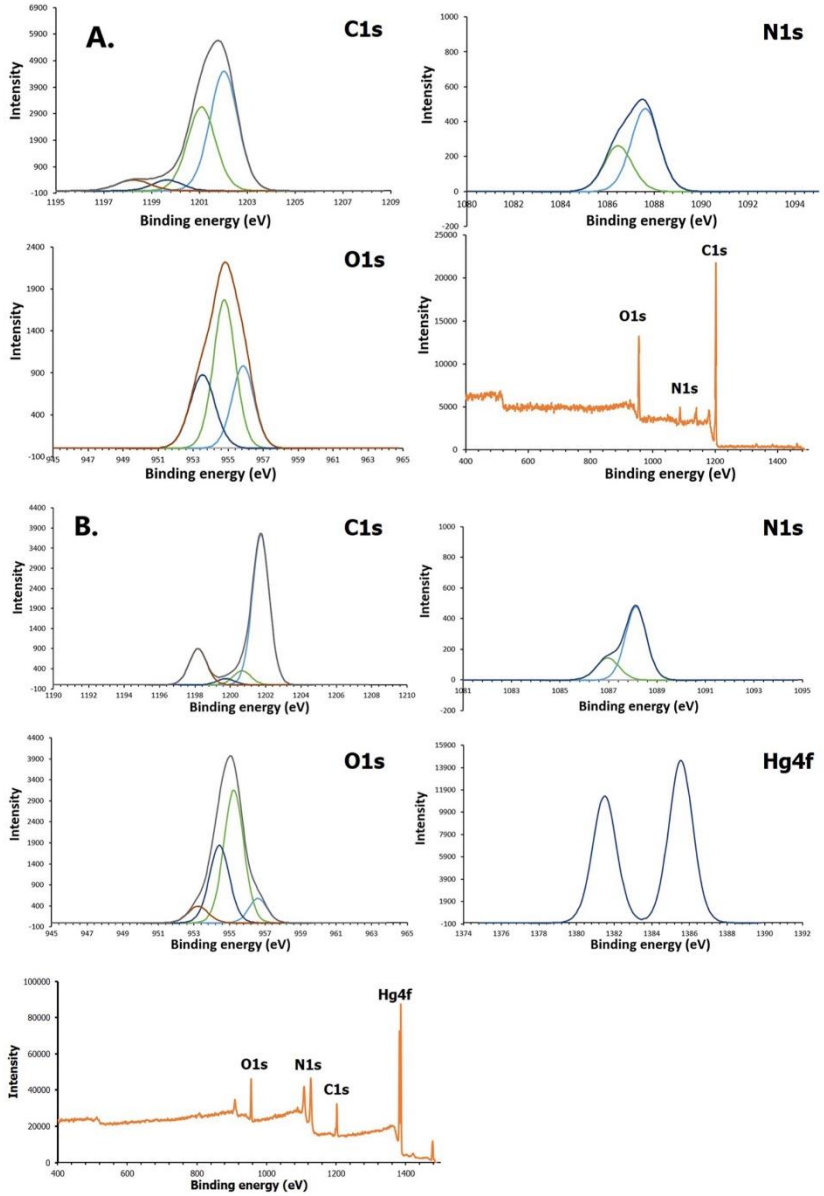

Figure 3. XPS spectra of the CD (A) and Hg-CD products (B) obtained.

https://doi.org/10.1021/acsomega.2c07175
ACS Omega 2023, 8, 7615−7625

Furthermore, elemental compositions of CDs and Hg-CDs were also investigated by the XPS technique.[37,47,48] Figure 3 presents the high-resolution XPS spectra of C (1s), N (1s), O (1s), and Hg (4f) of CDs and Hg-CDs. The XPS survey scan spectrum of the CDs (Figure 3A) revealed three apparent binding peaks corresponding to the O (1s), N (1s), and C (1s). The deconvolution spectrum of C (1s) showed four peaks at 284.64, 285.59, 287.05, and 288.44 eV, which can be attributed to C═C (sp^2), C−N, C−OH/C−O−C, and C═O groups, respectively.[49] The high-resolution N (1s) spectrum (Figure 3A) was deconvoluted into two peaks at 399.07 and 400.22 eV, corresponding to C−NH_2 and O═N—C functional groups, respectively. The O (1s) spectrum (Figure 3A) was deconvoluted to three peaks at 530.84, 531.91, and 533.14 eV, indicating the presence of −C−O/−N−O, —C═O, and C−O−C functional groups, respectively.[50,51] The XPS results confirmed that there are many functional groups (−NH_2, −COOH, and −OH) on the surface of CDs corresponding with FT-IR results. The XPS spectra of the Hg-CDs (Figure 3B) are composed of O, N, C, and Hg elements. The C (1s) spectrum could be deconvoluted into four peaks at 284.94, 286.03, 286.96, and 288.52 eV, corresponding to the C═C (sp^2), C−N, O—C═O, and C═O groups, respectively.[49] The N (1s) spectrum reveals the presence of the amine group (C−NH_2 (398.56 eV) and O═N—C (399.74 eV)). The O (1s) spectrum was deconvoluted to four peaks at 530.09, 531.47, 532.28, and 533.47 eV, suggesting the presence of −C−O/−N−O, —C═O, C−OH, and C−O−C groups, respectively.[48,50,51] For Hg, the (4f) spectrum found two peaks of 4f5/2 and 4f7/2 at 105.18 and 101.13 eV, respectively.[52] The results showed that mercury was adsorbed on CDs via oxygen-containing functional groups and amine group in the adsorption of mercury ions.[48,52]

3.3. Detection of Mercury Ions Using the Batch Method. Fluorescence quenching of CDs was achieved by hand mixing the aqueous solutions of CDs and Hg^{2+}. At first, Figure 4 presents images of the untreated CDs and products after reacting with Hg^{2+} under visible (Figure 4A) and UV light (Figure 4B). The bright blue photoluminescence is strong and easily seen with the naked eyes. In addition, 100 μL of the diluted CDs was added to 3.00 mL of deionized water in a quartz cuvette, and the fluorescence intensity of CDs was recorded as blank. Then, the standard solution of 0−100 μL of 1000 mg L^{-1} Hg^{2+} was added into 10 μL of solution increment each time. Afterward, the solution was mixed by shaking the cuvette. After Hg^{2+} was introduced into the CD solution, Hg-CD aggregation was induced; thus, fluorescence intensity of the CDs disappears soon. The aggregation of CDs is enforced upon the addition of the mercury ion. Consequently, the color of solution turns from pale yellow to colorless. However, UV−visible absorption of CDs and CDs after adding Hg^{2+} solution is less sensitive, and it could not be applied to real samples. Therefore, photoluminescence was used by measuring the maximum emission peak at 452 nm with an excitation at 365 nm. As shown in Figure 5A,B, the fluorescence intensity decreased gradually with the increase in Hg^{2+} concentration. The formation of non-luminescent Hg-CD aggregation might lead to quenching of fluorescence intensity. A linear calibration curve (Figure 5C) was obtained, and it shows that the untreated CDs could be utilized for quantitative analysis of Hg^{2+}. Based on the above results, high selectivity toward Hg^{2+} in aqueous solution could be probably a coordinative interaction with Hg^{2+} and the carboxyl and hydroxyl groups on the surface of CDs. The photoluminescence intensity decreases with the increasing concentrations of Hg^{2+}. The photoluminescence quenching of CDs was caused by Hg^{2+}chelation between surface functional groups of CDs and Hg^{2+} via charge transfer, leading to the fluorescence quenching of the CDs.[53−56]

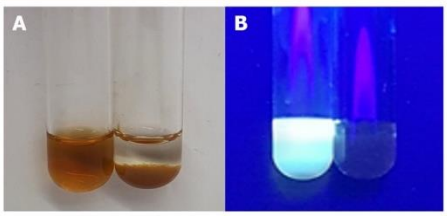

Figure 4. Photographs under visible (A; daylight lamp) and UV light (B; λ_{ex} = 365 nm). (The concentration of CDs is 0.27 mg mL^{-1}, and the concentration of Hg^{2+} is 60 mmol L^{-1}). All photos were taken by S.C.

A dependence of the CD fluorescence intensity on the pH value was reported. Similar to previous works,[21] we found that the intensity decreased when the pH value of the CD solution was lower than 5. The fluorescence intensity of Hg-CDs is also pH-dependent (Figure 5D). At the acidic medium, low quenching efficiency was observed, which results from the dissociation of the Hg-CD compound caused by the protonation of surface-binding carboxyls. With the increase in pH, the deprotonation of the carboxylic groups in the CDs occurs. This phenomenon may strengthen the covalent bond between Hg^{2+} and CDs, which leads to higher quenching efficiency and lower fluorescence intensity.[37] At the high basic medium, the precipitate of mercury hydroxide might occur and reduce the Hg-CD compound. From the results, pH 7.0 was used. Various types of medium solutions at pH 7 were further studied, which are DI water, acetate buffer, and phosphate buffer, and the results show that acetate buffer at pH 7 gives the best sensitivity.

3.4. Optimization of Physical Parameters Affecting the SIA Performance. The experiment is shown in Figure 1. The working standard solution of 0.3−600 mg L^{-1} Hg^{2+} was used to optimize the physical parameters. First, the volumes of the sample and reagent were optimized to reduce their amount (Figure 6A,B). Notably, the solution volume needed for the proposed SIA method can be reduced to the microliter level. We found that 200 μL of the sample (divided in two aliquots of 100 μL intercalated with the reagent aliquot) was sufficient to cover the analysis range with a satisfactory signal, and the CD reagent solution at 300 μL was selected for all further experiments. Next, the flow rate sent to the spectrofluorometer, which has a significant effect on the measured signal, was studied. In this experiment, the flow rate varied from 2.5, 5, 10, and 15 mL min^{-1}. As shown in Figure 6C, the sensitivity decreased when the flow rate was increased. In accordance with the sensitivity, we selected 2.5 mL min^{-1} as the optimal flow rate. In addition, we observed that even if a flow rate higher than 10 mL min^{-1} was used, sample throughput was not significantly improved, but a large noise was observed. At a 2.5 mL min^{-1} flow rate, we obtained a satisfactorily high throughput of 20 sample h^{-1}.

3.5. Effect of Other Metal Ions. Figure 7 shows the results of the effect of coexisting metal ions. First, batch experiments were performed by evaluating the fluorescence intensity under UV light. A hundred microliters of diluted CDs was added to a medium of 3.00 mL of DI water in a vial, and then, 80 μL of 100

https://doi.org/10.1021/acsomega.2c07175
ACS Omega 2023, 8, 7615−7625

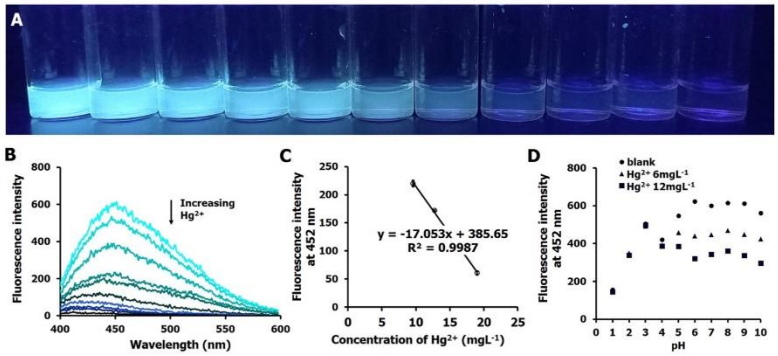

Figure 5. Corresponding fluorescence images under a 365 nm UV lamp (A) taken by S.C. and fluorescence emission spectra of a mixture of CDs with the addition of Hg^{2+} (B). Calibration curve plot of fluorescence intensity at 452 nm at various concentrations of Hg^{2+} (C). Effect of pH on the fluorescence intensity (D).

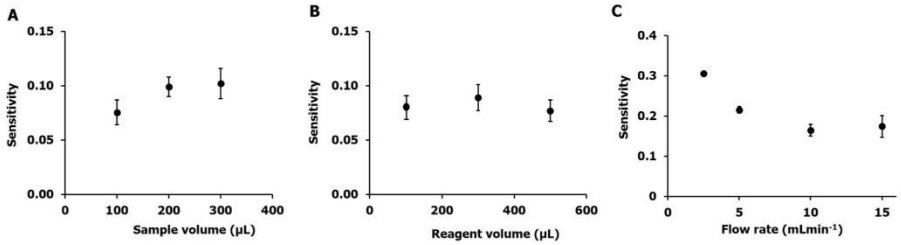

Figure 6. Sensitivity of calibration curves obtained from physical parameter studies: sample volume (A), reagent volume (B), and flow rate to detector (C). The optimized conditions are as follows: a flow rate of 2.5 mL min^{-1}, volumes of the sample and reagent of 0.2 and 0.3 mL, respectively, and no waiting time.

mg L^{-1} metal ion solution was added (Figure 7A). The fluorescence intensity was recorded with an emission wavelength of 452 nm and excitation wavelength of 360 nm (Figure 7B). The effect of metal ions on Hg^{2+} detection was also investigated by injecting 200 μL of 100 mg L^{-1} for each metal ion solution into the SIA system, and the signal profile and bar graph are shown in Figure 7C and Figure 7D, respectively, which were consistent with the data obtained from the batch experiment (Figure 7A,B). Notably, interferences were not observed from Cd^{2+}, Ba^{2+}, Ni^{2+}, Ca^{2+}, Na^{+}, K^{+}, and Zn^{2+}. Pb^{2+} and Mn^{2+} had a slight effect on the fluorescence intensity, which could be negligible. This result may be due to the stability constants between the Hg^{2+} and carboxylic group, which are higher than other metal ions leading to the formation of a Hg−O non-fluorescent metal adduct.[52] In the case of Fe^{2+} and Cu^{2+}, less fluorescence intensity might result from metal hydroxide precipitation. Quenching of CDs by Fe^{2+} and Cu^{2+} was also found in previous works.[33] In addition, 2 and 20 mg L^{-1} Fe^{2+} and Cu^{2+} were tested by injecting to the SIA system. The results showed that our method can tolerate the presence of Fe^{2+} and Cu^{2+} at the tested levels. However, these ions are rarely found in the tested skincare products.

3.6. Analytical Features. Figure 8A illustrates the signal profile obtained from the SIA system with various concentrations of Hg^{2+} and calibration curve obtained from the signal profile for the determination of Hg^{2+} in samples (Figure 8B). The horizontal axis is the concentration of Hg^{2+} in mg L^{-1}, and the vertical axis is the difference between fluorescence intensity of blank (I_0) and fluorescence intensity of the sample (I_s). The linear equation of 0.3−10 mg L^{-1} is $y = (0.846 \pm 0.040)x + (4.243 \pm 0.192)$ with $R^2 = 0.991$ and of 10−600 mg L^{-1} is $y = (0.129 \pm 0.006)x + (12.123 \pm 2.119)$ with $R^2 = 0.991$. The results showed that good precision with standard deviation and relative standard deviation for Hg^{2+} are 2.30 and 1.53%, respectively (n = 12). This method has short-time analysis with a sample throughput of 20 samples per hour. The limit of detection, that is, the ratio of 3 times the standard deviation of the background and the slope of the linear function (3 s/S), was calculated to be as low as 0.1 mg L^{-1}, which is lower than the permitted limit of mercury in skincare products in Thailand.[4] In addition, the U.S. FDA regulations also say about prohibited and restricted ingredients in cosmetics, which are limited to 65 mg Hg L^{-1} for eye area products and 1 mg Hg L^{-1} for all other cosmetics. Its presence is unavoidable under conditions of good manufacturing practice (21 CFR 700.13).[57] It should be noted that the analytical features of our proposed method are sufficient for determination of mercury in skincare products. Table 2 shows the figures of merit for some of the previously reported

https://doi.org/10.1021/acsomega.2c07175
ACS Omega 2023, 8, 7615−7625

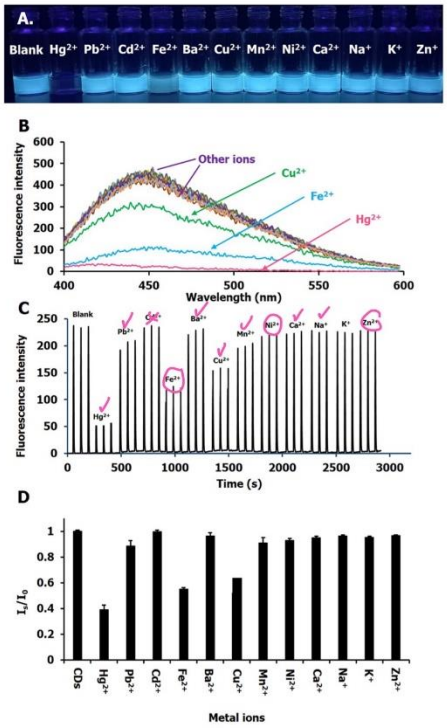

Figure 7. Photograph of fluorescence change under UV light (A) taken by S.C. and emission spectra (B) of diluted CDs in acetate buffer pH 7.0 solution upon the addition of various metal ions, including Hg^{2+}, Pb^{2+}, Cd^{2+}, Fe^{2+}, Ba^{2+}, Cu^{2+}, Mn^{2+}, Ni^{2+}, Ca^{2+}, Na^{+}, K^{+}, and Zn^{2+}. SIA experiments with the same set of foreign metal ions used acetate buffer pH 7.0 solution as the carrier (C, D).

methods and our method. This method has easy synthesis, and it uses untreated CDs without the need of any modifications. In addition, the measuring procedure is controlled automatically by a computer.

3.7. Sample Analysis and Method Validation. The applicability of the proposed method was evaluated by analyzing skincare products (sampled from Nakhon Pathom, Thailand) as real samples. First, the original samples were analyzed using the proposed SIA method and the reference ICP-MS. Notably, no Hg^{2+} was observed in all samples. Although Hg^{2+} was not found in the tested skincare samples, the result agreed well with that obtained from ICP-MS (with a detection limit of Hg^{2+} as low as 0.001 mg L^{-1}). The matrix effect of skincare was investigated by using spiked samples of 1 mg L^{-1} Hg^{2+}. For SIA, the sample solutions were directly injected into the system. For ICP-MS, a dilution factor of 100 was applied and then calculated backwards. Recoveries of each method are calculated and reported in Table 3. By comparison of %recoveries obtained from the SIA and ICP-MS, although %relative errors of some samples were carried out at ±5%,[58] their %recoveries are acceptable according to the AOAC method performance requirements for heavy metal analysis, which are in the range of 80−115.[59] The accuracy of our method was further evaluated by triplicate measurements of reference solution Hg^{2+} (Agilent part number 8500-6940-HG), certified as 1.0 mg L^{-1}.[60] The analysis of this sample using the proposed system showed that the fluorescence intensity measurement Hg^{2+} was 1.01 ± 0.02 mg L^{-1}. This result indicates the potential application of this procedure in monitoring hazardous Hg^{2+}.

4. CONCLUSIONS

Photoluminescent CDs have shown great application in potential health and medical fields. Here, we have utilized the microwave-assisted synthesis of untreated CDs as a specific reagent in the SIA system for the detection of heavy metal ions, which is mercury. In this work, although our CDs have a size of 14.7 ± 4.8 nm in average, the CDs exhibited good optical properties investigated corresponding to the "dots".[61] The CDs showed potential as mercury ion sensors with a detection limit of 0.1 mg L^{-1}. There are several advantages, such as a wider linear range and easy synthesis without the need for later purification and modification steps. No significant difference was observed between the results from our method and the results from ICP-

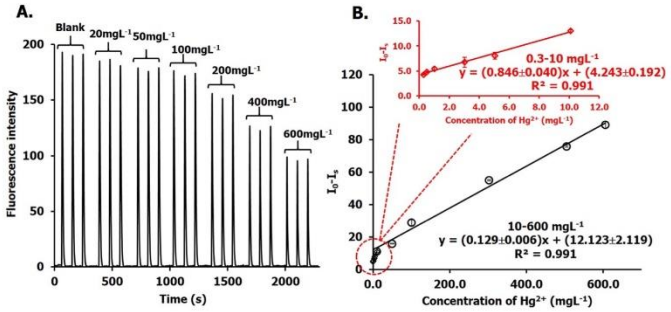

Figure 8. Signal profile (A) and calibration curve (B) obtained from the proposed SIA operated under the optimum conditions. Error bars are derived from three injections.

https://doi.org/10.1021/acsomega.2c07175
ACS Omega 2023, 8, 7615−7625

Table 2. Figures of Merit for Some of the Previous Reports Utilizing CDs as a Reagent for Mercury Analysis

Sample	CD precursor	Synthesis procedure	Linear range	Precision	LOD	Automatics	Reference
Lake water	Flour	Microwave-assisted	0.0005–0.01 μmol L^{-1}	Not reported	0.5 nmol L^{-1}	×	37
Tap water	Urea and ethylenediamine tetraacetic acid (EDTA)	One-step pyrolysis	0.001–8 μmol L^{-1}	Not reported	6.2 nmol L^{-1}	×	51
Tap water	Citric acid and triethylamine	Hydrothermal	0.05–7 μmol L^{-1}	Not reported	2.8 nmol L^{-1}	×	52
Breast milk	Citric acid and melamine	Solid thermal method	2–14 μmol L^{-1}	%RSD < 6	0.44 μmol L^{-1}	×	33
Tap water and packed water	Citrus lemon juice and ethylenediamine	Hydrothermal	0.001–1 μmol L^{-1}	%RSD 1.32	5.3 nmol L^{-1}	×	34
Tap water	Citric acid and 2,2-dimethyl-1,3-propanediamine	Microwave-assisted pyrolysis	0–4.2 μmol L^{-1}	%RSD < 2	7.63 nmol L^{-1}	×	28
Tap water and lake water	Eggshell membrane	Hydrothermal	10–100 μmol L^{-1}	Not reported	2.6 μmol L^{-1}	×	29
skincare products	Acetic and urea	Microwave-assisted (untreated)	1.5–2991 μmol L^{-1} (0.3–600 mg L^{-1})	%RSD 1.53	0.5 μmol L^{-1} (0.1 mg L^{-1})	✓ 20 sample h^{-1}	This work

Table 3. Analysis Results of the Detection of Hg^{2+} in Real Samples from Triplicate Analysis Comparison with ICP-MS and Recovery Results of the Actual Samples (ND = Not Detectable)

	Hg^{2+} (mg L^{-1})				
	standard method (ICP-MS)	proposed method			
sample[a]	original	%recovery[b,c]	original	%recovery[b,c]	%relative error[d]
1	ND	101.10	ND	87.1 ± 2.4	−13.8
2	ND	100.83	ND	82.4 ± 3.9	−18.3
3	ND	90.77	ND	86.6 ± 1.0	−4.6
4	ND	98.66	ND	81.8 ± 6.6	−17.1
5	ND	109.56	ND	114.0 ± 5.7	4.05
6	ND	105.42	ND	104.2 ± 3.8	−1.16
7	ND	93.94	ND	85.2 ± 2.7	−9.30
8	ND	100.60	ND	88.7 ± 2.9	−11.8
9	ND	105.94	ND	92.6 ± 3.4	−12.6

[a]Sample nos. 1−5 were the whitening face serum, no. 6 was the soothing gel, and nos. 7−9 were serum lotion. [b]%recovery = [(concentration of spiked standard mercury solution − concentration of the sample)/concentration of standard mercury solution] × 100. [c]The concentration of spiked standard mercury solution for ICP-MS and the proposed method is 1 mg L^{-1}. [d]%relative error = [(%$recovery_{proposed\ method}$ − %$recovery_{std\ method}$)/%$recovery_{std\ method}$] × 100.

MS with an acceptable percentage recovery of 81.8−114. This method provides less recovery; however, the feature of cost-effectiveness and convenience is better compared to the standard ICP-MS. The SIA application based on CDs was developed for the first time, providing a simple, automatic, rapid, and low-cost analysis platform for the detection of mercury ions in skincare products and heavy metal ion contamination. Our method is environmentally friendly because the detection does not rely on any toxic chemical reaction. Therefore, this system has received considerable attention from scientists working with quality control or working for agencies of safety and inspection service. Furthermore, the SIA system could be further developed as a portable device for on-site analysis.

AUTHOR INFORMATION

Corresponding Author

Sumonmarn Chaneam − *Department of Chemistry, Faculty of Science, Silpakorn University, Nakhon Pathom 73000, Thailand; Flow Innovation Research for Science and Technology Laboratories (FIRST Labs), Bangkok 10400, Thailand;* orcid.org/0000-0002-2753-9642; Phone: +66 3 4255797; Email: chaneam_s@su.ac.th; Fax: +66 3 4271356

Authors

Kanokwan Sakunrungrit − *Department of Chemistry, Faculty of Science, Silpakorn University, Nakhon Pathom 73000, Thailand*

Cheewita Suwanchawalit − *Department of Chemistry, Faculty of Science, Silpakorn University, Nakhon Pathom 73000, Thailand*

Kanokwan Charoenkitamorn − *Department of Chemistry, Faculty of Science, Silpakorn University, Nakhon Pathom 73000, Thailand;* orcid.org/0000-0003-4166-8181

https://doi.org/10.1021/acsomega.2c07175
ACS Omega 2023, 8, 7615−7625

Apisake Hongwitayakorn − *Department of Computing, Faculty of Science, Silpakorn University, Nakhon Pathom 73000, Thailand*
Kamil Strzelak − *University of Warsaw, Faculty of Chemistry, 02-093 Warsaw, Poland*

Complete contact information is available at: https://pubs.acs.org/10.1021/acsomega.2c07175

Notes

The authors declare no competing financial interest.

■ ACKNOWLEDGMENTS

Financial support from the Reinventing University System Program by the Ministry of Higher Education, Science, Research, and Innovation is gratefully acknowledged (fiscal year 2021). The authors wish to express their gratitude to the Faculty of Science, Silpakorn University, for the support of this work.

■ REFERENCES

(1) Bourgeois, M.; Dooms-Goossens, A.; Knockaert, D.; Sprengers, D.; Van Boven, M.; Van Tittelboom, T. Mercury intoxication after topical appilcation of a metallic mercury ointment. *Dermatologica* **2004**, *172*, 48−51.
(2) Dyall-Smith, D. J.; Scurry, J. P. Mercury pigmentation and high mercury levels from the use of a cosmetic cream. *Med. J. Aust.* **1990**, *153*, 409−415.
(3) Chan, T. Y. K. Inorganic mercury poisoning associated with skin-lightening cosmetic products. *Clin. Toxicol.* **2011**, *49*, 886−891.
(4) Ministry of Public Health, Ed., *List of Prohibited in Cosmetic Production.*; Ministry of Public Health: Bangkok: 2559.
(5) EARTH, E. A. a. R. T. *Study of mercury contamination in face whitening products in Thailand*; EARTH, E. A. a. R. T.: Thailand, 2021. DOI: https://ipen.org/sites/default/files/documents/EARTH%20Hg%20in%20Whitening%20-%20Report.pdf.
(6) Gaál, F. F.; Abramović, B. F. Determination of mercury content of some pharmaceutical products by catalytic titration. *Microchim. Acta* **1972**, *1*, 465−472.
(7) Margosis, M.; Tanner, J. T. Determination of mercury in pharmaceutical products by neutron activation analysis. *J. Pharm. Sci.* **1972**, *61*, 936−938.
(8) Mallkuci, I.; Lazo, P. MERCURY DETERMINATION IN DRUG AND COSMETIC PRODUCTS. *Int. J. of Curr. Res.* **2014**, *6*, 8077−8082.
(9) Passariello, B.; Barbaro, M.; Quaresima, S.; Casciello, A.; Marabini, A. Determination of mercury by Inductively Coupled Plasma-Mass Spectrometry. *Microchem. J.* **1996**, *54*, 348−354.
(10) Allibone, J.; Fatemian, E.; Walker, P. J. Determination of mercury in potable water by ICP-MS using gold as a stabilising agent. *J. Anal. At. Spectrom.* **1999**, *14*, 235−239.
(11) Kraithong, S.; Sangsuwan, R.; Worawannotai, N.; Sirirak, J.; Charoenpanich, A.; Thamyongkit, P.; Wanichachewa, N. Triple detection modes for Hg^{2+} sensing based on a NBD-fluorescent and colorimetric sensor and its potential in cell imaging. *New J. Chem.* **2018**, *42*, 12412−12420.
(12) Petdum, A.; Panchan, W.; Sirirak, J.; Promarak, V.; Sooksimuang, T.; Wanichacheva, N. Colorimetric and fluorescent sensing of a new FRET system via [5]helicene and rhodamine 6G for Hg^{2+} detection. *New J. Chem.* **2018**, *42*, 1396−1402.
(13) Rasheed, T.; Nabeel, F.; Li, C.; Bilal, M. Rhodamine-assisted fluorescent strategy for the sensitive and selective in-field mapping of environmental pollutant Hg(II) with potential bioimaging. *J. Lumin.* **2019**, *208*, 519−526.
(14) Kaewnok, N.; Sirirak, J.; Jungsuttiwong, S.; Wongnongwa, Y.; Kamkaew, A.; Petdum, A.; Panchan, W.; Sahasithiwat, S.; Sooksimuang, T.; Charoenpanich, A.; Wanichacheva, N. Detection of hazardous mercury ion using [5]helicene-based fluorescence probe with "Turn ON" sensing response for practical applications. *J. Hazard. Mater.* **2021**, *418*, 126242.
(15) Bauzá De Mirabó, F. M.; Thomas, A. C.; Rubí, E.; Forteza, E.; Cerdá, V. Sequential injection analysis system for determination of mercury by cold-vapor atomic absorption spectroscopy. *Anal. Chim. Acta* **1997**, *355*, 203−210.
(16) Punrat, E.; Chuanuwatanakul, S.; Kaneta, T.; Motomizu, S.; Chailapakul, O. Method development for the determination of mercury(II) by sequential injection/anodic stripping voltammetry using an in situ gold-film screen-printed carbon electrode. *J. Electroanal. Chem.* **2014**, *727*, 78−83.
(17) Rattanakit, P.; Prasertboonyai, K.; Liawruangrath, S. Development of sequential injection spectrophotometric method for determination of mercury (II) using pyrogallol red. *Int. J. Environ. Anal. Chem.* **2016**, *96*, 1415−1429.
(18) Du, J.; Zhu, B.; Peng, X.; Chen, X. Optical reading of contaminants in aqueous media based on gold nanoparticles. *Small* **2014**, *10*, 3461−3479.
(19) Zangeneh Kamali, K.; Pandikumar, A.; Jayabal, S.; Ramaraj, R.; Lim, H. N.; Ong, B. H.; Bien, C. S. D.; Kee, Y. Y.; Huang, N. M. Amalgamation based optical and colorimetric sensing of mercury(II) ions with silver@graphene oxide nanocomposite materials. *Microchim. Acta* **2016**, *183*, 369−377.
(20) Lee, J.-S.; Han, M. S.; Mirkin, C. A. Colorimetric Detection of Mercuric Ion (Hg^{2+}) in Aqueous Media using DNA-Functionalized Gold Nanoparticles. *Am. Ethnol.* **2007**, *119*, 4171−4174.
(21) Baker, S. N.; Baker, G. A. Luminescent carbon nanodots: emergent nanolights. *Angew. Chem., Int. Ed.* **2010**, *49*, 6726−6744.
(22) Berlina, A. N.; Zherdev, A. V.; Dzantiev, B. B. Progress in rapid optical assays for heavy metal ions based on the use of nanoparticles and receptor molecules. *Microchim. Acta* **2019**, *186*, 172.
(23) Yoo, D.; Park, Y.; Cheon, B.; Park, M. H. Carbon Dots as an Effective Fluorescent Sensing Platform for Metal Ion Detection. *Nanoscale Res. Lett.* **2019**, *14*, 272.
(24) Li, P.; Li, S. F. Y. Recent advances in fluorescence probes based on carbon dots for sensing and speciation of heavy metals. *NANO* **2021**, *10*, 877−908.
(25) El-Shafey, A. M. Carbon dots: Discovery, structure, fluorescent properties, and applications. *Green Process. Synth.* **2021**, *10*, 134−156.
(26) Sekar, A.; Yadav, R.; Basavaraj, N. Fluorescence quenching mechanism and the application of green carbon nanodots in the detection of heavy metal ions: a review. *New J. Chem.* **2021**, *45*, 2326−2360.
(27) Nazri, N. A. A.; Azeman, N. H.; Luo, Y.; Bakar, A. A. A. Carbon quantum dots for optical sensor applications: A review. *Opt. Laser Technol.* **2021**, *139*, 106928.
(28) Ghanem, A.; Al-Qassar Bani Al-Marjeh, R.; Atassi, Y. Novel nitrogen-doped carbon dots prepared under microwave-irradiation for highly sensitive detection of mercury ions. *Heliyon* **2020**, *6*, No. e03750.
(29) Ye, Z.; Zhang, Y.; Li, G.; Li, B. Fluorescent Determination of Mercury(II) by Green Carbon Quantum Dots Synthesized from Eggshell Membrane. *Anal. Lett.* **2020**, *53*, 2841−2853.
(30) Omer, K. M.; Hama Aziz, K. H.; Mohammed, S. J. Improvement of selectivity via the surface modification of carbon nanodots towards the quantitative detection of mercury ions. *New J. Chem.* **2019**, *43*, 12979−12986.
(31) Yahyazadeh, E.; Shemirani, F. Easily synthesized carbon dots for determination of mercury(II) in water samples. *Heliyon* **2019**, *5*, No. e01596.
(32) Mohammadpour, Z.; Safavi, A.; Shamsipur, M. A new label free colorimetric chemosensor for detection of mercury ion with tunable dynamic range using carbon nanodots as enzyme mimics. *Chem. Eng. J.* **2014**, *255*, 1−7.
(33) Pajewska-Szmyt, M.; Buszewski, B.; Gadzala-Kopciuch, R. Carbon dots as rapid assays for detection of mercury(II) ions based on turn-off mode and breast milk. *Spectrochim. Acta, Part A* **2020**, *236*, 118320.

(34) Tadesse, A.; Hagos, M.; RamaDevi, D.; Basavaiah, K.; Belachew, N. Fluorescent-Nitrogen-Doped Carbon Quantum Dots Derived from Citrus Lemon Juice: Green Synthesis, Mercury(II) Ion Sensing, and Live Cell Imaging. *ACS Omega* **2020**, *5*, 3889−3898.
(35) Zhang, Q.; Zhang, X.; Bao, L.; Wu, Y.; Jiang, L.; Zheng, Y.; Wang, Y.; Chen, Y. The Application of Green-Synthesis-Derived Carbon Quantum Dots to Bioimaging and the Analysis of Mercury(II). *J. Anal. Methods Chem.* **2019**, *2019*, 8183134.
(36) Qu, S.; Wang, X.; Lu, Q.; Liu, X.; Wang, L. A biocompatible fluorescent ink based on water-soluble luminescent carbon nanodots. *Angew. Chem., Int. Ed.* **2012**, *51*, 12215−12218.
(37) Qin, X.; Lu, W.; Asiri, A. M.; Al-Youbi, A. O.; Sun, X. Microwave-assisted rapid green synthesis of photoluminescent carbon nanodots from flour and their applications for sensitive and selective detection of mercury(II) ions. *Sens. Actuators, B* **2013**, *184*, 156−162.
(38) Sk, M. P.; Chattopadhyay, A. Induction coil heater prepared highly fluorescent carbon dots as invisible ink and explosive sensor. *RSC Adv.* **2014**, *4*, 31994−31999.
(39) Han, Z.; He, L.; Pan, S.; Liu, H.; Hu, X. Hydrothermal synthesis of carbon dots and their application for detection of chlorogenic acid. *Luminescence* **2020**, *35*, 989−997.
(40) Bajpai, S. K.; D'Souza, A.; Suhail, B. Blue light-emitting carbon dots (CDs) from a milk protein and their interaction with Spinacia oleracea leaf cells. *Int. Nano Lett.* **2019**, *9*, 203−212.
(41) Fu, Y.; Zhao, S.; Wu, S.; Huang, L.; Xu, T.; Xing, X.; Lan, M.; Song, X. A carbon dots-based fluorescent probe for turn-on sensing of ampicillin. *Dyes Pigm.* **2020**, *172*, 107846.
(42) Li, X.; Zhang, S.; Kulinich, S. A.; Liu, Y.; Zeng, H. Engineering surface states of carbon dots to achieve controllable luminescence for solid-luminescent composites and sensitive Be^{2+} detection. *Sci. Rep.* **2014**, *4*, 4976.
(43) Hoan, B. T.; Van Huan, P.; Van, H. N.; Nguyen, D. H.; Tam, P. D.; Nguyen, K. T.; Pham, V. H. Luminescence of lemon-derived carbon quantum dot and its potential application in luminescent probe for detection of $Mo^{(6+)}$ ions. *Luminescence* **2018**, *33*, 545−551.
(44) Wang, C.; Hu, T.; Wen, Z.; Zhou, J.; Wang, X.; Wu, Q.; Wang, C. Concentration-dependent color tunability of nitrogen-doped carbon dots and their application for iron(III) detection and multicolor bioimaging. *J. Colloid Interface Sci.* **2018**, *521*, 33−41.
(45) Liu, W.; Diao, H.; Chang, H.; Wang, H.; Li, T.; Wei, W. Green synthesis of carbon dots from rose-heart radish and application for Fe^{3+} detection and cell imaging. *Sens. Actuators, B* **2017**, *241*, 190−198.
(46) Askarinejad, A.; Morsali, A. Synthesis and characterization of mercury oxide unusual nanostructures by ultrasonic method. *Chem. Eng. J.* **2009**, *153*, 183−186.
(47) Tang, Q.; Zhu, W.; He, B.; Yang, P. Rapid Conversion from Carbohydrates to Large-Scale Carbon Quantum Dots for All-Weather Solar Cells. *ACS Nano* **2017**, *11*, 1540−1547.
(48) Wei, X.-M.; Xu, Y.; Li, Y.-H.; Yin, X.-B.; He, X.-W. Ultrafast synthesis of nitrogen-doped carbon dots via neutralization heat for bioimaging and sensing applications. *RSC Adv.* **2014**, *4*, 44504−44508.
(49) Zhao, C.; Li, X.; Cheng, C.; Yang, Y. Green and microwave-assisted synthesis of carbon dots and application for visual detection of cobalt(II) ions and pH sensing. *Microchem. J.* **2019**, *147*, 183−190.
(50) Edison, T. N.; Atchudan, R.; Sethuraman, M. G.; Shim, J. J.; Lee, Y. R. Microwave assisted green synthesis of fluorescent N-doped carbon dots: Cytotoxicity and bio-imaging applications. *J. Photochem. Photobiol., B* **2016**, *161*, 154−161.
(51) Barati, A.; Shamsipur, M.; Arkan, E.; Hosseinzadeh, L.; Abdollahi, H. Synthesis of biocompatible and highly photoluminescent nitrogen doped carbon dots from lime: analytical applications and optimization using response surface methodology. *Mater. Sci. Eng., C* **2015**, *47*, 325−332.
(52) Kuzmenko, V.; Naboka, O.; Staaf, H.; Haque, M.; Göransson, G.; Lundgren, P.; Gatenholm, P.; Enoksson, P. Capacitive effects of nitrogen doping on cellulose-derived carbon nanofibers. *Mater. Chem. Phys.* **2015**, *160*, 59−65.
(53) Shah, H.; Xin, Q.; Jia, X.; Gong, J. R. Single precursor-based luminescent nitrogen-doped carbon dots and their application for iron (III) sensing. *Arabian J. Chem.* **2019**, *12*, 1083−1091.
(54) He, J. H.; Cheng, Y. Y.; Yang, T.; Zou, H. Y.; Huang, C. Z. Functional preserving carbon dots-based fluorescent probe for mercury (II) ions sensing in herbal medicines via coordination and electron transfer. *Anal. Chim. Acta* **2018**, *1035*, 203−210.
(55) Yan, F.; Kong, D.; Luo, Y.; Ye, Q.; He, J.; Guo, X.; Chen, L. Carbon dots serve as an effective probe for the quantitative determination and for intracellular imaging of mercury(II). *Microchim. Acta* **2016**, *183*, 1611−1618.
(56) Li, L.; Yu, B.; You, T. Nitrogen and sulfur co-doped carbon dots for highly selective and sensitive detection of Hg (II) ions. *Biosens. Bioelectron.* **2015**, *74*, 263−269.
(57) U.S. Food and Drug Administration. *Prohibited & Restricted Ingredients in Cosmetics*.; U.S. Food and Drug Administration https://www.fda.gov/cosmetics/cosmetics-laws-regulations/prohibited-restricted-ingredients-cosmetics. (accessed 2022-12-13).
(58) Codex Alimentarius Commission. *CAC/GL 40−1993 Guidelines on Good Laboratory Practice in Pesticide Residue Analysis*; Codex Alimentarius Commission: Rome, Italy: 2010.
(59) AOAC International. *AOAC SMPR 2012.007 Standard Method Performance Requirements for Heavy Metals in a Variety of Foods and Beverages*; AOAC International: Rockville, USA: 2021.
(60) Agilent Technologies, I. *Multi-element calibration standard-2A*.; Agilent Technologies, I. https://www.agilent.com/store/en_US/Prod-8500-6940/8500-6940 . (accessed 2022-12-10).
(61) Liu, J.; Li, R.; Yang, B. Carbon Dots: A New Type of Carbon-Based Nanomaterial with Wide Applications. *ACS Cent. Sci.* **2020**, *6*, 2179−2195.

https://doi.org/10.1021/acsomega.2c07175
ACS Omega 2023, 8, 7615−7625

REFERENCES

1. Bourgeois, M., et al., *Mercury intoxication after topical application of a metallic mercury ointment.* Dermatologica, 1986. **172**(1): p. 48–51.
2. Dyall-Smith, D.J. and J.P. Scurry, *Mercury pigmentation and high mercury levels from the use of a cosmetic cream.* Med. J. Aust., 1990. **153**(7): p. 409-415.
3. Chan, T.Y., *Inorganic mercury poisoning associated with skin-lightening cosmetic products.* Clin. Toxicol., 2011. **49**(10): p. 886-891.
4. Alvarez-Rivera, G., et al., *Preservatives in Cosmetics*, in *Analysis of Cosmetic Products*. 2018. p. 175-224.
5. Hamilton, T. and G.C.d. Gannes, *Allergic contact dermatitis to preservatives and fragrances in cosmetics.* Skin ther. lett., 2011. **14**: p. 1-4.
6. Kumari, P.K., et al., *Alternative to artificial preservatives.* Sys. Rev. Pharm., 2019: p. 99-102.
7. Deza, G. and A.M. Gimenez-Arnau, *Allergic contact dermatitis in preservatives: current standing and future options.* Curr. Opin. Allergy Clin. Immunol., 2017. **17**(4): p. 263-268.
8. Charoenkitamorn, K., et al., *Simple portable voltammetric sensor using anodized screen-printed graphene electrode for the quantitative analysis of p-hydroxybenzoic acid in cosmetics.* ACS Omega, 2022. **7**(18): p. 16116-16126.
9. Verma, R.J. and V. Asnani, *Ginger extract ameliorates paraben induced biochemical changes in liver and kidney of mice.* Acta Pol. Pharm., 2017. **64**(3): p. 217-220.
10. Bussan, D.D., R.F. Sessums, and J.V. Cizdziel, *Direct mercury analysis in environmental solids by ICP-MS with on-line sample ashing and mercury pre-concentration using a direct mercury analyzer.* J. Anal. At. Spectrom., 2015. **30**(7): p. 1668-1672.
11. Youngvises, N., et al., *Greener liquid chromatography using a guard column with micellar mobile phase for separation of some pharmaceuticals and determination of parabens.* Talanta, 2013. **106**: p. 350-359.

12. Katakam, L.N.R., S.K. Ettaboina, and T. Dongala, *A simple and rapid HPLC method for determination of parabens and their degradation products in pharmaceutical dosage forms.* Biomed. Chromatogr., 2021. **35**(10): p. e5152.
13. Khesina, Z.B., et al., *Microextraction by packed sorbent optimized by statistical design of experiment as an approach to increase the sensitivity and selectivity of HPLC-UV determination of parabens in cosmetics.* J. Pharm. Biomed. Anal., 2021. **195**: p. 113843.
14. Armarego, W.L., *Chapter 5 - Nanomaterials*, in *Purification of laboratory chemicals: part 2 inorganic chemicals, catalysts, biochemicals, physiologically active chemicals, nanomaterials.* 2022: Butterworth, Heinemann.
15. Liu, J., R. Li, and B. Yang, *Carbon Dots: A New Type of Carbon-Based Nanomaterial with Wide Applications.* ACS Cent. Sci., 2020. **6**(12): p. 2179-2195.
16. Daniel, S. and S. Thomas, *Layered double hydroxides: fundamentals to applications*, in *Layered double hydroxide polymer nanocomposites*. 2020, Woodhead Publishing.
17. Munyemana, J.C., et al., *A review on optical sensors based on layered double hydroxides nanoplatforms.* Microchim. Acta, 2021. **188**(3): p. 1-19.
18. Ruiz-Medina, A., *Flow injection analysis—clinical and pharmaceutical applications*, in *Reference module in chemistry, molecular sciences and chemical engineering*. 2018.
19. Borowska, S. and M.M. Brzoska, *Metals in cosmetics: implications for human health.* J. Appl. Toxicol., 2015. **35**(6): p. 551-572.
20. Abbas, H.H., et al., *Mercury exposure and health problems of the students using skin-lightening cosmetic products in makassar, south sulawesi, indonesia.* Cosmetics, 2020. **7**(3): p. 1-10.
21. Sun, G.F., et al., *Characteristics of mercury intoxication induced by skin-lightening products.* Chin. Med. J., 2017. **130**(24): p. 3003-3004.
22. Ministry of Public Health, *List of prohibited in cosmetic production*. 2559, Ministry of Public Health: Bangkok.
23. U.S. Food and Drug Administration. *Prohibited & restricted ingredients in cosmetics*. [cited 2023-05-14]; Available from:

https://www.fda.gov/cosmetics/cosmetics-laws-regulations/prohibited-restricted-ingredients-cosmetics.

24. Gaal F. F. and B.F. Abramovic, *Determination of mercury content of some pharmaceutical products by catalytic titration.* Mikrochim. Acta, 1982. **1**: p. 465-472.
25. Margosis, M. and J.T. Tanner, *Determination of mercury in pharmaceutical products by neutron activation analysis.* J. Pharm. Sci., 1972. **61**(6): p. 936-938.
26. Ang, H.H., E.L. Lee, and H.S. Cheang, *Determination of mercury by cold vapor atomic absorption spectrophotometer in Tongkat Ali preparations obtained in Malaysia.* Int. J. Toxicol., 2004. **23**(1): p. 65-71.
27. Petdum, A., et al., *Colorimetric and fluorescent sensing of a new FRET system via [5]helicene and rhodamine 6G for Hg^{2+} detection.* New J. Chem., 2018. **42**(2): p. 1396-1402.
28. Rasheed, T., et al., *Rhodamine-assisted fluorescent strategy for the sensitive and selective in-field mapping of environmental pollutant Hg(II) with potential bioimaging.* J. Lumin., 2019. **208**: p. 519-526.
29. Huang, C.C. and H.T. Chang, *Selective gold-nanoparticle-based "turn-on" fluorescent sensors for detection of mercury (II) in aqueous solution.* Anal. Chem., 2006. **78**(24): p. 8332-8338.
30. Kraithong, S., et al., *Enhancing Sensitivity of Novel Hg^{2+} Fluorescent Sensor via Plasmonic Enhancement of Silver Nanoparticles.* Sens. Actuators B Chem., 2018. **258**: p. 694-703.
31. Qiao, G., et al., *Signal transduction from small particles: Sulfur nanodots featuring mercury sensing, cell entry mechanism and in vitro tracking performance.* J. Chem. Eng., 2020. **382**.
32. Chien, C.-T., et al., *Tunable photoluminescence from graphene oxide.* Angew. Chem. Int. Ed., 2012. **51**(27): p. 6662-6666.
33. Carbonaro, et al., *On the emission properties of carbon dots: reviewing data and discussing models.* C J. Carbon Res., 2019. **5**(4): p. 1-15.
34. Sciortino, L., et al., *Tailoring the emission color of carbon dots through nitrogen-induced changes of their crystalline structure.* J. Phys. Chem. C, 2018. **122**(34):

p. 19897-19903.

35. Qu, S., et al., *A biocompatible fluorescent ink based on water-soluble luminescent carbon nanodots.* Angew. Chem. Int. Ed., 2012. **51**(49): p. 12215-12218.
36. Yoo, D., et al., *Carbon dots as an effective fluorescent sensing platform for metal ion detection.* Nanoscale Res. Lett., 2019. **14**(1): p. 1-13.
37. He, J.H., et al., *Functional preserving carbon dots-based fluorescent probe for mercury (II) ions sensing in herbal medicines via coordination and electron transfer.* Anal. Chim. Acta, 2018. **1035**: p. 203-210.
38. Qin, X., et al., *Microwave-assisted rapid green synthesis of photoluminescent carbon nanodots from flour and their applications for sensitive and selective detection of mercury(II) ions.* Sens. Actuators B Chem., 2013. **184**: p. 156-162.
39. Barati, A., et al., *Synthesis of biocompatible and highly photoluminescent nitrogen doped carbon dots from lime: analytical applications and optimization using response surface methodology.* Mater. Sci. Eng. C, 2015. **47**: p. 325-332.
40. Kuzmenko, V., et al., *Capacitive effects of nitrogen doping on cellulose-derived carbon nanofibers.* Mater. Chem. Phys., 2015. **160**: p. 59-65.
41. Pajewska-Szmyt, M., B. Buszewski, and R. Gadzala-Kopciuch, *Carbon dots as rapid assays for detection of mercury(II) ions based on turn-off mode and breast milk.* Spectrochim. Acta A Mol. Biomol. Spectrosc., 2020. **236**: p. 118320.
42. Tadesse, A., et al., *Fluorescent-Nitrogen-Doped Carbon Quantum Dots Derived from Citrus Lemon Juice: Green Synthesis, Mercury(II) Ion Sensing, and Live Cell Imaging.* ACS Omega, 2020. **5**(8): p. 3889-3898.
43. Ghanem, A., R. Al-Qassar Bani Al-Marjeh, and Y. Atassi, *Novel nitrogen-doped carbon dots prepared under microwave-irradiation for highly sensitive detection of mercury ions.* Heliyon, 2020. **6**(4): p. e03750.
44. Ye, Z., et al., *Fluorescent Determination of Mercury(II) by Green Carbon Quantum Dots Synthesized from Eggshell Membrane.* Anal. Lett., 2020. **53**(18): p. 2841-2853.
45. Cerdà, V., et al., *Evolution and description of the principal flow techniques*, in

Flow analysis. 2014. p. 1-42.

46. De Mirabo, F.B., et al., *Sequential injection analysis system for determination of mercury by cold-vapor atomic absorption spectroscopy.* Anal. Chim. Acta, 1997. **355**(2-3): p. 203-210.
47. van Staden, J.F. and R.E. Taljaard, *Determination of Lead(II), Copper(II), Zinc(II), Cobalt(II), Cadmium(II), Iron(III), Mercury(II) using sequential injection extractions.* Talanta, 2004. **64**(5): p. 1203-1212.
48. Punrat, E., et al., *Method development for the determination of mercury(II) by sequential injection/anodic stripping voltammetry using an in situ gold-film screen-printed carbon electrode.* J. Electroanal. Chem., 2014. **727**: p. 78-83.
49. Rattanakit, P., K. Prasertboonyai, and S. Liawruangrath, *Development of sequential injection spectrophotometric method for determination of mercury (II) using pyrogallol red.* Int. J. Environ. Anal. Chem., 2016. **96**(15): p. 1415-1429.
50. Kashani, F.Z., et al., *A carbon paste electrode modified with a nickel titanate nanoceramic for simultaneous voltammetric determination of ortho- and para-hydroxybenzoic acids.* Microchim. Acta, 2018. **186**(1): p. 1-8.
51. Shivashankara, A.R., et al., *Hepatoprotective effects of Zingiber officinale roscoe (ginger)*, in *Bioactive food as dietary interventions for liver and gastrointestinal disease*. 2013. p. 657-671.
52. Food and Drug Administration, U.S., *Annex VI – List of preservatives allowed for use in cosmetic products*. 2022: United States.
53. EU Cosmetics Regulation, *Annex V – List of preservatives allowed in cosmetic products*. 2022: England.
54. Huang, H.Y., I.Y. Huang, and H.Y. Lin, *Separation of parabens in capillary electrochromatography using poly(styrene-divinylbenzene-methacrylic acid) monolithic column.* J. Sep. Sci., 2006. **29**(13): p. 2038-2048.
55. Uysal, U.D. and T. Güray, *Determination of parabens in pharmaceutical and cosmetic products by capillary electrophoresis.* J. Anal. Chem., 2008. **63**(10): p. 982-986.
56. Cheng, Y.C., et al., *Large volume sample stacking with EOF and sweeping in CE for determination of common preservatives in cosmetic products by*

chemometric experimental design. Electrophoresis, 2012. **33**(9-10): p. 1443-1448.

57. Weisenberg, E., B. Gershon, and J. Schoenberg, *Micro-determination of p-hydroxybenzoic esters in pharmaceuticals and cosmetics.* J. Assoc. Off. Anal. Chem., 1977. **60**(1): p. 56-59.
58. Yang, T.J., et al., *Determination of additives in cosmetics by supercritical fluid extraction on-line headspace solid-phase microextraction combined with gas chromatography-mass spectrometry.* Anal. Chim. Acta, 2010. **668**(2): p. 188-194.
59. Wang, P.G. and W. Zhou, *Rapid determination of parabens in personal care products by stable isotope GC-MS/MS with dynamic selected reaction monitoring.* J. Sep. Sci., 2013. **36**(11): p. 1781-1787.
60. Dhahir, S.A. and H.J. Hussein, *Spectrophotometric determination of methyl paraben in pure and pharmaceutical oral solution.* Adv. Nat. Sci., 2013. **6**(4): p. 69-74.
61. Ahmed, A.M.K., A.S. Khazaal, and A.H. Ahmed, *Spectrophotometric determination of methyl paraben in pharmaceutical formulations by oxidative coupling reaction.* Tik. J. of Pure Sci., 2018. **21**(6): p. 85-89.
62. Kitchawengkul, N., et al., *Mimicking peroxidase-like activity of nitrogen-doped carbon dots (N-CDs) coupled with a laminated three-dimensional microfluidic paper-based analytical device (laminated 3D-μPAD) for smart sensing of total cholesterol from whole blood.* Anal. Chem., 2021. **93**(18): p. 6989-6999.
63. Zhuang, J., et al., *Ex vivo detection of iron oxide magnetic nanoparticles in mice using their intrinsic peroxidase-mimicking activity.* Mol. Pharm., 2012. **9**(7): p. 1983-1989.
64. Wongsing, B., et al., *Vanadium-doped porous cobalt oxide for its superior peroxidase-like activity in simultaneous total cholesterol and glucose determination in whole blood based on a simple two-dimensional paper-based analytical device.* Anal. Chem., 2022. **94**(40): p. 13785-13794.
65. Lee, N., et al., *Application of peroxidase-mimic Mn_2BPMP boosted by ADP to enzyme cascade assay for glucose and cholesterol.* Chemosensors, 2022. **10**(2): p. 1-10.

66. Tummala, S., R. Bandi, and Y.P. Ho, *Synthesis of Cu-doped carbon dot/chitosan film composite as a catalyst for the colorimetric detection of hydrogen peroxide and glucose.* Microchim. Acta, 2022. **189**(8): p. 284.

67. Jouyban, A. and R. Amini, *Layered double hydroxides as an efficient nanozyme for analytical applications.* Microchem. J., 2021. **164**: p. 105970.

68. Zhan, T., et al., *NiFe layered double hydroxide nanosheets as an efficiently mimic enzyme for colorimetric determination of glucose and H_2O_2.* Sens. Actuators B Chem., 2018. **255**: p. 2635-2642.

69. Ponlakhet, K., et al., *$Fe^{II}Fe^{III}$ layered double hydroxide nanosheets ($Fe^{II}Fe^{III}$ LDHNS) as an enzyme mimic for colorimetric detection of H_2O_2.* Anal. Methods, 2019. **11**(37): p. 4785-4794.

70. Prakobkij, A., et al., *Nitrogen-doped carbon dots/Ni-MnFe-layered double hydroxides (N-CDs/Ni-MnFe-LDHs) hybrid nanomaterials as immunoassay label for low-density lipoprotein detection.* Microchim. Acta, 2022. **189**(2): p. 72.

71. Sk, M.P. and A. Chattopadhyay, *Induction coil heater prepared highly fluorescent carbon dots as invisible ink and explosive sensor.* RSC Adv., 2014. **4**(60): p. 31994-31999.

72. Bajpai, S.K., A. D'Souza, and B. Suhail, *Blue light-emitting carbon dots (CDs) from a milk protein and their interaction with Spinacia oleracea leaf cells.* Int. Nano Lett., 2019. **9**(3): p. 203-212.

73. Khunkhong, N., et al., *A novel spirooxazine derivative as a colorimetric probe for Fe^{2+} and Pb^{2+} determination on microfluidic paper-based analytical device (**μ**PAD) for maintaining in photochromic efficiency.* Dyes Pigm., 2023. **208**: p. 110869.

74. Dong, Y.L., et al., *Graphene oxide-Fe_3O_4 magnetic nanocomposites with peroxidase-like activity for colorimetric detection of glucose.* Nanoscale, 2012. **4**(13): p. 3969-3976.

75. Aumiller, W.M., Jr., et al., *Interactions of macromolecular crowding agents and cosolutes with small-molecule substrates: effect on horseradish peroxidase activity with two different substrates.* J. Phys. Chem. B, 2014. **118**(36): p. 10624-

10632.

76. Fu, Y., et al., *A carbon dots-based fluorescent probe for turn-on sensing of ampicillin.* Dyes Pigm., 2020. **172**: p. 107846.

77. Li, X., et al., *Engineering surface states of carbon dots to achieve controllable luminescence for solid-luminescent composites and sensitive Be^{2+} detection.* Sci. Rep., 2014. **4**(1): p. 4976.

78. Hoan, B.T., et al., *Luminescence of lemon-derived carbon quantum dot and its potential application in luminescent probe for detection of Mo($^{6+}$) ions.* Luminescence, 2018. **33**(3): p. 545-551.

79. Wang, C., et al., *Concentration-dependent color tunability of nitrogen-doped carbon dots and their application for iron(III) detection and multicolor bioimaging.* J. Colloid Interface Sci., 2018. **521**: p. 33-41.

80. Liu, W., et al., *Green synthesis of carbon dots from rose-heart radish and application for Fe^{3+} detection and cell imaging.* Sens. Actuators B Chem., 2017. **241**: p. 190-198.

81. Askarinejad, A. and A. Morsali, *Synthesis and characterization of mercury oxide unusual nanostructures by ultrasonic method.* Chem. Eng. J., 2009. **153**(1-3): p. 183-186.

82. Tang, Q., et al., *Rapid conversion from carbohydrates to large-scale carbon quantum dots for all-weather solar cells.* ACS Nano, 2017. **11**(2): p. 1540-1547.

83. Wei, X.-M., et al., *Ultrafast synthesis of nitrogen-doped carbon dots via neutralization heat for bioimaging and sensing applications.* RSC Adv., 2014. **4**(84): p. 44504-44508.

84. Zhao, C., et al., *Green and microwave-assisted synthesis of carbon dots and application for visual detection of cobalt(II) ions and pH sensing.* Microchem. J., 2019. **147**: p. 183-190.

85. Edison, T.N., et al., *Microwave assisted green synthesis of fluorescent N-doped carbon dots: Cytotoxicity and bio-imaging applications.* J. Photochem. Photobiol. B, Biol., 2016. **161**: p. 154-161.

86. Shah, H., et al., *Single precursor-based luminescent nitrogen-doped carbon dots and their application for iron (III) sensing.* Arab. J. Chem., 2019. **12**(7): p. 1083-

1091.

87. Yan, F., et al., *Carbon dots serve as an effective probe for the quantitative determination and for intracellular imaging of mercury(II).* Microchim. Acta, 2016. **183**(5): p. 1611-1618.

88. Li, L., B. Yu, and T. You, *Nitrogen and sulfur co-doped carbon dots for highly selective and sensitive detection of Hg (II) ions.* Biosens. Bioelectron., 2015. **74**: p. 263-9.

89. Baker, S.N. and G.A. Baker, *Luminescent carbon nanodots: emergent nanolights.* Angew. Chem. Int. Ed., 2010. **49**(38): p. 6726-6744.

90. AOAC Official Methods of Analysis, *Standard method performance requirements for heavy metals in a variety of foods and beverages*. 2012.

91. Agilent Technologies, I. *Multi-element calibration standard-2A*. [cited 2023-05 -03]; Available from: https://www.agilent.com/store/en_US/Prod-8500-6940/8500-6940.

92. Codex Alimentarius Commission, *CAC/GL 40-1993 Guidelines on Good Laboratory Practice in Pesticide Residue Analysis*. 2010: Italy.

93. Magario, I., et al., *Mechanisms of radical generation in the removal of phenol derivatives and pigments using different Fe-based catalytic systems.* J. Mol. Catal. A: Chem., 2012. **352**: p. 1-20.

94. Sagone Jr, A.L., et al., *A new method for the detection of hydroxyl radical production by phagocytic cells.* Biochim. Biophys. Acta Gen. Subj., 1980. **628**: p. 90-97.

95. Baba, Y., et al., *Hydroxyl radical generation in the photo-Fenton process: Effects of carboxylic acids on iron redox cycling.* J. Chem. Eng., 2015. **277**: p. 229-241.

96. Gu, G.H., et al., *Mechanism of dehydration of phenols on noble metals via first-principles microkinetic modeling.* ACS Catal., 2016. **6**(5): p. 3047-3055.

97. Patel, A.K., et al., *Biochemical and spectroscopic characterization of morning glory peroxidase from an invasive and hallucinogenic plant weed Ipomoea carnea.* J. Agric. Food Chem., 2008. **56**(19): p. 9236-9245.

98. Mohamed, S.A., et al., *Properties of a cationic peroxidase from Citrus jambhiri cv. Adalia.* Appl. Biochem. Biotechnol., 2008. **150**(2): p. 127-137.

99. Lai, L.S., et al., *Catalytic characteristics of peroxidase from wheat grass.* J. Agric. Food Chem., 2006. **54**(22): p. 8611-8616.

100. Elsayed, A.M., et al., *Purification and biochemical characterization of peroxidase isoenzymes from Ficus carica latex.* Biocatal. Agric. Biotechnol., 2018. **16**: p. 1-9.

101. Rani, D.N. and T.E. Abraham, *Kinetics and thermal stability of two peroxidase isozymes from Eupatorium odoratum. Applied Biochemistry and Biotechnology.* Appl. Biochem. Biotechnol., 2006. **128**: p. 215-226.

102. Zhang, K., et al., *Determination of hemoglobin based on its enzymatic activity for the oxidation of o-phenylenediamine with hydrogen peroxide.* Anal. Chim. Acta, 2000. **413**(1-2): p. 109-113.

103. Lai, L.-S., et al., *Catalytic characteristics of peroxidase from wheat grass.* J. Agric. Food Chem., 2006. **54**(22): p. 8611-8616.

104. Elsayed, A.M., et al., *Purification and biochemical characterization of peroxidase isoenzymes from Ficus carica latex.* Biocatal. Agric. Biotechnol., 2018. **16**: p. 1-9.

105. Rani, D.N. and T.E. Abraham, *Kinetics and thermal stability of two peroxidase isozymes from Eupatorium odoratum.* Appl. Biochem. Biotechnol., 2006. **128**: p. 215-226.

106. AOAC Official Methods of Analysis, *Appendix F: Guidelines for Standard Method Performance Requirements*. 2016.

มหาวิทยาลัยศิลปากร

VITA

NAME Kanokwan Sakunrungrit

INSTITUTIONS ATTENDED B.Sc. (Chemistry), Silpakorn University

PUBLICATION Sukaram T., Sakunrungrit K., Juanjankarn J., Siriboon J., Sirisakwisut P., Yensamran Y., and Chaneam S.* Application of Natural Reagent from Orchid Flower as Indicator for Volumetric Acid-base Titration. Thai Science and Technology Journal. (2020), 1545-1557.

Sakunrungrit K., Suwanchawalit C., Charoenkitamorn K., Hongwitayakorn A., Strzelak K., and Chaneam S.* Sequential Injection Analysis for Rapid Determination of Mercury in Skincare Products Based on Fluorescence Quenching of Eco-Friendly Synthesized Carbon Dots. ACS Omega. (2023), 8, 8, 7615–7625.

AWARD RECEIVED Best poster presentation award from the 4th Materials Research Society of Thailand International Conference (MRS-Thailand 2023), Ubon Ratchathani, Thailand, “Fluorometric Determination of Preservatives in Skincare Products using Layered Double Hydroxides as Peroxidase Enzyme Mimicking”, February 28 – March 4, 2023.

Silver prize award in Young Rising Stars of Science 2021 from the 47th International Congress on Science, Technology, Technology-Based Innovation (STT 47th), Nakhon Pathom, Thailand, “Rapid and sensitive method for determination of mercury in pharmaceutical products based on green synthesis of carbon nanodots” October 5 – 7, 2021.

มหาวิทยาลัยศิลปากร